

Modeling First Flush and Particle Destabilization:
Implications for Design and Operation of Stormwater BMPs



Joohyon Kang

UNIVERSITY OF CALIFORNIA

Los Angeles

2005

UNIVERSITY OF CALIFORNIA

Los Angeles

Modeling First Flush and Particle Destabilization:
Implications for Design and Operation of Stormwater BMPs

A dissertation submitted in partial satisfaction of the
requirements for the degree Doctor of Philosophy
in Civil Engineering

by

Joohyon Kang

2005

© Copyright by

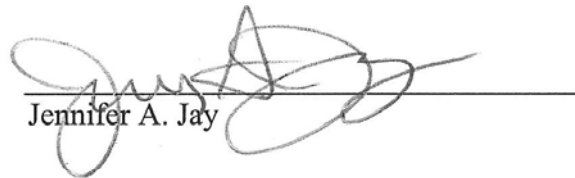
Joohyon Kang

2005

The dissertation of Joohyon Kang is approved.



Richard F. Ambrose



Jennifer A. Jay



Keith D. Stolzenbach



Michael K. Stenstrom, Committee Chair

University of California, Los Angeles

2005

To my parents and brother

Table of Contents

Chapter 1. Introduction / 1

Chapter 2. Background and Literature Review / 5

- 2.1 CHARACTERISTICS OF URBAN RUNOFF / 5
 - 2.1.1 Pollutants sources in Urban Runoff / 6
 - 2.1.2 Pollutant Buildup and Washoff / 8
 - 2.1.3 First Flush Phenomena / 13
- 2.2 MODELS FOR STORMWATER RUNOFF / 17
 - 2.2.1 Water Quantity Models / 18
 - 2.2.2 Water Quality Models / 19
 - 2.2.3 Numerical Solutions for Partial Differential Equations / 20
- 2.3 PARTICLE REMOVAL IN STORMWATER RUNOFF / 24
 - 2.3.1 Particle Settling in Highway Runoff / 24
 - 2.3.2 Particle Destabilization / 27

Chapter 3. Model Development / 30

- 3.1 MODEL EQUATIONS / 30
 - 3.1.1 Kinematic Wave Equation / 32
 - 3.1.2 Diffusion wave equation / 33
 - 3.1.3 Infiltration / 34
 - 3.1.4 Pollutant Transport / 35
 - 3.1.5 Pollutant Erosion from a Plane Surface / 35
- 3.2 NUMERICAL SOLUTIONS / 38
 - 3.2.1 Method of Characteristics for 1-D Flow / 38
 - 3.2.2 Characteristics Averaging Method for Radial Flow / 39
 - 3.2.3 Stability and Convergence in Numerical Solutions / 41
- 3.3 PARAMETER ESTIMATION / 48

Chapter 4. Methodology for Highway Runoff Coagulation/Flocculation / 50

- 4.1 PREPARATION OF RUNOFF SAMPLE / 50
- 4.2 MIXING TESTS / 51
- 4.3 PROTOCOLS FOR JAR TESTS / 51
- 4.4 WATER QUALITY MEASUREMENTS / 53

Chapter 5. First Flush Simulation / 54

- 5.1 PARAMETER ESTIMATION IN 1-D HIGHWAY RUNOFF MODEL / 54
 - 5.1.1 Flow Calculation / 54
 - 5.1.2 Calibration of Water Quality Parameters / 62

- 5.1.3 Pollutant Buildup / 63
- 5.2 FIRST FLUSH SIMULATIONS IN 1-D FLOW / 66
 - 5.2.1 Maximum MFF Ratio and Optimum Watershed Length / 66
 - 5.2.2 Evaluation of Affecting Factors / 68
- 5.3 RADIAL FLOW SIMULATION / 77
- 5.4 DESIGN IMPLICATIONS / 81
 - 5.4.1 MFF Ratio as a Design Parameter / 82
 - 5.4.2 BMP design for Highway Runoff / 88
 - 5.4.3 BMP Design for Parking Lots / 90
 - 5.4.4 Potential Improvement of BMP Performance by Optimal Design / 92

Chapter 6. Particle Destabilization in Highway Runoff / 95

- 6.1 PARTICLE AGGREGATION OVER TIME / 95
- 6.2 LOW DOSE FLOCCULATION / 98
- 6.3 SWEEP FLOC COAGULATION / 100
- 6.4 FLOCCULATION WITH CATIONIC POLYMER / 104
- 6.5 REMOVAL OF DISSOLVED HEAVY METALS / 108
- 6.6 DISCUSSION / 112

Chapter 7. Conclusion / 114

Appendix A. Site Descriptions / 118

Appendix B. Numerical Tests for Radial Flow Problem / 120

Appendix C. Measured and Simulated Polluto-graphs / 130

Appendix D. Regressions for Buildup / 139

Appendix E. Program Codes (MATLAB) / 141

Appendix F. Calculation of Metal Removal Efficiency / 151

REFERENCES / 152

List of Figures

- FIGURE 2.1 Definition of mass first flush ratio / 15
- FIGURE 2.2 Hydrograph with TSS, turbidity, conductivity and PSD for site 2, event 1/7/05 / 25
- FIGURE 3.1 Concept of 1-D flow model for highway runoff / 31
- FIGURE 3.2 Two-phase washoff of the pollutants / 37
- FIGURE 3.3 Procedure of the node value calculation in MOC / 39
- FIGURE 3.4 Characteristics averaging – Interior points / 40
- FIGURE 3.5 Calculated outflow using different values of Δt with different Δx_0 / 43
- FIGURE 3.6 Water depth profile at $t = 70$ min using different values of Δt with $\Delta x_0 = 1\text{m}$ / 44
- FIGURE 3.7 Calculated outflow using different values of Δx_0 with $\Delta t = 1/8$ min / 45
- FIGURE 3.8 Water depth profile at $t = 70$ min using different values of Δx_0 with $\Delta t = 1/8$ min / 45
- FIGURE 3.9 Outflow concentration profiles calculated for the same storm event using different values of Δx with $\Delta t = 1/8$ min / 46
- FIGURE 3.10 Mass profiles along the distance at $t = 30$ min calculated for the same storm event using different values of Δx with $\Delta t = 1/8$ min / 46
- FIGURE 5.1 Measured and simulated runoff volumes with different values of pavement hydraulic conductivity / 55
- FIGURE 5.2 Measured and simulated peak flows with different values of pavement hydraulic conductivity / 57
- FIGURE 5.3 Runoff coefficients with respect to the total rainfall volume at $K_p = 10^{-5}$ cm/sec / 58
- FIGURE 5.4 Measured and calculated hydrographs and polluto-graphs / 61
- FIGURE 5.5 Regressions for COD buildup using different curve forms / 64
- FIGURE 5.6 MFF changes with different watershed lengths at $I = 3$ mm/hr and $T = 3$ hr / 67
- FIGURE 5.7 Maximum MFF₂₀, optimum watershed length, and watershed length at MFF₂₀ = 2.5 / 68
- FIGURE 5.8 MFF₁₀ and MFF₂₀ with respect to the watershed length for different rainfall intensities and durations / 70
- FIGURE 5.9 MFF₁₀ and MFF₂₀ with respect to the watershed length for different slopes / 71
- FIGURE 5.10 MFF₁₀ and MFF₂₀ with respect to the watershed length for different values of pavement hydraulic conductivity / 72
- FIGURE 5.11 MFF₁₀ and MFF₂₀ with respect to the watershed length for different values of $m_{b,s}^0$ / 74
- FIGURE 5.12 MFF₁₀ and MFF₂₀ with respect to the watershed for different erosion coefficients of short-term pollutant source / 75
- FIGURE 5.13 MFF₁₀ and MFF₂₀ with respect to the watershed for different erosion rates of long-term pollutant source / 76

- FIGURE 5.14 MFF₁₀ and MFF₂₀ with respect to the watershed length for different inlet radius in the radial flow / 79
- FIGURE 5.15 Maximum MFF ratio and optimum watershed length in the radial flow simulation in Figure 5.14 / 80
- FIGURE 5.16 Mass distribution on the converging watershed / 81
- FIGURE 5.17 Contours of the optimal watershed length for maximum MFF₂₀ as a function of rainfall intensity and duration for different values of $m_{b,s}^o$ at $S_o = 0.02$ and $K_p = 10^{-5}$ cm/sec / 84
- FIGURE 5.18 Contours of the maximum MFF₂₀ as a function of rainfall intensity and duration for different values of $m_{b,s}^o$ at $S_o = 0.02$ and $K_p = 10^{-5}$ cm/sec / 85
- FIGURE 5.19 Contours of the maximum watershed length at MFF₂₀ = 2.5 as a function of rainfall intensity and duration for different values of $m_{b,s}^o$ at $S_o = 0.02$ and $K_p = 10^{-5}$ cm/sec / 87
- FIGURE 5.20 Contours of the maximum watershed length at MFF₂₀ = 2.5 as a function of rainfall intensity and duration for different slopes at $m_{b,s}^o = 1.0$ g/m² and $K_p = 10^{-5}$ cm/sec / 88
- FIGURE 5.21 Collection system design in the highway runoff BMPs / 89
- FIGURE 5.22 Different inlet location and watershed length in a square type watershed / 91
- FIGURE 5.23 Determination of design watershed length based on a MFF₂₀ curve for Cu / 93
- FIGURE 6.1 TSS and TDS changes over time from the observation of natural aggregation on 2/6/05 / 97
- FIGURE 6.2 PSD changes over time on 2/6/05 / 98
- FIGURE 6.3 Turbidity changes in the samples in low dose coagulation: (a) Alum; (b) Ferric chloride / 99
- FIGURE 6.4 Turbidity removal from sweep floc coagulation / 102
- FIGURE 6.5 Optimum coagulant dose and initial conductivity / 103
- FIGURE 6.6 Turbidity and ZP changes after adding same serious of amounts for alum and ferric chloride on 3/18/05 / 103
- FIGURE 6.7 ZP changes in the sample after adding two different molecular weight polyDADMACs on 2/6/05 / 104
- FIGURE 6.8 Optimum polymer dose and initial sample conductivity / 105
- FIGURE 6.9 Effect of mixing time on the turbidity removal with and without polymer on 1/28/05 / 105
- FIGURE 6.10 Effect of alum addition on the mixing time using polymer coagulation on 1/28/05 / 107
- FIGURE 6.11 PSD changes with different molecular weight polymers on 2/11/05 / 107
- FIGURE 6.12 Dissolved metal concentrations in the treated runoff from different coagulation/flocculation tests on 3/18/05 / 109
- FIGURE 6.13 Coagulation results with different polymer doses at alum = 8 mg/L on 4/28/05 / 110
- FIGURE 6.14 Coagulation results with different polymer doses at alum = 16 mg/L on 4/28/05 / 111

List of Tables

TABLE 2.1	Metal Concentrations for Different Particle Size Ranges / 7
TABLE 2.2	Quantitative Definitions of First Flush in the Stormwater Runoff from Different Researchers / 14
TABLE 2.3	Deterministic Studies for Pollutant Washoff Simulation / 21
TABLE 2.4	FDMs used for the Overland Flow Calculation / 22
TABLE 3.1	Model Equations and Numerical Schemes / 31
TABLE 3.2	Summary of Storm Events Used for the Estimation of Water Quality Parameters / 49
TABLE 4.1	Characteristics of 1 hr Composite Samples from Site 2 / 50
TABLE 4.2	Protocols for the Coagulation / Flocculation Tests / 52
TABLE 5.1	Input Parameters for the Flow Calculation / 58
TABLE 5.2	Calibrated Parameters for Site 3 / 62
TABLE 5.3	Buildup Equations Fitted by Different Curve Forms for COD, Conductivity, Zn and Cu / 63
TABLE 5.4	Comparison of Buildup Equations / 65
TABLE 5.5	Qualitative Relationship between MFF_{20} and Design factors / 82
TABLE 5.6	Design Factors Applied in the MFF Simulations / 83
TABLE 5.7	Performances of BMPs with Different Designs / 94

ACKNOWLEDGMENTS

I am deeply grateful to my advisor, Prof. Stenstrom, M.K., who has constantly given me inspiration in the research as well as physical supports. He has always been a model of what a scholar ought to be. Also, it is pleasant duty to express special thanks to Dr. Lau, S.-L. and Dr. Li, Y.-X. at UCLA. This dissertation would not have been completed without their contribution. Finally, I would like to thank Caltrans (California Department of Transportation) for funding the stormwater monitoring project.

VITA

September 6, 1971	Born, Pusan, Korea
1996	B.S., Civil and Environmental Engineering Korea University Seoul, Korea
1998	M.S., Civil and Environmental Engineering Korea University Seoul, Korea
1998-2001	Staff, Water and Wastewater Treatment Project Team LG Engineering and Construction Corporation Seoul, Korea
2002-05	Graduate Student Researcher University of California, Los Angeles

PUBLICATION AND PRESENTATIONS

- Kang, J.-H. (1998). Nutrient removal in wastewater using supernatant of septage as an external carbon source, *Master's thesis*, Dept. of Civil and Environmental Engineering, Korea University, Seoul, Korea, Feb.
- Kang, J.-H., Li, Y., Lau, S., Kayhanian, M., and Stenstrom, M.K. (2005). Application of particle size distribution in highway runoff: Optimization of settling tank design to remove particles, *Proceedings of the 4th south pacific conference on storm-water and aquatic resource protection*, Auchland, New Zealand.

ABSTRACT OF THE DISSERTATION

Modeling First Flush and Particle Destabilization:
Implications for Design and Operation of Highway Stormwater BMPs

by

Joohyon Kang

Doctor of Philosophy in Civil Engineering

University of California, Los Angeles, 2005

Professor Michael K. Stenstrom, Chair

First flush, which describes a greater pollutant discharge rate in the earlier part of a storm event, is an important phenomenon to understand pollutant washoff behavior of stormwater runoff and to establish appropriate best management practices (BMPs). A number of partially successful efforts have been made to reveal the relationship between first flush and the factors involved in the physical processes, including the characteristics of the rainfall and the watershed.

In this study, a deterministic model was developed to predict the mass first flush (MFF) and to utilize it for better design of BMPs focusing on treating the first flush. The model used the kinematic wave equation to calculate flow. For the water quality calculation, the mass transport equation and erosion equation were used with the concept of two different sources of pollutant mass. The model parameters were calibrated by a parameter estimation procedure using three years' monitoring data from a highway runoff site. The MFF simulation results showed that there exists an optimum watershed size to maximize MFF and by maximizing MFF, BMPs can improve overall reduction of pollutant mass. Contours of watershed length, developed using MFF simulations for different conditions of rainfall and watershed geometry, can be used to design runoff collection system of a BMP for highways and parking lots.

Another aspect of BMP design is how to enhance pollutant removal efficiency. Although most stormwater BMPs use gravity settling to remove particulates, particles in highway runoff are generally too small to be removed effectively. Therefore, additional means to destabilize particles are required. Alum, ferric chloride and cationic polymers were evaluated to destabilize particle in the runoff. Alum or ferric chloride alone was not successful due to large dose requirement and sludge production. A small dose addition of polymer followed by a long period of gentle mixing was successful. The required dose for polymer and coagulant were proportional to the initial conductivity of the runoff and therefore, unattended operation in the field might be possible by controlling the dose based on the initial conductivity.

Introduction

Non-point source (NPS) pollution such as urban stormwater runoff is receiving considerable attention because it has been identified as a major pollutant source, impairing receiving water bodies ([Furumai et al., 2002](#)). In the United States, the Clean Water Act (CWA) was amended by Congress in 1987 for the United States Environmental Protection Agency (USEPA) to establish phased National Pollutant Discharge Elimination System (NPDES) for stormwater discharges, to address permit applications, regulatory guidance and management and treatment requirements Under the CWA, California Department of Transportation (Caltrans) also instituted a statewide stormwater program in an effort to control stormwater pollution from the transportation facilities including highways in the State of California.

Urbanized landuses generate significantly greater pollutant loads as well as high peak flow and flow volume than undeveloped landuse, causing contamination and flood risk in ecosystems. Highway runoff readily transports heavy metals, oil and grease and other

toxic compounds that are accumulated during dry periods (Roger et al., 1998; Furumai et al., 2002; Lau and Stenstrom, 2005). To mitigate this problem, selection of appropriate controlling strategies, which are referred to as “best management practices” (BMPs), is essential. BMPs encompass all possible methods including public education, regulatory procedures and treatment facilities. A treatment facility is classified as a structural BMP and has been a preferred approach among BMPs because educational or regulatory methods are institutionally difficult (Kim, 2002).

Most structural BMPs adapt physical and chemical mechanisms such as sedimentation and filtration to remove pollutants. In these treatment systems, particle removal mechanisms play an important role, determining overall efficiency of pollutant removal. Suspended solids in urban runoff are composed of relatively fine particles, providing high surface to volume ratio for adsorption of reactive organics and metals on surface or within pores (Characklis and Wiesner, 1997; Roger et al., 1998; Sansalone et al., 1998). Particles in the highway runoff are unexpectedly stable in the solution because particles' density and shape are heterogeneous. Therefore, particle destabilization processes are required (Kang et al., 2005).

Characterizing pollutant washoff behavior is also crucial for design and operation of BMPs. Pollutant washoff is generally characterized by the “first flush”, a popularly used concept to indicate the high discharge of constituent mass or concentration in the early part of the runoff volume (Geiger, 1987). First flush is frequently observed in the runoff of the urbanized area including highly impervious landuses such as highways and parking lots. Therefore, characterizing first flush phenomena has been an important goal in the

stormwater pollution studies to establish better treatment strategies. First flush is strongly associated with the hydraulic condition that depends on meteorological and geometrical characteristics of the watershed. Numerous efforts have been made to reveal the relationship between the pollutant washoff behavior and associated factors including rainfall intensity, flow rate, watershed area and bed slope (Gupta and Saul, 1996; Deletic and Maksimovic, 1998; Cristina and Sansalone, 2003a; Taebi and Droste, 2004). However, no clear relationships among those factors have been yet verified.

Research Objectives

This research is composed of two main categories: Mass first flush (MFF) simulation using deterministic models for the stormwater runoff and experimental studies on particle destabilization using coagulation and flocculation.

The first objective of this study is to explore the first flush behavior quantitatively and qualitatively as a function of major factors that are related to the physical processes occurring during runoff using deterministic runoff models. The kinematic wave and diffusive wave theories were used to calculate flow depth and velocity. In addition, erosion and transport equations were coupled with water quantity solutions from the wave equations. The model was calibrated using three years' monitored concentration data using an optimization technique to solve the inverse problem. Using the calibrated model, a series of simulations was performed, exploring design relationships in order to develop a design tool to maximize first flush from small watersheds.

The second goal was to develop ways of increasing particle size in the runoff from highway sites. A series of coagulation and flocculation studies of highway runoff were performed to remove particles and associated pollutants. Various kinds of particle removal mechanisms including sweep floc coagulation and charge neutralization were tested using different coagulants and operating conditions. The goal of this study was to suggest the appropriate strategies for the particle destabilization in highway runoff.

Organization of Dissertation

The dissertation is organized into seven chapters. Chapter 2 introduces background and previous work on the mathematical models for urban runoff as well as previous particle destabilization studies. Chapter 3 describes model development and calculation methods. Chapter 4 discusses the protocols for the coagulation and flocculation tests. Chapter 5 provides the results of model verification, first flush simulation with discussion of the implications for practice. Chapter 6 presents the results of coagulation and flocculation tests. Finally, chapter 7 concludes the dissertation with summary on the induced results and those applications.

Background and Literature Review

2.1 CHARACTERISTICS OF URBAN RUNOFF

Non-point source pollution has long been recognized for its potential to degrade surface waters in the United States. The 1972 Amendments to the Clean Water Act recognized non-point source pollution under its “208” requirements. Early work was limited mostly to planning for non-point source management and identified agricultural runoff as being different and requiring alternative management strategies than point sources such as municipal and industrial wastewaters. Highways and streets were among the first to be investigated as non-point source pollutants very early in [Sartor and Boyd \(1972\)](#). Other early research included the Nationwide Urban Runoff Program ([U.S. EPA, 1983](#)) which addressed different types of land use. The first work in our laboratory investigated transportation land use such as parking lots and commercial as sources of oil and grease ([Stenstrom et al. 1984](#)).

2.1.1 Pollutants sources in Urban Runoff

Heavy Metals. Urban stormwater runoff is known to be the largest contribution of metals to the local receiving water bodies (Characklis and Wiesner, 1997). The Metals from anthropogenic sources include As, Pb, Na, Zn, Ba, Cd, Fe and Cr whereas Al, Ca, Mg, Sr, Hg and Mn are usually from natural sources (Zartman et al., 2001). The chemical nature and source of the individual metals lead to different partitioning between solid and liquid. Particulate metals in the urban runoff are typically associated with organic matter from the tire wear, pavement surface wear and dust from exhausted pipes as well as minerals from soil, pavement and sources in the watershed (Roger et al., 1998).

A pollutant's partition between solid and liquid phases is of concern because particulate fraction plays an important role in determining BMP efficiency. Hunter et al. (1981) reported that approximately 50% of total metals in stormwater were associated with particles. Characklis and Wiesner (1997) concluded that Zn exists mainly in the dissolved phase up to 80% of total concentration, while Fe is usually combined with coarse materials. Roger et al. (1998) stated that Pb and Zn were often found in the sediments from motorways and Zn was associated with the fine particles (< 50 μm). Furumai et al. (2002) stated that the particulate fractions accounted for 55 ~ 89%, 56 ~ 89% and 79 ~ 96% of total load of Zn, Cu and Pb, respectively, in highway runoff. Pb concentrations are declining in urban runoff because of elimination of lead in the gasoline (Furumai et al., 2002; Characklis and Wiesner, 1997). A large fraction of a particulate metal is usually associated with fine particles as shown in Table 2.1 (Li et al., 2005b).

TABLE 2.1 Metal Concentrations for Different Particle Size Ranges (Li et al., 2005b)

Size Ranges (μm)	Heavy Metal Concentration ($\mu\text{g/g}$)								Sampling and Experimental Methods	References	
	Al	Cd	Cr	Cu	Fe	Ni	Pb	Zn			
<i>Urban stormwater suspension</i>											
0.45-2				2894	29267		199	13540		Manually collected samples; Wet sieving	Morquecho and Pitt 2003, Birmingham and Tuscaloosa, Alabama
2-10				4668	18508		868	13641			
10-45				735	26221		229	1559			
45-106				1312	14615		226	2076			
106-250				2137	21730		375	3486			
>250				50	28604		117	266			
<i>Highway runoff sediments</i>											
25-38		16.8		364			265	1189		Manually collected from trough; Drying at 110°C-Sieving	Sansalone and Buchberger 1997b, Cincinnati, Ohio
38-45		17.2		353			236	996			
45-63		17.3		364			266	1027			
63-75		16.3		333			258	1057			
75-150		15		312			248	1014			
150-250		9.2		204			195	574			
250-425		8		78			65	325			
425-850		9.5		48			53	314			
850-2000		9.7		45			37	259			
<50	60000		350	420		230	1570	4370			
50-100	45000		400	250		250	1480	1700			
100-200	38000		410	200		220	1550	1100			
200-500	35500		150	100		220	850	930			
500-1000	37500		140	50		220	460	930			
<i>Street sweeping</i>											
<75				470				410		Vacuuming; Sieving	German and Svensson 2002, Jönköping, Sweden
75-125				270				230			
125-250				340				190			
250-500				200				120			
500-1000				50				70			
<43		5	46	220		65	350	960		Vacuuming; Air Drying-Sieving	Lau and Stenstrom 2004, Los Angeles, California
43-100		5	58	230		50	300	805			
100-250		2	38	230		40	210	500			
250-841		na	12	240		5	44	150			
Average		1	28	238		25	142	360			

Organics and Nutrients. Polynuclear aromatic hydrocarbons (PAHs) and microorganisms such as fecal coliforms and pathogens are of concern because of their potential toxicity to human health and ecosystems. PAHs are usually combined with the other organic matter (Schueler, 1987) and the origins of PAHs in urban runoff are usually pavement leaching, tire abrasion, automobile's combustion processes and lubricating oils (Latimer et al., 1990; Takada et al., 1991; Ngabe et al., 2000; Krein and Schorer, 2000; Kamalakkannan et al., 2004). Atmospheric deposition and regional air pollution emission is also a significant PAH source (Herricks, 1995).

Urban runoff also carries significant amount of nutrients such as nitrogen and phosphorous (Abustan et al., 1998). Nutrients sources include fertilizer applied to the yards, roof runoff, various household chemicals and street runoff. Vaze et al. (2002) performed an experimental study of pollutant accumulation on urban road surfaces and found that majority of total phosphorous and nitrogen in the solid samples was associated with particles less than 50 µm in diameter.

Borst and Selvakumar (2003) found large concentrations of fecal coliforms and pathogens in urban runoff. Microorganisms are self-suspended or absorbed to suspended particles, and prefer particles that are larger than 30 µm in diameter (Schillinger and Gannon, 1985).

2.1.2 Pollutant Buildup and Washoff

A variety of pollutants originating from vehicles, atmospheric deposition and pavement degradation are accumulated in the dry season and washed out during the next storm

event. The two stages, pollutant accumulation and emission, are referred to as “buildup” and “washoff”. Understanding the behavior of buildup and washoff is important to predict pollutant load emissions and establish treatment strategy. Most of buildup/washoff studies have adapted empirical approaches based on analysis of large databases because the physical and chemical processes involved in buildup and washoff are complicated and difficult to generalize.

Buildup. Landuse type is considered an important factor that determines the buildup characteristics for pollutants from different sources and having varying characteristic such as particle size, partitioning between particulate and liquid phases and density. [Sartor and Boyd \(1972\)](#) monitored pollutant buildup in the ten US cities to identify the types and characteristics of pollutants accumulating on streets and reported that the buildup of solids, COD and heavy metals is strongly associated with landuses. The buildup mass in industrial areas was the largest among three different landuses: residential, industrial and commercial. [Manning et al. \(1977\)](#) performed field measurements of accumulated pollutants in the four different landuses (i.e. single family residential, multi family residential, commercial and industrial) and calculated relative fractions of organics, nutrients and heavy metals in the total solids.

Many researchers have tried to develop appropriate mathematical expressions for buildup. Among several types of buildup formulas, exponential and Michaelis-Menton types have been common because the upper limit of mass accumulation is clearly defined in the formulas. A linear-type buildup formula is sometimes preferred because the

formulation and calculations are simple (Barbé et al., 1995). Buildup formulas are typically site specific but include the antecedent dry days (ADD) as a common variable. Other parameters such as atmospheric deposition, traffic load, street sweeping, biological degradation and wind speed can be incorporated in a buildup formula as positive or negative affecting factors (James and Shivalingaiah, 1985). Shahbeen (1975) particularly emphasized the contribution of traffic loading by assigning the dust and dirt (DD) production per vehicle as 800-1200 mg/axle-km travel.

Washoff. The physical processes involved in washoff are erosion and transport. During a storm, pollutants accumulated on the watershed are exposed to the energy of flow and rainfall, initiating pollutant mobilization. In urban runoff, the mass deficiency on the impervious surface results in relatively high washoff rate at the beginning of the storm. This phenomenon is called “first flush” and will be discussed in a separate section of this chapter.

Lacking theoretical studies, constituent washoff might be described utilizing the erosion and transport theories developed for sediment. Sediment transport by water flow is typically classified into two different modes of discharge: bed load and suspended load discharges. The commencement of particle mobilization is usually estimated by the ratio of the shear velocity of the flow, u^* , to the settling velocity of the particle, w (Graf, 1998). Most prediction models for the bed load discharge are based on the empirical or semi-empirical formulas, most of which are functions of bed shear stress, τ_b . A conventional empirical formula for bed load discharge is Dubois equation:

$$q_b = \Psi \tau_b (\tau_b - \tau_c) \quad (2.1)$$

where q_b is the bed load transport in lb/sec-ft, Ψ is the coefficient for a given bed, τ_b is the bed shear stress ($= \gamma h S$), γ is the specific weight of fluid, h is the flow depth, S is the channel slope, and τ_c is the critical bed shear stress to cause movement of the bed.

Conventional prediction methods for the suspended load discharge involve the shear velocity and boundary conditions, which depend on the concentration of bed load discharge. A theoretical equation (Rouse, 1938; Einstein, 1950) gives the vertical distribution of concentration of suspended solids for 2-D flow as follows:

$$\frac{C_y}{C_a} = \left(\frac{D-y}{y} \frac{a}{D-a} \right)^z \quad (2.2)$$

with
$$z = \frac{w}{\kappa u_*} \quad (2.3)$$

where C_y is the concentration at a distance y above the streambed, C_a is the concentration at a distance a above the streambed, D is the flow depth, w is the fall velocity of the particles, κ is the turbulence constant (Karman constant), and u_*^* is the shear velocity ($= \sqrt{gRS}$, where R = hydraulic radius). Most of the theories on the bed load and suspended load discharges were developed for the non-cohesive sediment, which is larger than 20 μm in diameter.

Cohesive sediment particles, which are less than 20 μm in diameter, are subject to the van der Waals attractive force and the double layer repulsive force. It can be therefore assumed that particles are transported as suspended load rather than as bed load (Deletic,

2001). For the mobilization of cohesive sediment, critical boundary shear stress should be exerted, which is proportional to the plastic yield strength τ . Mehta (1994) suggested the following equation for the erosion rate from consolidated cohesive bed:

$$E = M \frac{\tau_b - \tau_s}{\tau_s} \quad (2.4)$$

where E is the erosion rate, τ_b and τ_s are the bed shear stress and shear strength, respectively, and M is the constant for a given bed.

Zhang et al. (2002) investigated the effects of flow rate, flow depth and slope gradient on the soil detachment rate. According to their experiments using an artificial channel, the detachment rate could be estimated by the power function of flow rate and bed slope.

For overland flow caused by excess rainfall (i.e. Hortonian overland flow) such as stormwater runoff, rainfall energy also influences on pollutant erosion. Gabet and Dunne (2003) described the relationship between the rain power and sediment detachment in the hill slope area using the following equation:

$$\Psi = \alpha R^\beta A(h, d) \quad (2.5)$$

where Ψ is the sediment detachment rate ($\text{g m}^{-2} \text{s}^{-1}$), α and β are empirical constants, $A(h, d)$ is the attenuation function ($0 \sim 1$), R is the rain power (W m^{-2}), h is the flow depth, and d is the raindrop diameter.

2.1.3 First Flush Phenomena

The “first flush” is defined as the emission of a greater fraction of constituent mass or higher concentration in the early part of the runoff volume (Geiger, 1987). The first flush phenomenon is frequently observed in the runoff of small, highly impervious urbanized areas, such as highways and parking lots (Sansalone and Cristina, 2004).

Characterizing the first flush phenomena is important to establish treatment strategies. If a large portion of pollutant mass is contained in the first portion of the runoff, a BMP that is optimized to treat the first portion may be economically advantageous. The first flush phenomenon is strongly related to hydraulic conditions. A number of efforts have been performed to determine the relationship between pollutant washoff behavior and rainfall intensity, flow rate, watershed area or bed slope, using statistical analysis of empirical observations. Unfortunately no clear, general relationships among have been found.

Because no consensual definition of “first flush” has yet been established, different criteria are used according to the researchers as summarized in table 2.2. Among several criteria for occurring of first flush, a criterion proposed by Geiger (1987) is common, which suggests that the occurrence of a first flush when the initial slope of the curve of the normalized cumulative mass emission with respect to the normalized cumulative runoff volume is greater than 45%.

In order to quantify the high initial pollutant load of the first flush, Ma et al. (2002) suggested a concept of mass first flush (MFF) ratio as depicted in Figure 2.1. Figure 2.1

can be created by plotting normalized discharged mass versus normalized runoff volume using the following equation:

$$\frac{y}{x} = \frac{\int_0^{t_i} C(t)Q(t)dt / M}{\int_0^{t_i} Q(t)dt / V} = \frac{\int_0^{t_i} C(t)Q(t)dt / \int_0^{t_i} Q(t)}{M / V} \quad (2.6)$$

where $C(t)$ is pollutant concentration (M/L^3), $Q(t)$ is stormwater flow discharged at time t (L^3/T), M is total pollutant mass (M), V is total flow volume (L^3), and t_i is elapsed time (T). The existence of a mass first flush can be determined if the plotted line lies above the

TABLE 2.2 Quantitative Definitions of First Flush in the Stormwater Runoff from Different Researchers

Quantitative Definition or Criteria for FF	Reference
Initial slope of normalized cumulative mass emission plotted against normalized cumulative runoff volume > 45%	Geiger (1987)
40 ~ 60% of the pollutant load in the initial 25% of the runoff volume	Vorreiter and Hickey (1994)
80% of pollutant load in the first 30% of the runoff volume	Saget et al. (1996)
Maximum gap between normalized cumulative mass emission and corresponding normalized cumulative runoff volume during a storm event	Gupta and Saul (1996)
Generalized quantitative definition of mass first flush using the ratio of mass washoff fraction to the runoff volume fraction (Mass First Flush ratio, MFF)	Ma et al. (2002)
Particle number first flush (PNFF) ratio defining particle first flush, which is an extension of the MFF ratio developed by Ma et al. (2002)	Li et al. (2005a)

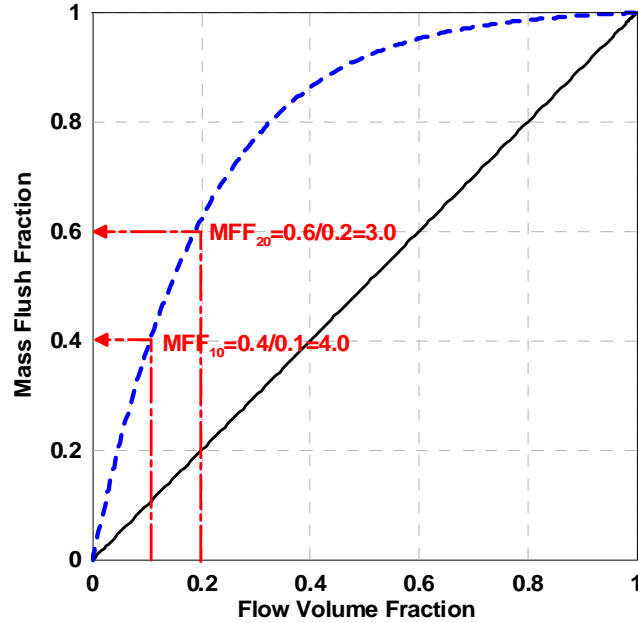


FIGURE 2.1 Definition of mass first flush ratio

straight line indicating the proportional mass delivery according to the amount of runoff volume. The intersection of the a vertical line at a specific normalized volume and the mass line is used to calculate the MFF_n , by dividing the normalized mass at same normalized volume, designated as n , which is expressed as a percentage from 0 to 100%. Therefore, the MFF_{10} and MFF_{20} for the constituent at 10% and 20% of the runoff volume are respectively calculated as 3.0 and 4.0 in the Figure 2.1.

First flush phenomena might or might not be observed depending on meteorological and geometrical characteristics of the watershed. Generally, small size watersheds with high imperviousness tend to show strong first flush (Ma et al., 2002). There have been numerous studies to establish the relationship between first flush phenomena and associated parameters such as watershed types, rainfall characteristics and other factors

(Gupta and Saul, 1996; Charneneau and Barrette, 1998; Deletic and Maksimovic, 1998; Taebi and Droste, 2004; Cristina and Sansalone, 2003a; Lee et al., 2003). Gupta and Saul (1996) conducted correlation studies in the combined sewer system and reported that total suspended solids (TSS) load in the first flush was well correlated with rainfall intensity, storm duration and ADD whereas mean concentration of the first flush was not. Deletic and Maksimovic (1998) performed statistical analysis using monitored data from paved road runoff and concluded that washoff TSS load were merely influenced by ADD as opposed to the conductivity. Taebi and Droste (2004) examined the runoff from an urbanized landuse in Iran and stated that first flush load of total solids (TS) and chemical oxygen demand (COD) were not closely related to the characteristics of rainfall-runoff. Meanwhile, Cristina and Sansalone (2003a) observed the high first flush effect in mass-limited high runoff volume events compared to the flow-limited low runoff volume events. Lee et al. (2003) investigated the first flush of organics, nutrients and iron from four different landuses (i.e. apartments, commercial, single residential and mixed area) and proposed polynomial equations to represent first flush, which were site and event specific.

As shown from the proceeding discussion, no consensus exists for hydrodynamic behavior of pollutant washoff, and therefore no clear methodology for quantifying the first flush exists.

2.2 MODELS FOR STORMWATER RUNOFF

Stormwater model is basically composed of water quantity and water quality models. A water quantity model calculates runoff volume or flow rate resulting from excess rainfall, which is used for the flood control. The pollutant concentration or mass load in the runoff is estimated by a water quality model. Accurate water quantity calculation is prerequisite for the water quality calculation because most water quality models include hydrologic or hydraulic factors as independent variables (Zoppou, 2001).

There exist various kinds of mathematical models for water quantity and water quality from simple empirical models to complex deterministic models. Empirical or regression models are frequently adapted because they are mathematically simple and thus require less calculation efforts. Those models are limited in application because they are valid only for specific sites or events. Development of fast computing technology makes it easier to utilize a complicated deterministic model for the accurate solution of temporal and spatial varying water quantity and quality.

A deterministic stormwater model usually includes several components in the governing equations: rainfall-runoff, pollutant buildup, erosion, transport and sink/source of the pollutants mass such as settling or biodegradation. Complexity of the model depends on the mathematical expressions of those components in the model. Some of those components can be neglected or simplified according to their relative importance.

2.2.1 Water Quantity Models

One of the simplest water quantity models is the *rational formula*, which calculates the runoff volume. However, the simulation of temporal and spatial flow behavior can be performed by deterministic models such as the Saint-Venant system of equations and their simplifications. The Saint-Venant equations are composed of two conservative laws and have been popularly used for the open channel flow problems (Graf, 1998). Shallow water flow can be also described by these equations. One-dimensional form considering uniform rainfall and infiltration are written on a unit width basis as follows (Singh, 1996):

Continuity equation:

$$\frac{\partial h}{\partial t} + \frac{\partial}{\partial x}(uh) = I - f \quad (2.7)$$

Momentum equation:

$$\frac{\partial u}{\partial t} + \frac{\partial}{\partial x}\left(\frac{1}{2}u^2 + gh\right) = g(S_0 - S_f) \quad (2.8)$$

where h is flow depth (L), u is local mean velocity (L/T), I is rainfall intensity (L/T), f is infiltration rate (L/T), g is gravitational acceleration, x is space coordinate in the flow direction (L), t is time (T), S_0 is bed slope, and S_f is frictional slope. It is sometimes more convenient to use the reduced form of above equations (i.e. the kinematic wave and diffusive wave equations) in the simulation of sheet flow over plane surfaces by neglecting local acceleration, convective acceleration or pressure force effects. The kinematic wave equation has been a preferred modeling equation in the calculation of

surface runoff because the calculation is simple and accurate (Tomanovic and Maksimovic, 1996; Deletic, 2001; Singh, 2002a, 2002b; Jaber and Mohtar, 2002; Haque, 2002; Cristina and Sansalone, 2003b). The diffusion wave equation can be applied where the hydraulic diffusivity plays a major role such as a watershed with a very mild slope (Ponce and Klabunde, 1999).

2.2.2 Water Quality Models

As opposed to the water quantity model, the history of water quality models for the stormwater runoff is relatively short. Due to limited knowledge on the involving mechanisms in the pollutant washoff, the majority of the model equations that have been used are based on the empirical or statistical approaches. One of the simplest models (Grottker, 1987) is the exponential equation representing emission rate of pollutants as follows:

$$P_t = P_1 e^{-k_2 V_t} \quad (2.9)$$

where P_t is load remaining on the watershed after time t from the beginning of the runoff event (kg), P_1 is initial load (kg), k_2 is washoff coefficient (mm^{-1}), and V_t is total runoff to time t . The exponential-type equations have been used to approximate greater washoff at the beginning of a storm. Regression models relate water quality parameters with selected factors considered to be important using simple linear, simple linear, semi-log, log-log transformations. These models have been popularly used to estimate event mean concentrations and total load of the pollutant. However, regression models are limited in

use because those models are only site-specifically valid (Zoppou, 2001). Despite of this limitation, empirical and regression models are still popularly used because the calculations are simple.

Several researchers have focused on deterministic models addressing transport and erosion mechanisms of pollutants in the overland flow system (Tomanovic and Maksimovic, 1996; Singh, 2002a, 2002b). A deterministic model requires comparatively larger calculation efforts because spatial and time varying water quantity and quality equations are integrated. Table 2.3 summaries several previous works on the deterministic models for pollutant washoff. Singh (2002a, 2002b) performed simulation for hydrology and pollutant transport over the plane surfaces using hyperbolic equations. He investigated solute discharge patterns for different locations in a watershed, rainfall duration as well as hydraulic conditions. More recently, Deng et al. (2005) simulated first flush of salt in a flume using fractional kinetic theory in the transport equation to consider heavy tail effect in pollutant washoff.

2.2.3 Numerical Solutions for Partial Differential Equations

Finite difference methods (FDMs) have been widely used because this approach is conceptually easier and efficient in geometrically simple problems as opposed to finite element methods (FEMs). Most problems for water resources and mass transport are generally modeled by hyperbolic or parabolic partial differential equations, which can be effectively solved using various numerical schemes including explicit and implicit methods. Explicit schemes require less laborious program codes while implicit schemes

TABLE 2.3 Deterministic Studies for Pollutant Washoff Simulation ^a

Domain	Target Species	Governing equations			References
		Hydraulics	Transport	Sink/Source	
Asphalt surface	Suspended solid	1-D Kinematic wave equation $\frac{\partial h}{\partial t} + \frac{\partial(uh)}{\partial x} = I - f, u = \sqrt{S/n} \cdot h^{2/3}$	Classical 1-D advection dispersion equation	$\frac{\partial M}{\partial t} = -b_1 M E_k (1 - e^{-h_m/h}) + \begin{cases} 0, & \tau_u \leq \tau_c \\ b_2 M (\tau_u - \tau_c)^{1.5}, & \tau_u > \tau_c \end{cases}$	Tomanovic and Maksimovic (1996)
Agricultural Area	Suspended solid Particulate phosphorous	1-D St. Venant equations: $B \frac{\partial H}{\partial t} + \frac{\partial Q}{\partial x} = 0,$ $\frac{\partial Q}{\partial t} + gA \frac{\partial H}{\partial x} + \frac{\partial}{\partial x} (\alpha Qv) + \frac{g Q Q}{C^2 AR} = 0$	Classical 1-D advection dispersion equation	$\frac{dC_{SS}}{dt} = -\frac{w_{sed} C_{SS}}{z} + \begin{cases} 0, & v \leq v_c \\ \frac{\varepsilon(v^2 - v_c^2) C_{EM}}{z}, & v > v_c \end{cases}$ $\frac{dC_{EM}}{dt} = w_{sed} C_{SS} + \begin{cases} 0, & v \leq v_c \\ -\varepsilon(v^2 - v_c^2) C_{EM}, & v > v_c \end{cases}$	Stuck et al. (2001)
Impervious plane	Solute	1-D Kinematic wave equation	Classical 1-D advection dispersion equation	$\frac{\partial w}{\partial t} = -kShw$	Singh (2002a)
Infiltrating plane	Solute	1-D Kinematic wave equation	Classical 1-D advection dispersion equation	$\frac{\partial w}{\partial t} = -kShw$	Singh (2002b)
Grassed Area	Sediment	1-D Kinematic wave equation	$\frac{\partial(hq_s/q)}{\partial t} + \frac{\partial q_s}{\partial x} = D \frac{\partial^2(hq_s/q)}{\partial x^2} - \lambda_s q_s$	$Particle\ Deposition = \lambda_s q_s$	Deletic (2001)
Permeable surface (Soil)	Salt	1-D Kinematic wave equation	$\frac{\partial C}{\partial t} + u \frac{\partial C}{\partial x} = D \frac{\partial^F C}{\partial x^F} + EC_s - \frac{(I-f)}{h} C$	$C_s = C_0 \exp(-\mu t)$	Deng et al. (2005)

^a M -amount of sediments on the surface (g/m^2), τ_u -total shear stress (Pa), τ_c -Shields's critical shear stress (Pa), E_k -kinetic energy of rain drops per unit area [J/m^2s], h_m -penetration depth (m), h -flow depth (m), b_1 and b_2 -coefficients, B -cross-sectional storage width (m), H -water surface elevation (m), x -longitudinal distance (m), t -time (s), Q -flow (m^3/s), g -acceleration due to gravity (m/s^2), A -cross-sectional area (m^2), α -flow non-uniformity correction factor, v -mean velocity over cross-sectional area (m/s), w -mass of pollutant per unit surface area (g/m^2), k -washoff rate constant ($1/m/s$), S -bottom slope, C -constituent concentration (gm^3), D -dispersion coefficient (m^2/s), ε -erosion coefficient (s/m^2), C_{EM} -surface concentration of erodible mass for each event (g/m^2), C_{SS} -volumetric concentration of suspended solids (g/m^3), v_c -critical velocity for erosion (m/s), w_{sed} -sedimentation velocity (m/s), z -channel depth (m), u -velocity of the flow (m/s), I -rainfall intensity (m/s), f -infiltration rate (m/s), C_s -pollutant concentration on the fractal surface (g/m^3), E -transfer coefficient of pollutant, F -fractor, C_0 -initial value for C_s (g/m^3), μ -decay coefficient ($1/s$), q_s -sediment loading rate ($g/m/s$), λ_s -trapping efficiency ($1/m$).

allow larger time step without losing stability of the solution. Table 2.4 shows different FDMs adapted in solving overland flow problem by several researchers.

One of the important aspects in the numerical calculation is convergence of the solution. The convergence condition for a finite difference scheme for hyperbolic equations such as the kinematic wave equation is defined by the well-known Courant-Friedrichs-Lewy (CFL) condition as follows:

$$\frac{\Delta t}{\Delta x} \leq \frac{1}{c} \quad \text{or} \quad C_N = \frac{c\Delta t}{\Delta x} \leq 1 \quad (2.10)$$

where c is celerity (L/T), Δt is time step (T), Δx is grid size and C_N is the Courant number.

TABLE 2.4 FDMs used for the Overland Flow Calculation

Numerical Scheme	Classification	Flow Equation	Reference
Lax-Wendroff	Explicit	Kinematic wave	Singh (2002), Moramarco and Singh (2002), Cristina and Sansalone (2003)
Method of Characteristics	-	Kinematic wave	Henderson et al. (1964)
Preiss-Mann's 4 Point Implicit	Implicit	Kinematic wave	Deletic (2001)
MacCormack	Explicit	Saint-Venant	Fennema and Chaudhry (1986), Fiedler and Ramirez (2000)
Alternating Direction Explicit	Explicit	Diffusion wave	Fennema et al. (1994)

Convergence does not always guaranty accuracy of the solution. Numerical schemes often suffer from unfavorable “Noise”, which means spurious oscillations in space or time, resulting in erroneous solutions. Oscillatory solutions are introduced from inappropriate time step and grid size, sudden change in boundary conditions, initial noise and numerical dispersion (Wood, 1993). In the shallow water problem, oscillation control is exceedingly challenging due to non-linear nature of the governing partial differential equations (Govindaraju et al., 1988).

A smoothing operator is often required to attenuate oscillation in the numerical solution of the non-linear partial differential equations such as those of fluid dynamics (Shapiro, 1975). Fiedler and Ramirez (2000) claimed that additional oscillation control is needed for the overland flow simulation with extreme hydraulic conductivity and spatial variance. Sometimes a damping term such as artificial viscosity is introduced in the governing equation to smooth $2\Delta x$ oscillation (Fennema and Chaudhry, 1990, 1986; Fiedler and Ramirez, 2000).

The method of characteristics (MOC) is oscillation free and thus produces a very accurate solution because the characteristics trace the disturbance trajectories. This scheme, however, needs extra effort to interpolate the solution at the required points because the resulting matrix of grid points is non-uniformly spaced.

2.3 PARTICLE REMOVAL IN STORMWATER RUNOFF

Performance of a stormwater BMP is primarily determined by the particle removal efficiency because a great portion of pollutant mass is associated with particles (Pettersson, 1998). Most BMPs cannot remove soluble pollutants. A widely used particle removal mechanism for stormwater BMPs is gravity settling due its low cost and simplicity of operation and maintenance, as compared to other methods such as filtration (Aldheimer and Bennerstedt, 2003). A settling tank is a common stormwater BMP and uses gravity settling to remove pollutants. Its performance is a function of particle settling velocity, hydrologic and hydraulic conditions (Jacopin et al., 1999, 2001; Persson and Wittgren, 2003; Guo, 2004). There have been several studies to determine the settling profile of the stormwater particles to optimize the design and operation of a settling tank (Aiguier et al., 1996, 1998; Li et al., 2005b). However, majority of the stormwater particles are fine particles (Li et al., 2005a), which are stable in the water column and thus additional efforts to destabilize particles are sometimes required.

2.3.1 Particle Settling in Highway Runoff

A particle's terminal settling velocity depends on its size, shape, density, and is influenced by the liquid characteristics, such as temperature and viscosity. Particle size distribution (PSD) monitored in our three highway sites (see Appendix A) showed that 97% of particles were less than 30 μm in diameter (Li, et al., 2005a), which makes small

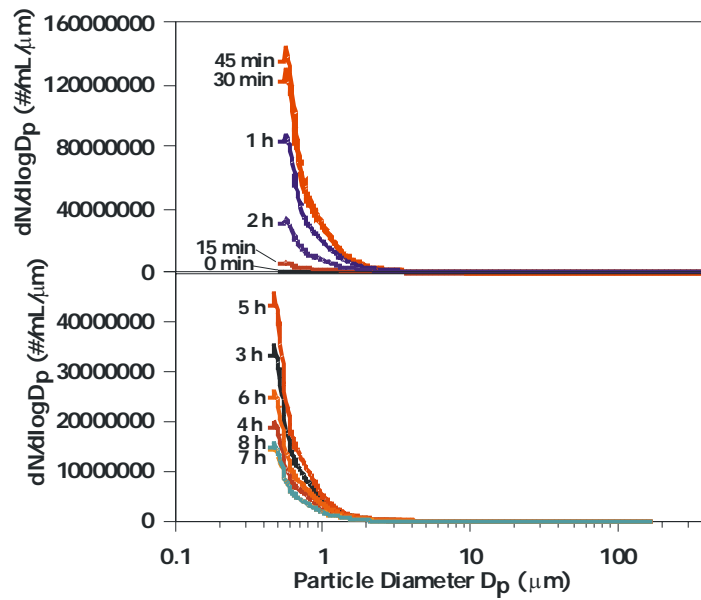
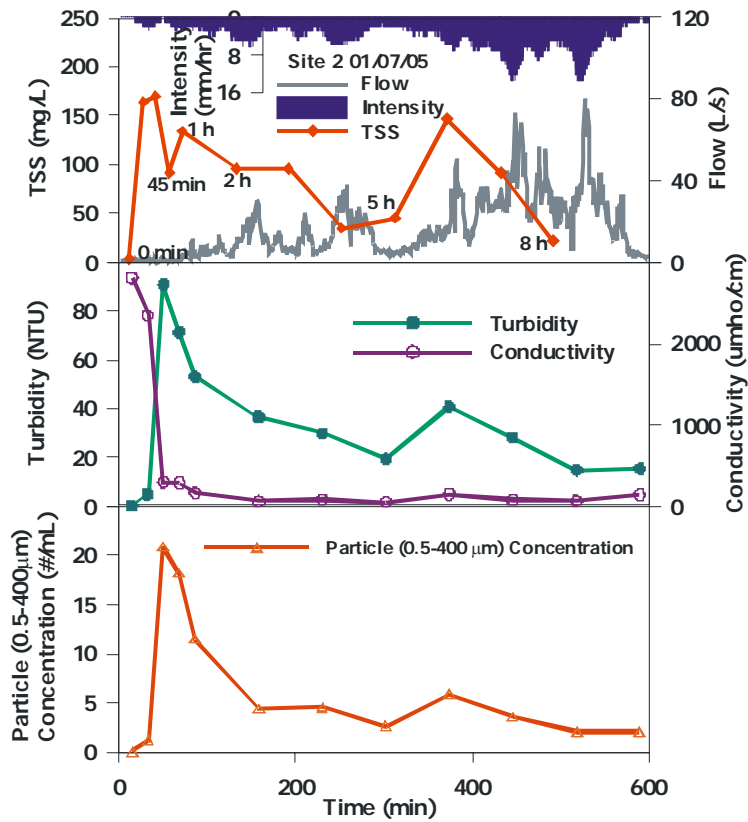


FIGURE 2.2 Hydrograph with TSS, turbidity, conductivity and PSD for site 2, event 1/7/05

particle removal extremely important in BMP design. Figure 2.2 shows the typical PSD of a series of grab samples collected through a storm event. Turbidity, TSS, specific conductivity are also shown, and additional information about measuring techniques and more events are available elsewhere (Li, et al., 2005a).

Li et al. (2005b) performed simulations for the removal efficiencies of the particles and associated pollutants for the entire 2002-2003 wet year using particle settling velocities calculated with Newton's and Stokes' law. Spherical particles corresponding to the measured PSD and having a uniform density 2.6 g/cm^3 were assumed. Continuous flow clarifiers with volumes sized to contain 1.6 mm to 26 mm of rainfall were simulated and were able to remove 75% to 92% of the particles between 2 and 1000 μm , respectively. The clarifier could remove only 3% to 29% of particles between 2 and 10 μm and was able to remove only 13% to 72% of particles between 2 and 25 μm . A series of settling column tests with fresh stormwater samples showed much less removal than predicted, which suggests that settling velocities of smaller particles are much lower than calculated by Newton's and Stokes' law with the stated assumptions. The difference is hypothesized to be caused by a distribution of densities and deviation from spherical shape. These results support anecdotal observations of poor performance of BMPs using sedimentation for removing smaller particles (Stenstrom and Kayhanian, 2005).

It is unfortunate that the smaller particles are not removed since they routinely have higher concentrations of heavy metals and PAHs than the larger particles (Sansalone and Buchberger, 1997; Roger, et al., 1998; German and Svensson, 2002; Morquecho and Pitt, 2003; Lau and Stenstrom, 2004). It is clear that using sedimentation for smaller particle

removal will require some type of particle destabilization in order to increase particle size and improve settling velocity. This is challenging because stormwater BMPs usually operate unattended in many locations. In addition, managing coagulation/flocculation systems will be difficult.

2.3.2 Particle Destabilization

Natural Aggregation of Particles. Particles in the aqueous system naturally aggregate due to the collision between particles resulting from Brownian diffusion, fluid shear and differential settling (McAnally and Mehta, 2000; Perigault et al., 2000; Li et al., 2005a). Microbiological activities such as degradation or polymer production change surface properties to enhance particle aggregation (Milligan and Loring, 1997; Krishnappan et al., 1999). Kranck and Milligan (1991) stated that gravitational settling and particle aggregation play an important role for the deposition of fine sediment in the ocean. However, colloidal particles are generally very stable in the solution by equilibrating between the gravitational force, van der Waals' attractive force and columbic repulsive force. The stability of particles retards their natural aggregation. It is thus necessary to destabilize particles and thereby accelerate particle aggregation rate to separate fine particles from the solution easily.

Particle Destabilization Mechanisms. Destabilization of dispersed particles in aqueous systems can be achieved by several different mechanisms. The formation of deltas in estuaries is a common example of the double layer compression mechanism.

Engineered systems, however, typically use coagulants and coagulant aids for colloid destabilization involving either charge neutralization, bridging, sweep floc, or a combination of those mechanisms. Among the metal ions, Al^{3+} and Fe^{3+} are commonly used in the water and wastewater treatment. Depending on their dosage and water characteristics, Al^{3+} , Fe^{3+} , and their hydrolysis products neutralize the negatively charged particles (stoichiometric destabilization) or precipitate as amorphous forms to enmesh colloidal particles (sweep floc coagulation) (Summ and O'Melia, 1968).

Natural and synthetic polymers have been used as a flocculating aid in water and wastewater treatment systems for many years. Cationic polymers are used to reduce the repulsive force between particles, both by neutralization and bridging mechanisms. Polymers bridge two or more particles by attaching themselves to the available sites on the particles. Anionic polymers are commonly used to flocculate negatively charged particles via bridging. Both bridging and neutralization mechanisms can fail with excessive concentrations of polymer. Restabilization resulting from charge reversal can easily occur.

Coagulation of Stormwater Runoff. In stormwater treatment, coagulation and flocculation have proposed as methods for enhancing colloid destabilization. Polyaluminum chloride (PACl) has frequently been employed because its low acidity is advantageous for weakly buffered stormwater. Heinzmann (1994) has shown that the mixture of PACl and cationic polymer (polyacrilamide) was effective in the filtration system of urban stormwater. Annadurai, et al. (2003) investigated the efficiency of PACl

to treat high turbidity stormwater (1,650 NTU). They stated that a high dose of PACl (>100 mg/L) is preferable to generate large flocs for easy solid-liquid separation (i.e., bridging). The California Department of Transportation (Caltrans) has recently conducted comprehensive coagulation studies using PACl along with polymer and ballast sand as coagulant aids to remove the turbidity and phosphorus in stormwater entering Lake Tahoe (Johnston and Patel, 2004). From the pilot plant tests, Johnston and Patel (2004) reported that the optimum dose of PACl ranged from 75 to 100 mg/L. Trejo-Gaytan et al. (2005) conducted a low dose coagulation study using several classes of coagulants to treat runoff into the Lake Tahoe. They tested new types of coagulants, which are prehydrolyzed aluminum salts with and without silica, sulfate and organic polymers and controlled the doses using inline particle surface charge detector. From their three phase coagulation study, PACl modified with silica or sulfate were most effective to obtain lower than 20 NTU under different conditions of initial water turbidity, temperature, mixing intensity and settling time.

Model Development

3.1 MODEL EQUATIONS

Because a highway is a longitudinally extended structure, highway runoff is simplified as 1-D flow problem in the longitudinal direction. Figure 3.1 conceptualizes the translation of 2-D problem into 1-D problem for the highway runoff simulation. The arrows in the 2-D domain show the vectors indicating real flow direction in the highway. In the simulation, a large arrow in 1-D domain is assumed to represent the velocity vectors in the corresponding section of 2-D domain.

Table 3.1 summaries the model equations and numerical schemes that were used in this study. The kinematic wave equation is used to calculate 1-D flow with a steep bed slope ($\sim 2\%$). For the radial flow simulation, the diffusion wave equation was used to consider the effect of backwater diffusion near the downstream where water mass accumulates. Non-oscillatory solutions for water depth and velocity are essential to

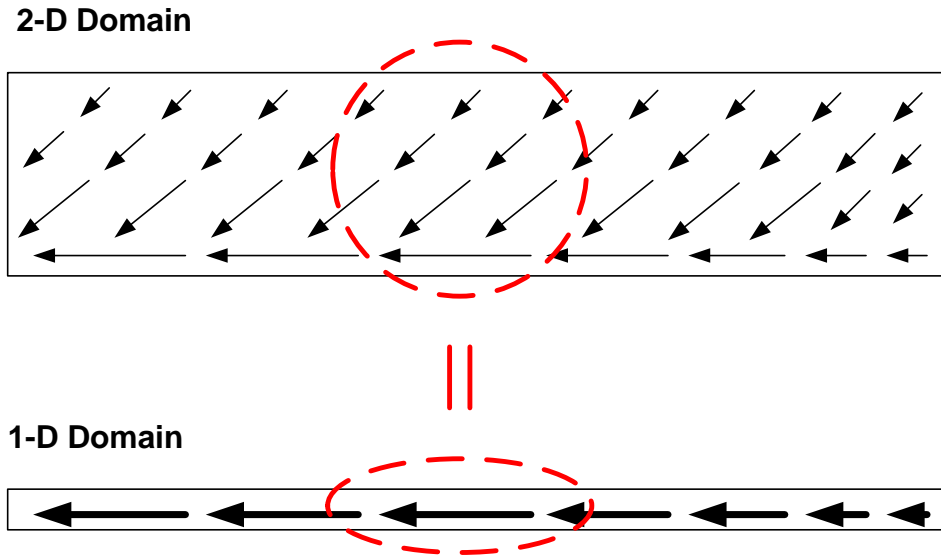


FIGURE 3.1 Concept of 1-D flow model for highway runoff

TABLE 3.1 Model Equations and Numerical Schemes

Models		1-D Flow	Radial Flow
Water quantity (Overland flow model)	Governing equation	Kinematic wave equation	Diffusion wave equation
	Equation type	Hyperbolic	Parabolic
	Numerical scheme	Method of characteristics (MOC)	Characteristics averaging method (CAM)
Water quality (Mass transport model)	Governing equation	Advection-diffusion equation	Advection-diffusion equation
	Equation type	Parabolic	Parabolic
	Numerical scheme	Crank-Nicolson method	Crank-Nicolson method

obtain accurate solutions for the mass transport equation. Therefore, the method of characteristics (MOC) and characteristics averaging method (CAM) were considered appropriate schemes to solve the kinematic wave and diffusion wave equations, which are hyperbolic and near-hyperbolic partial differential equations, respectively.

3.1.1 Kinematic Wave Equation

The kinematic wave equation is derived by simplifying equation (2.8). Neglecting the terms on the left hand side (i.e. the terms of acceleration, gravity and pressure force), Equation (2.8) is reduced to

$$S_f = S_0 \quad (3.1)$$

Manning's equation and equation (3.1) are plugged into equation (2.7), resulting in the kinematic wave equation as follows:

$$\frac{\partial h}{\partial t} + \alpha m h^{m-1} \frac{\partial h}{\partial x} = I - f \quad (3.2)$$

with
$$c = \alpha m h^{m-1} = mu, \quad \alpha = \sqrt{S_0} / n \quad (3.3)$$

where c is celerity (L/T), m is constant (=5/3), n is Manning's roughness coefficient.

The initial and boundary conditions for the overland flow can be reasonably assumed as (Singh, 1996)

$$h(0, t) = 0, \quad 0 \leq t \leq T \quad (3.4)$$

$$h(x, 0) = 0, \quad 0 \leq x \leq L \quad (3.5)$$

where T is storm duration and L is length of overland flow plane.

3.1.2 Diffusion wave equation

The diffusion wave equation is also a simplification of the Saint-Venant equations.

Equation (2.8) is reduced to equation (3.6) by ignoring acceleration and gravity force terms:

$$S_f = S_0 - \frac{\partial h}{\partial x} = -\frac{\partial H}{\partial x} \quad (3.6)$$

where H is water level above a datum (L).

By substituting equation (3.6) and the Manning's equation, Equation (2.7) yields a parabolic equation, called the "diffusion wave equation" as follows:

$$\frac{\partial H}{\partial t} = \frac{\partial}{\partial x} \left(K \frac{\partial H}{\partial x} \right) + I - f \quad (3.7)$$

or

$$\frac{\partial h}{\partial t} = -\frac{5}{3} u \frac{\partial h}{\partial x} + \frac{K}{2} \left(\frac{\partial^2 h}{\partial x^2} \right) + I - f \quad (3.8)$$

with

$$K = \frac{h^{5/3}}{n\sqrt{S_f}} \quad (3.9)$$

Radial flow can be also dealt with as a 1-D flow that includes additional lateral flow resulting from convergence of flow area to the downstream. Considering the tapering width in the flow direction, radial flow equation is derived from equation (3.8) as follows:

$$\frac{\partial h}{\partial t} = -\frac{5}{3}u \frac{\partial h}{\partial x} + \frac{K}{2} \left(\frac{\partial^2 h}{\partial x^2} \right) + \frac{hu}{L-x} + I - f \quad (3.10)$$

3.1.3 Infiltration

Although paved area such as highway and parking lots are classified as “impervious” landuses, infiltration, albeit small, inevitably occurs. In this study, 10-cm-thick asphalt pavement is assumed to approximate the infiltration through the bed surface.

Introducing Darcy’s law of permeability, infiltration rate can be expressed as

$$f = -K_p \left(\frac{\partial h}{\partial z} \right) = -K_p \left(\frac{h + T_p - p_p}{T_p} \right) = -K_p \left(\frac{h - p_p}{T_p} \right) - K_p \quad (3.11)$$

where K_p is hydraulic conductivity of the pavement (L/T), z is distance in the vertical direction (L), T_p is thickness of the pavement layer (L), p_p is pressure head under the pavement layer (L). Hydraulic conductivity of asphalt pavement has been reported in the range of 10^{-5} to 10^{-3} cm/sec (Allen, 2003; Bowders et al., 2003). By assuming the pavement is asphalt supported by well draining materials such as gravel, the pressure head under the pavement layer (p_p) becomes zero and equation (3.11) is reduced to a linear function of water flow depth (h) as

$$f = -\frac{K_A}{T_A} h - K_A = (10^{-6} \sim 10^{-4})h - (10^{-5} \sim 10^{-3}) \quad (3.12)$$

where the unit of the infiltration rate is [cm/sec].

3.1.4 Pollutant Transport

The conventional advection-dispersion equation (ADE) is used for the mass pollutant transport calculation. Ignoring mass transfer through infiltration, the ADE is expressed as

$$\frac{\partial m_w}{\partial t} = \frac{\partial}{\partial x} \left(D \frac{\partial m_w}{\partial x} \right) - \frac{\partial}{\partial x} (u \cdot m_w) - E \quad (3.13)$$

where m_w is pollutant mass in the water of the unit area (M/L^2) and D is dispersion coefficient (L^2/T) and E is pollutant erosion rate from the bed surface ($M/L^2/T$).

The dispersion coefficient can be calculated using the equation developed for the open channel flow (Elder, 1956) as follows:

$$D = 6.0hu^*, \quad u^* = \sqrt{ghS_0} \quad (3.14)$$

where u^* is friction velocity (L/T).

3.1.5 Pollutant Erosion from a Plane Surface

Pollutant erosion rate is generally assumed as a first order reaction in terms of mass available on the bed surface (Singh, 1996; Tomanovic and Maksimovic, 1996). The erosion coefficient of solutes or cohesive particles is typically related to the bed shear stress, which is reasonably correlated with mean flow velocity (Chien and Wan, 1999). Therefore, the erosion equation can be basically formulated as

$$E = \frac{dm_b}{dt} = -\varepsilon u^2 m_b \quad (3.15)$$

where m_b is mass available on the bed surface (M/L^2) and ε is erosion coefficient (T/L^2). However, equation (3.15) can not properly reflect polluto-graphs obtained from the monitoring data. Figure 3.2 displays an example of polluto-graph showing typical washoff behavior of COD, DOC and Oil and Grease. At the beginning of a storm, a pollutant is discharged with a considerably high concentration (phase I), declining to a low level in a short time followed by a prolonged residual concentration (phase II) to the storm end. This washoff behavior will be defined as “two-phase washoff” in this study.

Two-phase washoff was observed in the washoff of most of the measured constituents except suspended solids (SS). To model this phenomenon, two pollutant sources having different erosion rates were introduced: the short-term source and long-term source. The short-term source represents pollutant mass accumulated during antecedent dry period before a storm. Pollutants from the short-term source are easily detached from the surface under even small flow energy because they are on the outmost layer of the pollutant mass. In contrast, pollutants from the long-term source are not directly exposed to the flow shear or protected by the bed roughness; as a result, through the repeated storm events, survived pollutant is solidified on the surface and acts as a permanent pollutant source in the impervious watershed. Considering the terms for two different pollutant sources, equation (3.15) can be modified as follows:

$$E = \frac{dm_{b,t}}{dt} = \frac{dm_{b,s}}{dt} + \frac{dm_{b,l}}{dt} = -\varepsilon_s u^2 m_{b,s} - \varepsilon_l u^2 m_{b,l} \quad (3.16)$$

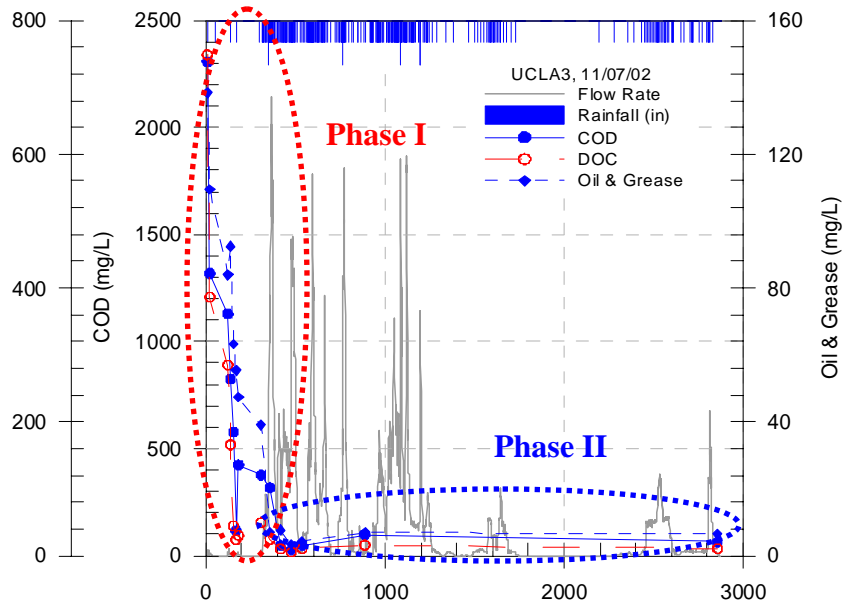


FIGURE 3.2 Two-phase washoff of the pollutants

where $m_{b,t}$ is total pollutant mass, $m_{b,s}$ is pollutant mass from the short-term source, $m_{b,l}$ is pollutant mass from the long-term source and $\varepsilon_s, \varepsilon_l$ are constants. The following relationships are valid if $m_{b,l}$ is large and ε_l is assumed to be negligibly small:

$$\frac{dm_{b,l}}{dt} \approx 0, \quad \varepsilon_l m_{b,l} = \varepsilon_l' \quad (3.17)$$

where ε_l' is constant.

By plugging equation (3.17) into equation (3.16), the erosion equation can be simplified as

$$E = \frac{dm_{b,t}}{dt} = \frac{dm_{b,s}}{dt} = -\varepsilon_s u^2 m_{b,s} - \varepsilon_l' u^2 \quad (3.18)$$

Now, ε_s and ε_l' are defined as erosion coefficients of pollutant mass from the short-term source and long-term source, respectively.

3.2 NUMERICAL SOLUTIONS

Model equations were calculated using FDMs as summarized in Table 3.1. The kinematic wave equation was solved by the method of characteristics (MOC) to avoid oscillatory solutions. Due to the near hyperbolic nature of the diffusion wave equation of this study, characteristics averaging method (CAM), was used for the radial flow problem. Mass transport equation is calculated using Crank-Nicolson method (C-N), which is a common method for parabolic differential equations.

3.2.1 Method of Characteristics for 1-D Flow

In the kinematic wave equation, the equation of characteristic curve can be obtained by calculating the determinant of the coefficient matrix as follows:

$$\frac{\partial h}{\partial t} = c = \frac{5}{3}\alpha h^{2/3} \quad (3.19)$$

Figure 3.3 illustrates the calculation procedure of node values using MOC. The destination of characteristic curve to the next time level at each node is determined explicitly using equation (3.19). For example, knowing the position (x_1, t_1) and value (h_1) of point X_1 , the position (x_2, t_2) and value (h_2) of point X_2 can be calculated as follows:

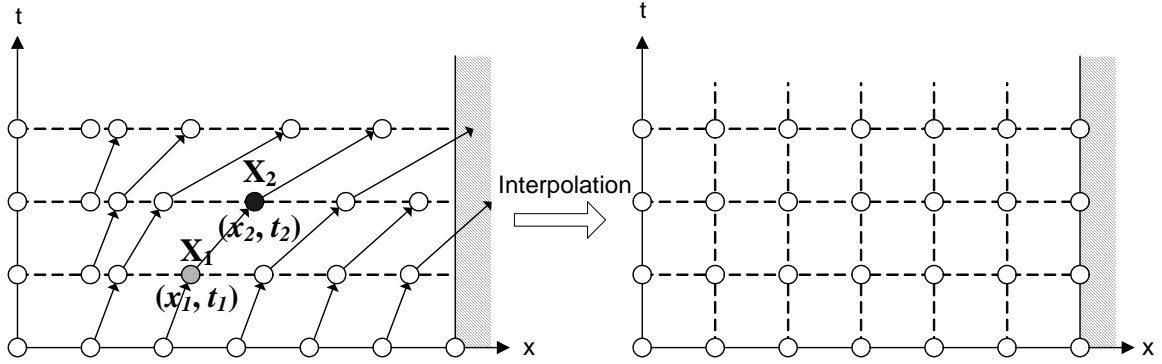


FIGURE 3.3 Procedure of the node value calculation in MOC

$$(x_2, t_2) = (x_1 + \Delta x_1, t_1 + \Delta t) = \left(x_1 + \frac{5}{3} \alpha h_1^{2/3} \Delta t, t_1 + \Delta t\right) \quad (3.20)$$

$$h_2 = h_1 + I(t_1) \cdot \Delta t \quad (3.21)$$

where $I(t_1)$ is rainfall intensity at $t = t_1$.

Starting with an evenly distributed node set at $t = 0$, the distance between nodes are disturbed as the calculation continues. The nodal values of the resulting non-homogeneous node set should finally be interpolated, obtaining a homogeneous node set.

3.2.2 Characteristics Averaging Method for Radial Flow

CAM is a modification of C-N to solve the near-hyperbolic equation of 1-D problems (Stenstrom, 1996). This method uses six node values to diagonally average the derivative terms as shown in Figure 3.4.

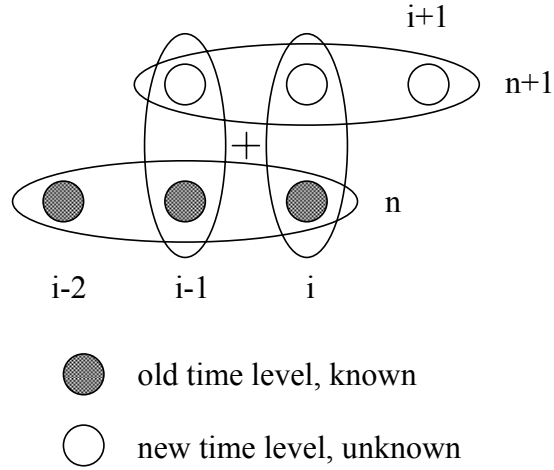


FIGURE 3.4 Characteristics averaging – Interior points (Stenstrom, 1996)

The diffusion wave equation can be formulated as follows:

$$\begin{aligned}
 & \left(\frac{1}{\Delta t} - \frac{K}{4\Delta x^2} - \frac{5u}{6\Delta x} \right) h_{i-1}^{n+1} & & \left(\frac{1}{2\Delta t} + \frac{K}{4\Delta x^2} - \frac{5u}{6\Delta x} \right) h_i^n \\
 + & \left(\frac{1}{2\Delta t} + \frac{K}{2\Delta x^2} + \frac{5u}{6\Delta x} \right) h_i^{n+1} & = & + \left(\frac{1}{2\Delta t} - \frac{K}{2\Delta x^2} + \frac{5u}{6\Delta x} \right) h_{i-1}^n \\
 - & \left(\frac{K}{4\Delta x^2} \right) h_{i-1}^{n+1} & & + \left(\frac{K}{4\Delta x^2} \right) h_{i-2}^n \\
 & & & + \frac{h_{i-1/2}^n u_{i-1/2}^n}{L - x_{i-1/2}} + \frac{I_{i-1/2}^n - f_{i-1/2}^n}{2}
 \end{aligned} \tag{3.22}$$

where i is node number and n is time step. In equation (3.22), K , u , I and f are assumed constants within a time step and determined at time n . This assumption is valid for the implicit methods (Wasantha Lal, 1998). A set of equations composed of equation (3.22) for each node can be constructed as a tri-diagonal matrix, which is solved using the Thomas algorithm (Von Rosenberg, 1969).

3.2.3 Stability and Convergence in Numerical Solutions

It is difficult to establish rigorous stability criteria for the grid size (Δx) and time step (Δt) because the overland flow equations are nonlinear (Fieldeler and Ramirez, 2000). MOC and implicit schemes are used for the stability of numerical solution in this study.

However, numerical sensitivity tests to determine appropriate Δx and Δt were necessary to insure that an accurate solution was obtained.

Solutions for 1-D Flow. The model domain size and input conditions used for the numerical sensitivity tests are shown bellow:

- Rainfall intensity = 6 mm/hr
- Rainfall duration = 1 hr
- Pavement hydraulic conductivity (K_p) = 0 cm/sec
- Slope = 0.02
- Watershed length (WL) = 244 m

Different values of Δt were evaluated for a given initial Δx (Δx_0) in MOC (Δx changes as MOC procedure proceeds). Figure 3.5 (a) and (b) show the outflow as a function of time calculated using six different values of Δt with 1 m and 2 m of Δx_0 , respectively. As Δt decreases, the solution converges to be an accurate solution. Large Δt produces overestimated solution, resulting from the error in the calculated position due to the linear assumption for the non-linear characteristics curve. Figure 3.6 shows the water

depth profile along the distance at $t = 70$ min using different values of Δt for a given Δx_0 . In the water depth profile shown in Figure 3.6, a sudden change in water depth indicates the wave propagation. Smaller Δt decreases the height of wave that moves along the distance during the Δt , providing better resolution in the water depth profile. From the results in Figure 3.5 and 3.6, 1/8 min was chosen for Δt to achieve sufficiently high accuracy in the solutions.

Effect of grid size was also tested. Figure 3.7 is the outflow profile over time using different values of Δx_0 at $\Delta t = 1/8$ min and Figure 3.8 is the water depth profile along the distance at $t = 70$ min under the same conditions for Δx_0 and Δt . According to those figures, different values of Δx_0 from 1 to 4 m make little difference in the solution of MOC.

The numerical solutions from C-N were also investigated to determine an appropriate grid size for the mass calculation in the 1-D flow model. Figure 3.9 is the pollutant concentration in the outflow with respect to time using different Δx from 1 to 6.1 m at $\Delta t = 1/8$ and Figure 3.10 is the profile of mass in the water along the distance using the same conditions for Δx and Δt . As shown in these figures, different grid sizes within the tested range make little change in calculated concentration of the outflow although 2 m or larger Δx causes slight oscillation in the spatial mass profile for a given time.

According to the numerical tests performed above, smaller Δx and Δt produce more accurate solutions for both MOC and C-N. Due to small grid size and time step, however, the computing time might be prohibitively long. In this study, the values of $\Delta x = 1$ m and $\Delta t = 1/8$ min were considered satisfactory. Occasionally, Δx larger than 1 m was also

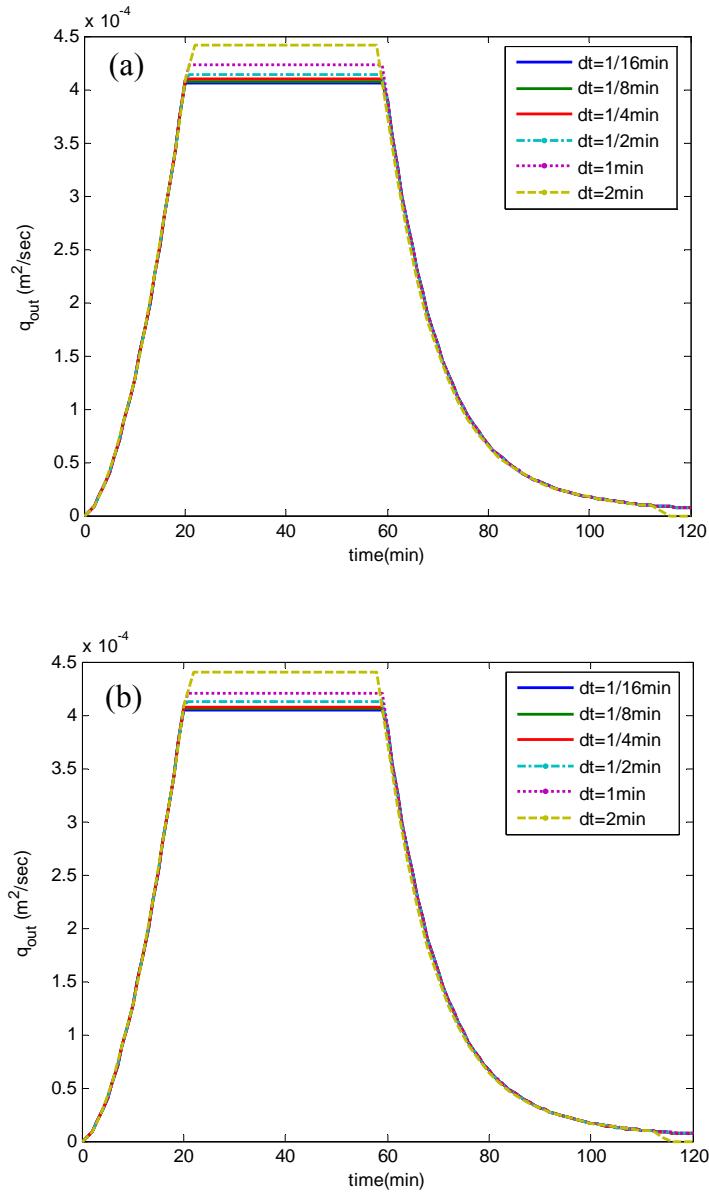


FIGURE 3.5 Calculated outflow using different values of Δt with different Δx_0 : (a) $\Delta x_0 = 1$ m; (b) $\Delta x_0 = 2$ m

used to reduce computing time without losing accuracy of the solution for the mass emission when the simulated watershed was longer than 1,000 m.

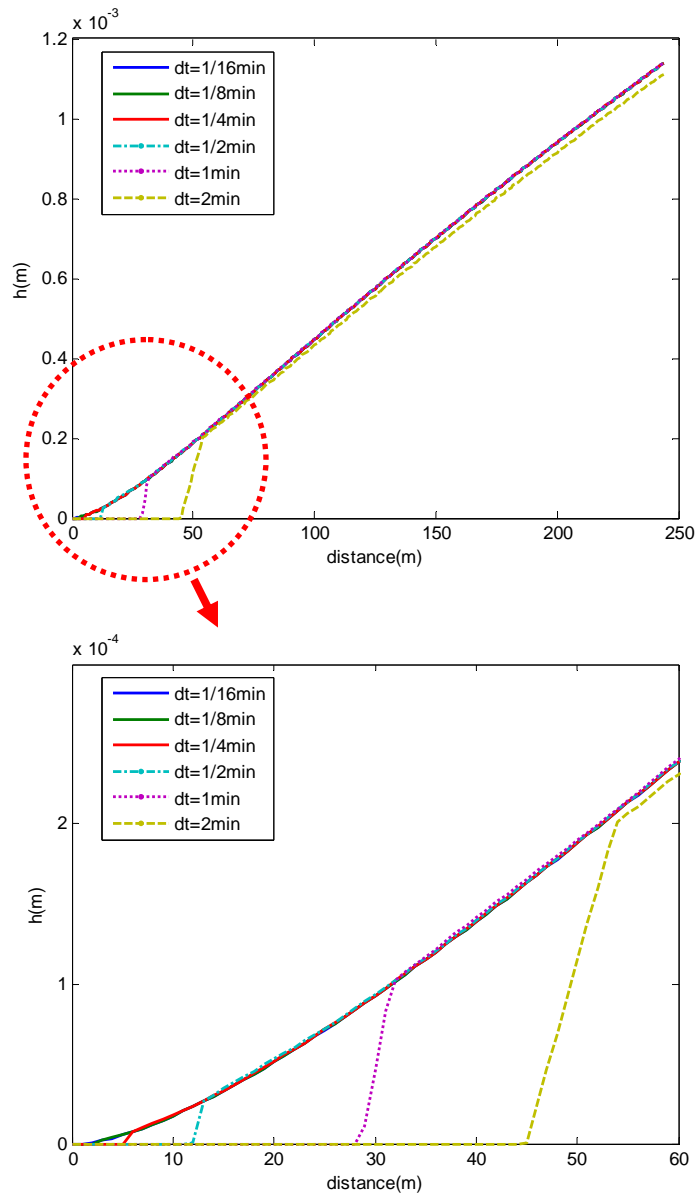


FIGURE 3.6 Water depth profile at $t = 70$ min using different values of Δt with $\Delta x_0 = 1$ m

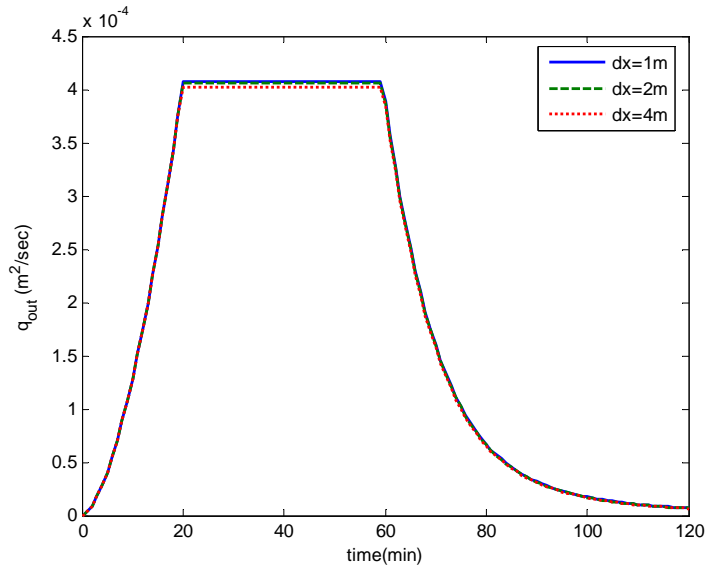


FIGURE 3.7 Calculated outflow using different values of Δx_0 with $\Delta t = 1/8$ min

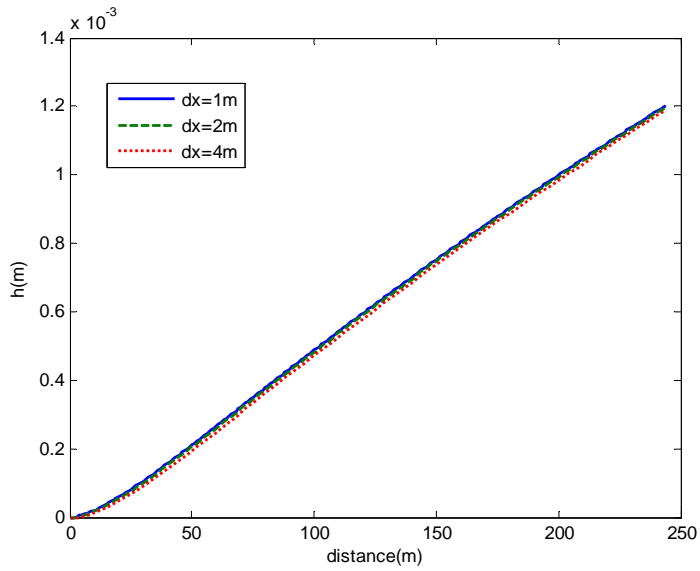


FIGURE 3.8 Water depth profile at $t = 70$ min using different values of Δx_0 with $\Delta t = 1/8$ min

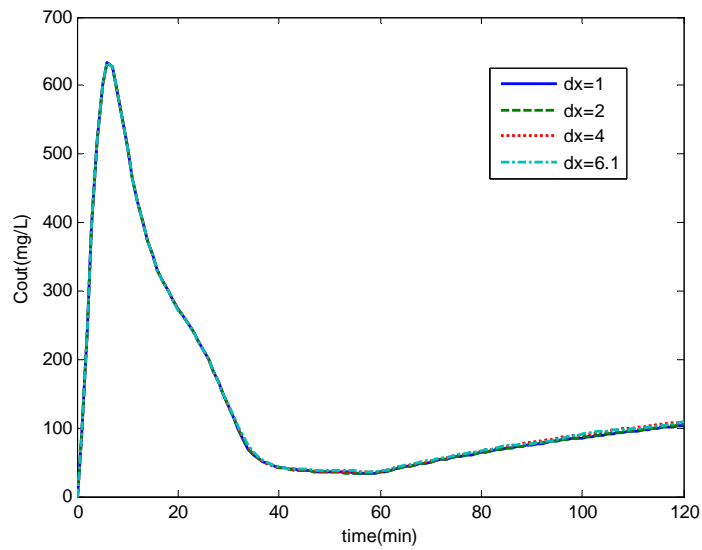


FIGURE 3.9 Outflow concentration profiles calculated for the same storm event using different values of Δx with $\Delta t = 1/8$ min

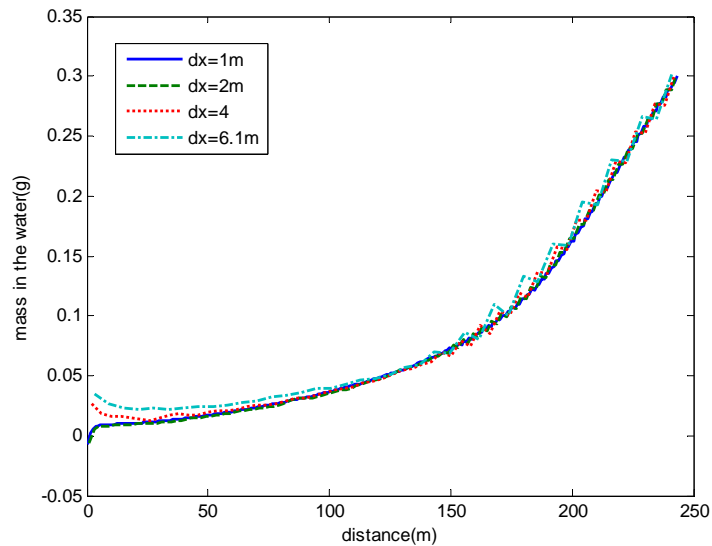


FIGURE 3.10 Mass profiles along the distance at $t = 30$ min calculated for the same storm event using different values of Δx with $\Delta t = 1/8$ min

Solutions for Radial Flow. Using the same inputs for rainfall, slope and pavement hydraulic conductivity with those of the numerical tests for 1-D flow, four different watershed dimensions were tested as follows:

- WL = 50 m, $r_o = 1$ m
- WL = 50 m, $r_o = 5$ m
- WL = 100 m, $r_o = 1$ m
- WL = 100 m, $r_o = 5$ m

where WL is length of converging-type watershed and r_o is the inlet radius. Tested ranges for Δx and Δt are 0.05 ~ 0.5 m and 1 ~ 1/32 min, respectively. By investigating the numerical solutions from the tests, following criteria were experimentally obtained.

- CAM
 - 1/8 min or smaller Δt is required to obtain non-oscillatory solution
 - Δx should be less than 1/10 ~ 1/20 of r_o for the accurate outflow calculation
- C-N
 - 1/8 min or smaller Δt is required to obtain accurate and non-oscillatory solution
 - Δx were to be less than 0.5 m to avoid $2\Delta x$ oscillation

Allowable size of Δx proportionally decreases as the inlet dimension decreases; as a result, extremely long computing time would be required for the solution of a watershed that has large WL and small r_o . In this case, the variable grid size might be useful. That is, the model domain can be discretized finer in the downstream domain than in the upstream domain. However, homogeneous grid sizes were used in this study because the

simulated watershed lengths were sufficiently short (1 ~200 m). The details results of the numerical tests can be found in Appendix B.

3.3 PARAMETER ESTIMATION

The model parameters were calibrated using measured runoff and pollutant concentration data obtained from selected storm events in site 3 (7-203) during 2000~2003 (see Appendix A). 22 storm events were used for the water quantity calculation and 12 storm events among them were selected for the water quality parameter calibration. The monitoring data used for these calibrations were selected based on the data availability for the constituent concentrations. Hydrologic characteristics of 12 storm events for the water quality parameter calibration are summarized in Table 3.2.

The calibrated model parameters were the initial value of $m_{b,s}$ ($m_{b,s}^0$), ε_s and ε_l' . A non-linear least-squares solver (i.e. “lscurvefit”) in the MATLAB toolbox was used to minimize equation (3.23) as the objective function.

$$\sum_i (C_{i,cal} - C_{i,obs})^2 \quad (3.23)$$

where $C_{i,cal}$ and $C_{i,obs}$ are the calculated and observed concentrations for i th grab sample, respectively.

TABLE 3.2 Summary of Storm Events Used for the Estimation of Water Quality Parameters

Date	Total Rainfall (mm)	Storm Duration (hr)	Antecedent Dry Days (Days)	Antecedent Rain (mm)	Average Rainfall Intensity (mm/hr)
1/10/2001	127.0	14.6	2.0	3.8	8.70
2/19/2001	7.1	6.9	5.3	128.8	1.03
2/24/2001	14.5	14.2	1.0	2.0	1.02
3/4/2001	11.9	3.7	4.0	10.7	3.22
11/24/2001	29.7	4.6	11.6	7.4	6.46
12/20/2001	12.2	12.7	6.3	2.0	0.96
1/27/2002	24.6	8.6	27.1	16.3	2.86
2/17/2002	7.4	2.0	20.3	24.6	3.70
3/17/2002	10.4	1.4	10.7	4.6	7.43
12/19/2002	32.5	10.4	3.1	40.6	3.22
2/11/2003	20.1	15.6	44.1	9.7	1.29
3/15/2003	123.2	21.7	11.7	1.5	5.68

Methodology for Highway Runoff Coagulation/Flocculation

4.1 PREPARATION OF RUNOFF SAMPLE

Multiple composite samples were collected during the first hour of runoff from site 2 (see Appendix A for site details) during the 2004-2005 storm season. One-hour composites were selected because this time is generally equal to the time of the first flush. Samples were returned to the laboratory within 1 hour and a series of jar tests were performed using different coagulants and mixing strategies. Table 4.1 shows a brief summary showing the range of sample characteristics.

TABLE 4.1 Characteristics of 1 hr Composite Samples from Site 2

Parameter	Range of Untreated Composite Samples
pH	6.3 ~ 7.1
Temp (°C)	13.2 ~ 19.8
Turbidity (NTU)	51 ~ 197
EC (μS)	141 ~ 1,014
ZP (mV)	-46.54 ~ -26.54

4.2 MIXING TESTS

Natural aggregation of the particles was investigated using runoff sample. Two 4 L bottles of runoff sample were prepared and labeled “no mixing” and “mixing” respectively. The bottle labeled “no mixing” was kept quiescent and the other labeled “mixing” was stirred by a magnetic bar exerting collision between particles to accelerate aggregation. The stirring speed of the magnetic bar was set to be as low as possible in order to minimize the breakup the particle flocs. The observation was performed for 385 hours in the normal temperature (20 °C). Samples were taken from each bottle (mixing and no mixing) and TSS, TDS and PSD were analyzed at 0, 24, 40.8, 76, 96, 240 and 385 hr, respectively.

4.3 PROTOCOLS FOR JAR TESTS

The jar tests were divided into three different experimental regimes: low dose coagulation, sweep floc coagulation and flocculation using organic polymers.

In the low dose coagulation, relatively small doses of alum or ferric chloride were applied and then slowly mixed for 4 to 8 hours. These procedures were intended to investigate the effect of metal ions on neutralizing and aggregating negatively charged particles in the water. The second regime used higher doses to produce sweep floc coagulation. The high alum or ferric chloride dosage formed a sweep floc enmeshing the colloidal particles. Optimum dose for each coagulant was estimated based on turbidity

removal. pHs were always adjusted to 7 both in low dose and sweep floc coagulation tests. Finally, a more extensive series of flocculation tests were performed using cationic organic polymers. Polydiallyldimethylammonium chlorides (polyDADMACs) with different molecular weights (Table 4.2) were used. Long periods of slow mixing were provided after 1 minute of rapid mixing to allow sufficient contact time for particle aggregation. The general procedures of each coagulation/flocculation test are shown in Table 4.2.

TABLE 4.2 Protocols for the Coagulation / Flocculation Tests

Experimental Regime	Rapid Mixing	Slow Mixing	Settling	Coagulant	Remark
Low dose coagulation	1min 100 rpm	4~8 hr 5~10 rpm	16~20 hr	Alum Ferric Chloride	pH adjusted to 7
Sweep floc coagulation	1min 100 rpm	10 min 5~10 rpm	40 min	Alum Ferric Chloride	pH adjusted to 7
Flocculation with polymer	1min 100 rpm	4~8 hr 5~10 rpm	16~20 hr	PolyDADMAC HMW: 400,000-500,000 MMW: 200,000-350,000 LMW: 100,000-200,000	

4.4 WATER QUALITY MEASUREMENTS

Turbidity, zeta potential (ZP) and particle size distribution (PSD) were the major parameters measured in the tests. Particle ZP was measured with ZetaPlus (Brookhaven Instruments Corp., Holtsville, New York). Water samples were diluted with de-ionized (DI) water before measured when they contained too high turbidity for measurement. Dilution with DI water was compared with samples diluted with filtered stormwater using 0.1 μ m filter and were not significantly different, showing that pre-dilution with DI water does not significantly alter the measured ZP of the particles.

PSD was measured with AccuSizer 780 Optical Particle Sizer module (Nicomp Particle Sizing Systems, Santa Barbra, California). The light scattering/extinction sensor attached on the AccuSizer can measure the particle number in the solution in different size range from 0.5 μ m to 400 μ m. Detail procedures for the PSD measurement are described in [Li et al. \(2005a\)](#).

First Flush Simulation

5.1 PARAMETER ESTIMATION IN 1-D HIGHWAY RUNOFF MODEL

5.1.1 Flow Calculation

The modeled highway site (site 3) was selected for modeling and considered as a 1-D catchment with 178 m in length. The measured rainfall data were used as the input rainfall and were assumed homogeneous along the distance. Flow was calculated on the basis of unit width and then multiplied by the site width (21.9 m) to be compared with the measured flow data. A value of 0.11 was used for Manning's roughness coefficient (n) assuming that the pavement surface is made of smooth asphalt or concrete.

It is necessary to estimate a representative hydraulic conductivity of the pavement (K_p). Three different values of K_p (i.e. 5×10^{-4} , 10^{-5} , and 2×10^{-5} cm/sec) were evaluated using 22 storm events data. Figure 5.1 shows the calculated and measured runoff volumes with values of R^2 for different K_p . As shown in the figure, the flow model predicts runoff

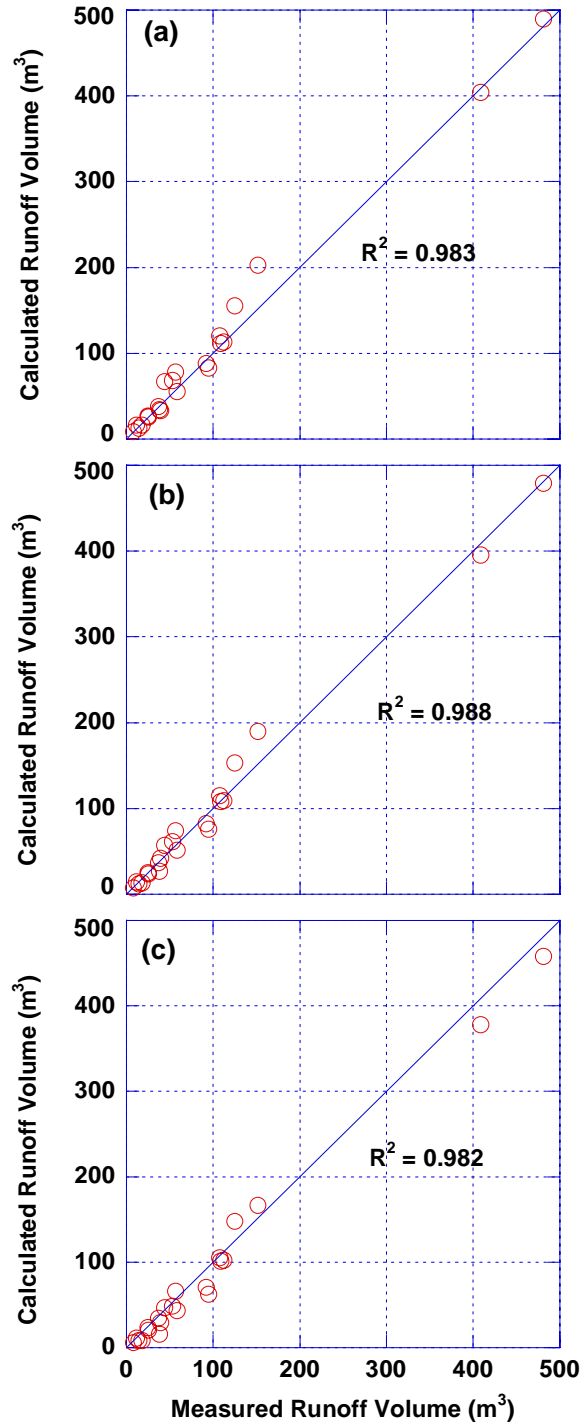


FIGURE 5.1 Measured and simulated runoff volumes with different values of pavement hydraulic conductivity: (a) 5×10^{-6} cm/sec; (b) 10^{-5} cm/sec; (c) 2×10^{-5} cm/sec

volume very well with R^2 larger than 0.980 and 10^{-5} cm/sec was the best value of K_p ($R^2 = 0.989$). Figure 5.2 compares the calculated and measured peak flow rates using the same plotting format with Figure 5.1. As opposed to the runoff volume calculation, calculated peak flows results were more scattered when compared to the measured peak flows. Despite this scattered correlation, Figure 5.2 suggested that peak flow can reasonably be simulated in the evaluated range of K_p ($5 \times 10^{-4} \sim 2 \times 10^{-5}$ cm/sec) and R^2 ranged from 0.437 to 0.440. Considering the results in Figure 5.1 and 5.2, 10^{-5} cm/sec was chosen as the best site-representative value of K_p .

Figure 5.3 shows the measured and calculated runoff coefficients with respect to the total rainfall volume at $K_p = 10^{-5}$ cm/sec. Both the measured and calculated runoff coefficients ranged from 0.60 ~ 0.96 and generally increased as the total rainfall increased. This demonstrates that the site infiltration can be reasonably modeled by Darcy's permeability theory.

Figure 5.4 contains the hydrographs for three different storm events. As can be seen, the 1-D runoff model can closely simulate the measured flow in peak flow rate, peak flow time and hydrodynamic flow patterns. More hydrographs can be found in Appendix C.

Based on the flow simulations described above, the parameters for the flow calculation were determined and summarized in Table 5.1. These parameters were used in the subsequent mass transport calculation.

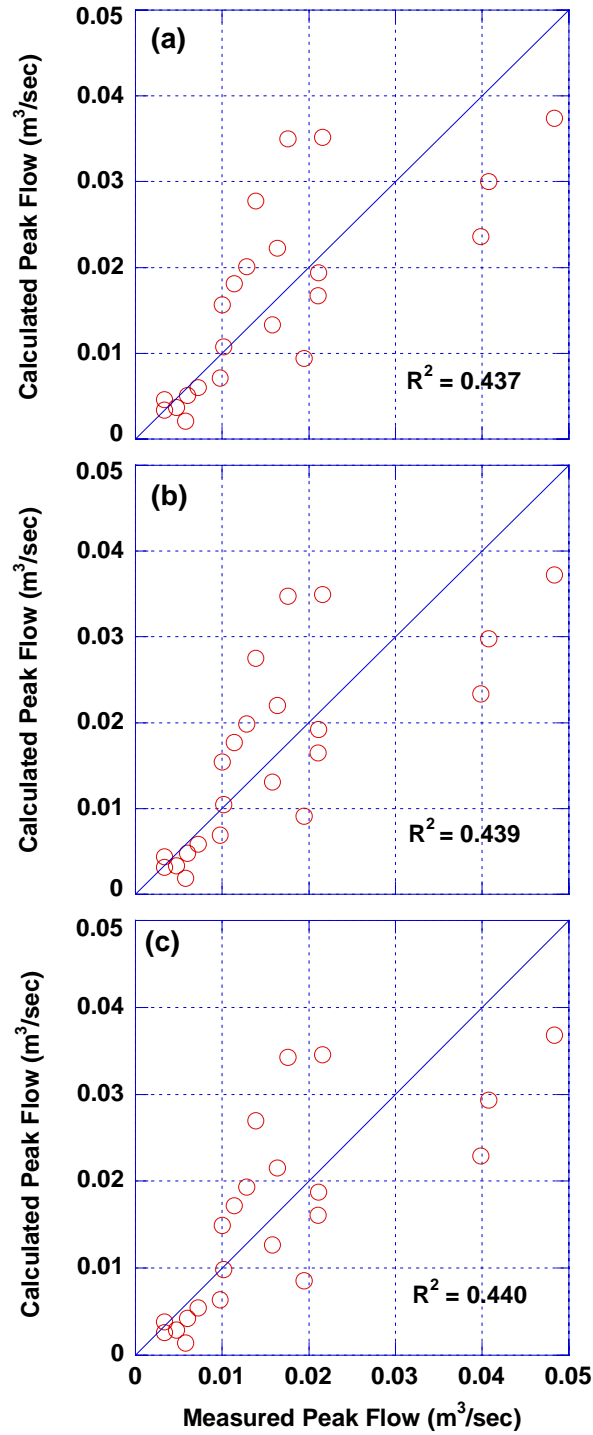


FIGURE 5.2 Measured and simulated peak flows with different values of pavement hydraulic conductivity: (a) 5×10^{-6} cm/sec; (b) 10^{-5} cm/sec; (c) 2×10^{-5} cm/sec

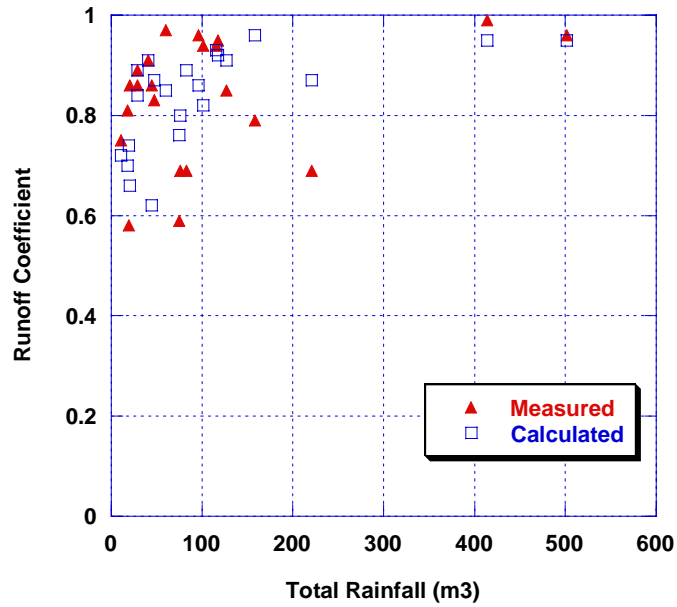
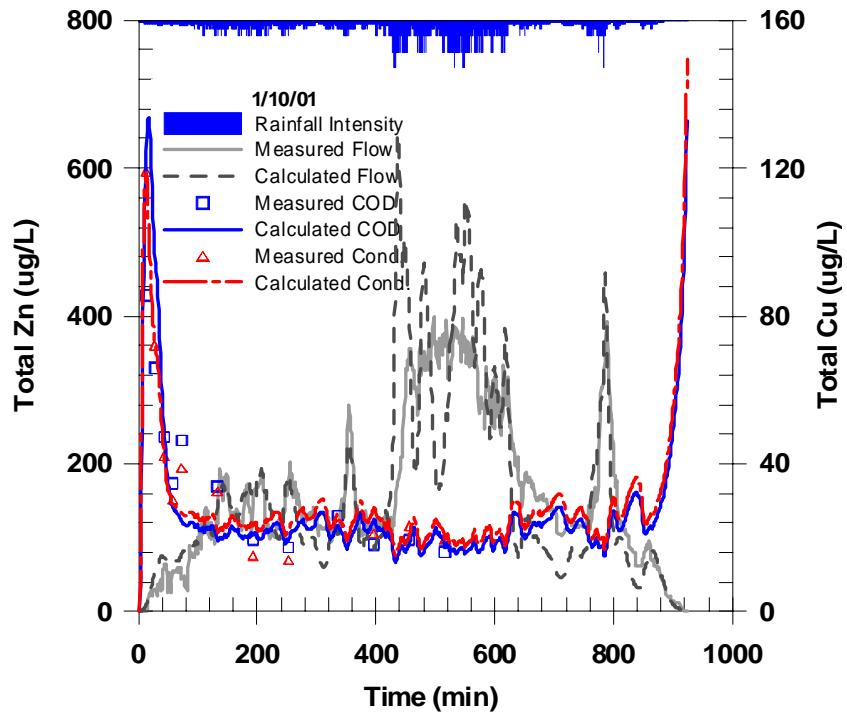
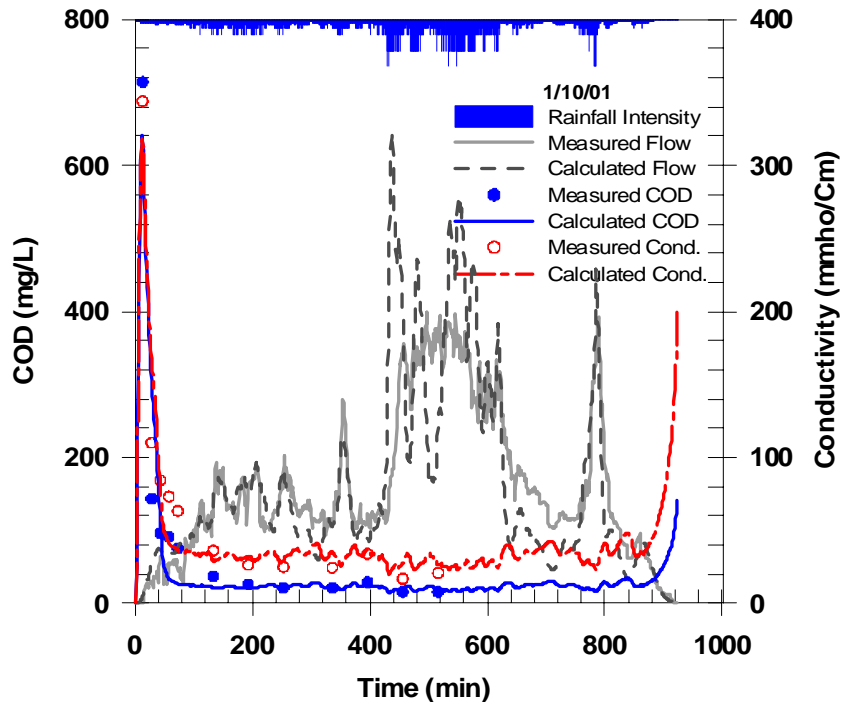


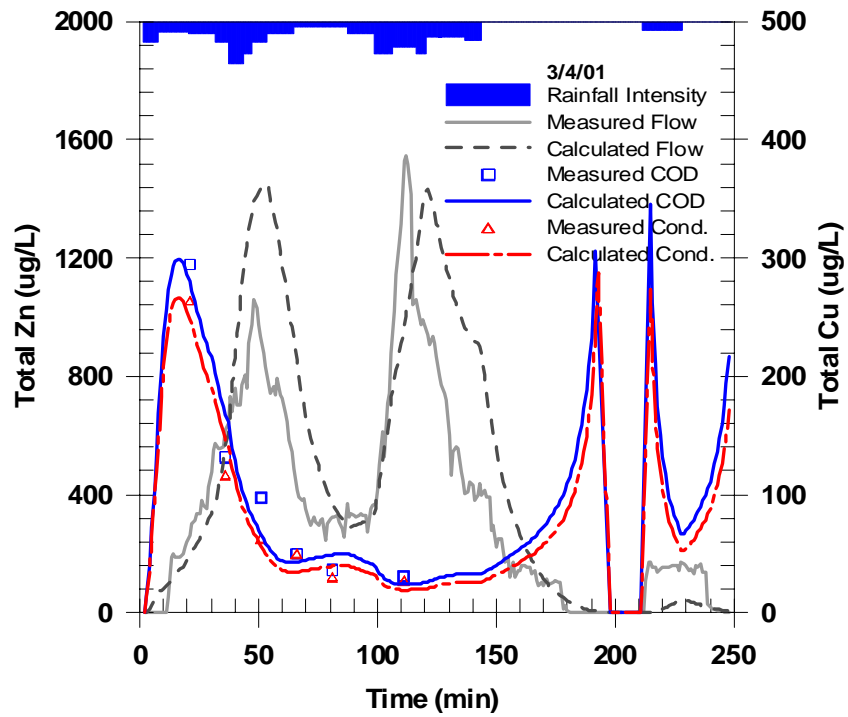
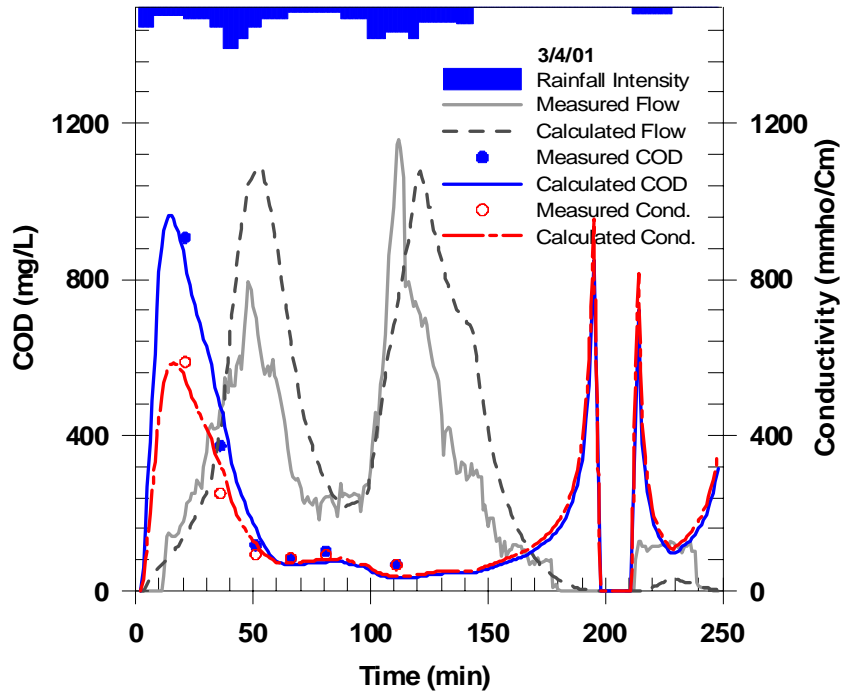
FIGURE 5.3 Runoff coefficients with respect to the total rainfall volume at $K_p = 10^{-5}$ cm/sec

TABLE 5.1 Input Parameters for the Flow Calculation

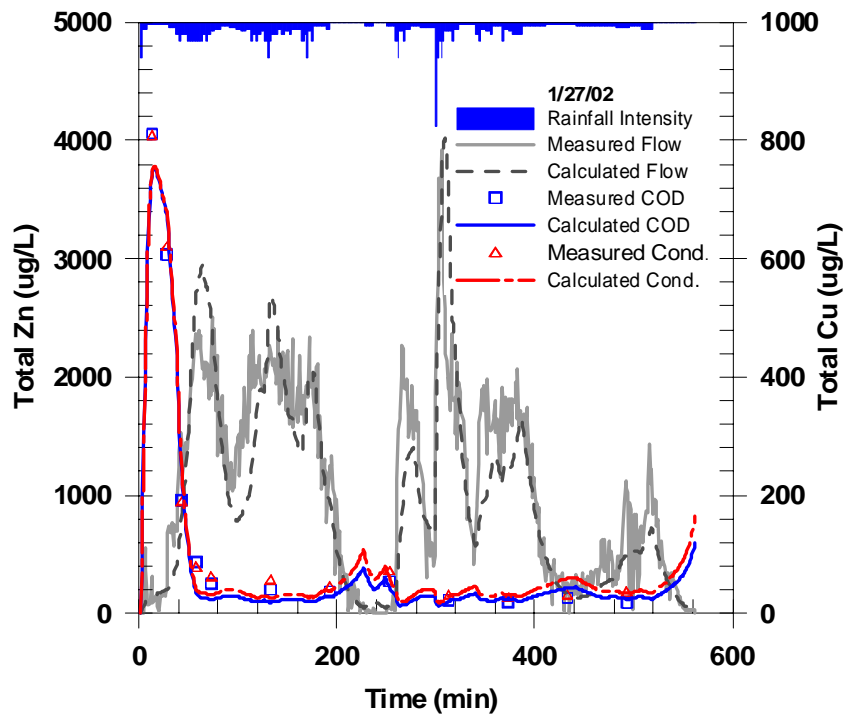
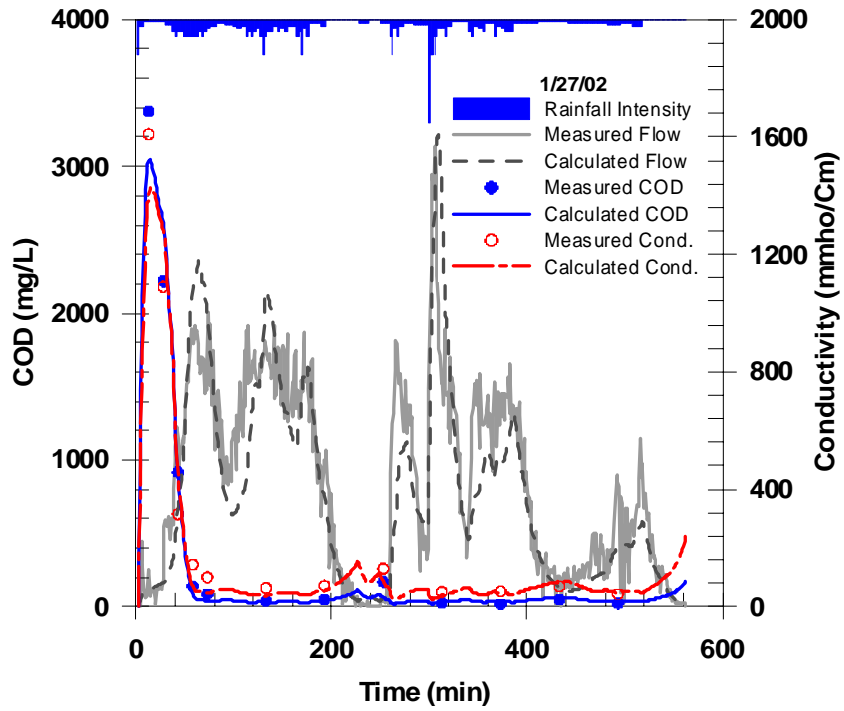
Input Parameters	Parameter Values
Watershed Length, WL (m)	178
Watershed Width, W (m)	21.9
Slope in the Longitudinal Direction, S_0	0.02
Manning's Coefficient, n	0.011
Hydraulic conductivity of the Pavement, K_p (cm/sec)	10^{-5}



(a) Storm event on 1/10/2001



(b) Storm event on 3/4/2001



(c) Storm event on 1/27/2002

FIGURE 5.4 Measured and calculated hydrographs and pollutographs

5.1.2 Calibration of Water Quality Parameters

Calculated concentrations were fitted with measured concentrations to calibrate the model parameters ($m_{b,s}^0$, ε_s and ε_l') for COD, conductivity, Zn and Cu, respectively. Before minimizing the sum of square errors between measured and calculated concentrations, the calibrated parameters were constrained to reasonable values by observing the measured and calculated concentration curves. Table 5.2 provides the calibrated parameters for four different constituents. ε_s ranged from 0.87 to 1.10 sec/m², without large variance among constituents. ε_l' , however, widely varies from one constituent to another. $m_{b,s}^0$ was different for individual storm events due to different ADD, which was as predicted.

Concentrations for each constituent were calculated using calibrated parameters and plotted with measured concentrations as illustrated in Figure 5.4. This figure provides polluto-graphs for three storm events on 1/10/2001, 3/4/2001 and 1/27/2002, respectively.

TABLE 5.2 Calibrated Parameters for Site 3^a

Parameters	$m_{b,s}^0$ (g/m ²)	ε_s (sec/m ²)	ε_l' (g·sec/m ⁴)
COD	0.10 ~ 1.18	1.09 (0.6 ~ 1.2)	0.0024 (0.001 ~ 0.004)
Conductivity	0.10 ~ 0.55	0.99 (0.4 ~ 1.2)	0.0027 (0.002 ~ 0.004)
Zn	0.05 ~ 1.46	0.87 (0.4 ~ 1.2)	0.0073 (0.004 ~ 0.014)
Cu	0.05 ~ 0.29	0.88 (0.4 ~ 1.2)	0.0016 (0.001 ~ 0.0028)

^a Average values with lower and upper boundaries in parentheses
 $m_{b,s}^0$ -Initial pollutant mass from the short-term sources

As can be seen, two-phase washoff phenomenon (high concentration first flush followed by prolonged emission in a low concentration level) was well simulated. A quick rise in the calculated concentration sometimes occurs at the end of rainfall as observed in Figure 4.3(a) and (b). This is due to the reduced dilution caused by the flow decrease. More polluto-graphs for the other storm events can be found in Appendix C.

5.1.3 Pollutant Buildup

Using calibrated $m_{b,s}^0$ values for each storm event, buildup equations were obtained as shown in Figure 5.5. This figure illustrates COD buildup as a function of ADD, showing the plots of calibrated values of $m_{b,s}^0$ fitted with four different curve forms using the least-square method. In the same manner, buildup formulas for the other constituents can be also obtained and presented in Table 5.3. Regressions for conductivity, Zn and Cu are provided in Appendix D.

TABLE 5.3 Buildup Equations Fitted by Different Curve Forms for COD, Conductivity, Zn and Cu ^a

Parameters	Linear	Power	Exponential	Michaelis-Menton
COD (g/m ²)	0.055t	0.178t ^{0.59}	1.29(1-e ^{-0.088t})	1.87t/(15.26+t)
Cond. (10 ² ×mmho)	0.027t	0.113t ^{0.50}	0.57(1-e ^{-0.113t})	0.76t/(10.19+t)
Zn (mg/m ²)	0.059t	0.173t ^{0.63}	1.55(1-e ^{-0.070t})	2.29t/(19.58+t)
Cu (mg/m ²)	0.012t	0.039t ^{0.60}	0.31(1-e ^{-0.078t})	0.45t/(16.95+t)

^a t - Antecedent dry days (days)

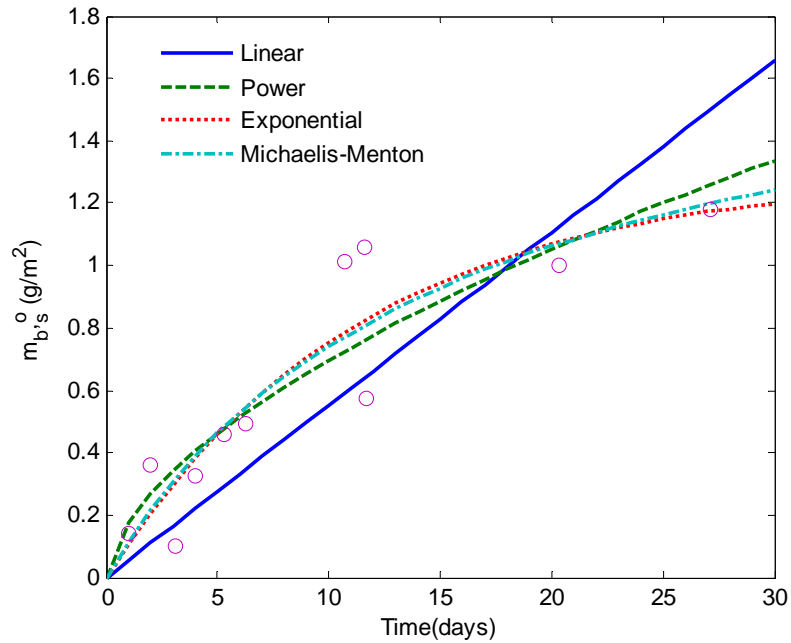


FIGURE 5.5 Regressions for COD buildup using different curve forms

Table 5.4 compares buildup formulas suggested by different researchers for urban landuses. Buildup mass of total solids (TS) for 30 days of ADD is calculated using each formula and compared in 4th and 5th columns of Table 5.4. Because a buildup formula for solid was not available in this study, The COD buildup formula was used and calculated COD mass was converted into the equivalent TS mass using the factor of 46,120 mgCOD/kgTS, reported for urban landuses by Manning et al. (1977). Table 5.4 implies that the solid accumulation estimated from this study (416 gTS/m) is reasonably well matched with that from Sartor’s formula (427 gTS/curb m) that represents 95% of TS accumulated across the street width. Tomanovic’s and Kim’s formulas slightly underestimated the total because their studies were only for suspended fraction of TS.

TABLE 5.4 Comparison of Buildup Equations

Application	Pollutant	Formula ^a	Equivalent solid mass accumulation for 30 days of ADD		References
			mass/length	mass/area	
Industrial landuse	TS	$TS(lb / curb\ mi) = \frac{t}{0.00187 + 0.000601t}$	427 gTS/m	-	Sartor et al. (1972)
Road pavement	TSS	$TSS(g / m^2) = 10(1 - e^{-0.045t})$	-	7.4 gTSS/m ²	Tomanovic and Maksimovic (1996)
Highway	TSS	$TSS(g / m^2) = 10.52(1 - e^{-0.062t})$	-	8.9 gTSS/m ²	Kim (2002)
Highway	COD	$COD(g / m^2) = 1.29(1 - e^{-0.088t})$	416 gTS/m ^b	26.0 gTS/m ^{2c}	This study (Exponential type)

^a *t* - Antecedent dry days (days)

^{b, c} calculated using the ratio of 46,120 mgCOD/kgTS reported by Manning et al. (1977)

5.2 FIRST FLUSH SIMULATIONS IN 1-D FLOW

All the MFF simulations in this study were based on the calibrated parameters (i.e. $m_{b,s}^0$, ε_s and ε_l') for COD. MFF_{10} and MFF_{20} were selected as the representative MFF ratios.

MFF was basically investigated as a function of watershed length (WL) under different conditions in rainfall intensity, rainfall duration, slope, pavement hydraulic conductivity, initial mass and erosion coefficients. Constant rainfall intensity was assumed for the input rainfall in the model equation. Different types of rainfall such as triangular or sinusoidal shaped rainfall patterns were remained for the future work.

5.2.1 Maximum MFF Ratio and Optimum Watershed Length

The MFF ratios (i.e. MFF_{10} and MFF_{20}) calculated for various watershed lengths (WLs) were investigated and it was found that there exists an optimum watershed length (WL_{opt}) that maximizes MFF_{10} or MFF_{20} in the range of 1 to 10,000 m. Figure 5.6 illustrates the MFF changes for different WLs. In this figure, both MFF_{10} and MFF_{20} are maximized at a 50 m-long-watershed. This demonstrates that neither of extremely small and large watersheds yields high MFF_n (e.g. MFF_{10} , MFF_{20}). In a small watershed, rainfall water rapidly flushes out without forming sufficiently high flow rate; as a result, pollutants are not well mobilized due to lack of flow energy. In a very large watershed, pollutants travel a long distance, resulting in retardation of mass emission although large flow energy effectively erodes pollutants out of the surface. MFF can be even inversed ($MFF_n < 1.0$) in an extremely large watershed (e.g. $WL > 5,000$ m in the Figure 5.6).

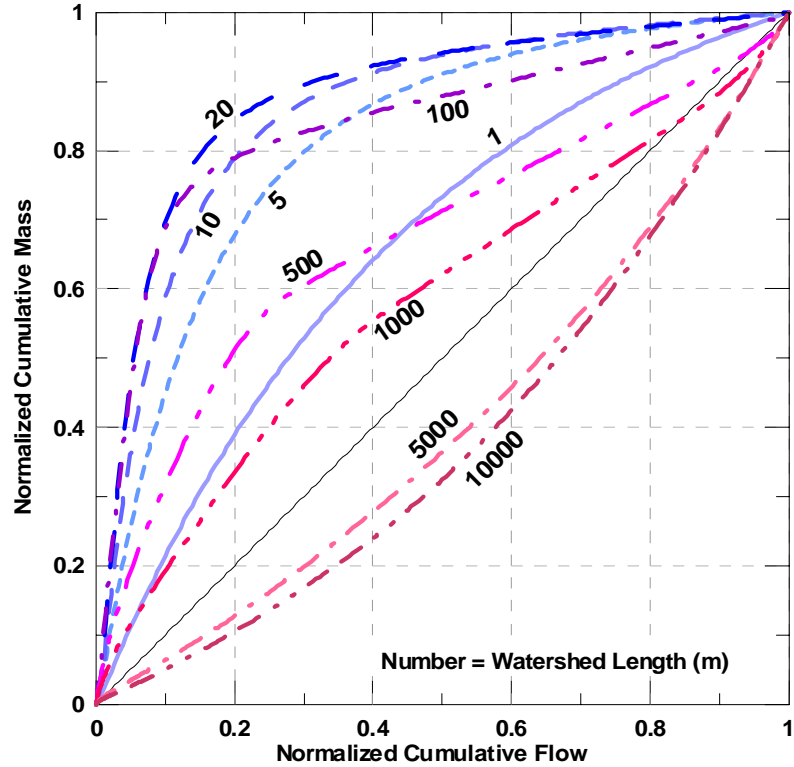


FIGURE 5.6 MFF changes with different watershed lengths at $I = 3$ mm/hr and $T = 3$ hr

Figure 5.7 illustrates how the maximum MFF ratio ($MFF_{n,max}$) and optimum watershed length (WL_{opt}) can be obtained from a MFF simulation. Because MFF_n is calculated at discrete points of WL , calculated values of MFF_n at those points are interpolated to produce a continuous function. A scalar-minimization solver (i.e. “fminbnd”) in the MATLAB toolbox was used to calculate maximum MFF_{10} ($MFF_{10,max}$), maximum MFF_{20} ($MFF_{20,max}$) and WL_{opt} from the non-linear continuous function obtained by interpolation. To calculate WL at a certain MFF_n value, a function solver (i.e. “fzero”) in the MATLAB was used. In Figure 5.7, $MFF_{20,max}$, WL_{opt} , and WL at $MFF_{20} = 2.5$ are calculated as 4.2, 30 and 550 m, respectively.

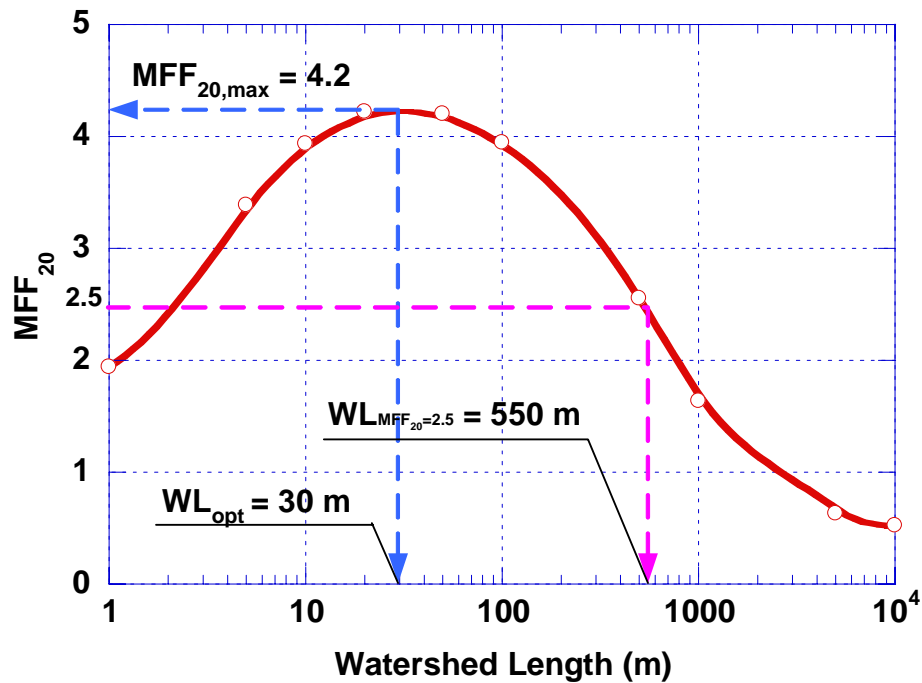


FIGURE 5.7 Maximum MFF_{20} , optimum watershed length, and watershed length at $MFF_{20} = 2.5$

5.2.2 Evaluation of Affecting Factors

Rainfall Intensity (I) and Duration (T). Six hypothetical rainfalls with different rainfall intensity and duration were simulated and calculated values of MFF_{10} and MFF_{20} were plotted as functions of WL in Figure 5.8. As can be seen, $MFF_{10,max}$ and $MFF_{20,max}$ occur at different WL s for each rainfall simulated. This is because different combinations of rainfall intensity and duration change hydraulic conditions, resulting in different emission rates of pollutants. Higher rainfall intensity and longer duration produce larger MFF_n and smaller WL_{opt} . As the watershed becomes longer, both MFF_{10} and MFF_{20} approach 1 or less. Storm events with the same total rainfall volume (e.g. *rainfall 1* and *5*,

or *rainfall 2* and *6*) showed similar curves in both cases of MFF_{10} and MFF_{20} , which implies total rainfall volume might be useful as a potential indicator for estimating $MFF_{n, \max}$ (e.g. $MFF_{10, \max}$, $MFF_{20, \max}$).

Slope (S_0) and Infiltration Rate (f). The effects of slope and infiltration rate were estimated using *rainfall 1* ($I = 3$ mm/hr and $T = 3$ hr). Figure 5.9 displays the effect of the bed slope on MFF_{10} and MFF_{20} for different WLs. As the slope increases, WL_{opt} tends to be shorter. $MFF_{10, \max}$ and $MFF_{20, \max}$ proportionally increase as the slope increases although the increments were insignificant in the simulated range of slope (0.01 ~ 0.06). $MFF_{10, \max}$ was more sensitive than $MFF_{20, \max}$ to slope change.

Figure 5.10 shows MFF_{10} and MFF_{20} with respect to WL for three different values of K_p ranging from 10^{-5} to 5×10^{-5} cm/sec. Corresponding runoff coefficients were also displayed in the figure. As can be seen, smaller K_p produces larger MFF_{10} and MFF_{20} , and requires smaller WL for $MFF_{n, \max}$. $MFF_{10, \max}$ and $MFF_{20, \max}$ also decrease as K_p increases. High infiltration rate reduces net precipitation, thereby retarding pollutant erosion rate because of lower flow energy. In the long watershed range ($WL > 300$ m), the curves of MFF_{10} and MFF_{20} under different infiltration rate become closer. That is, MFF_{10} and MFF_{20} are less sensitive to the infiltration rate in a large watershed.

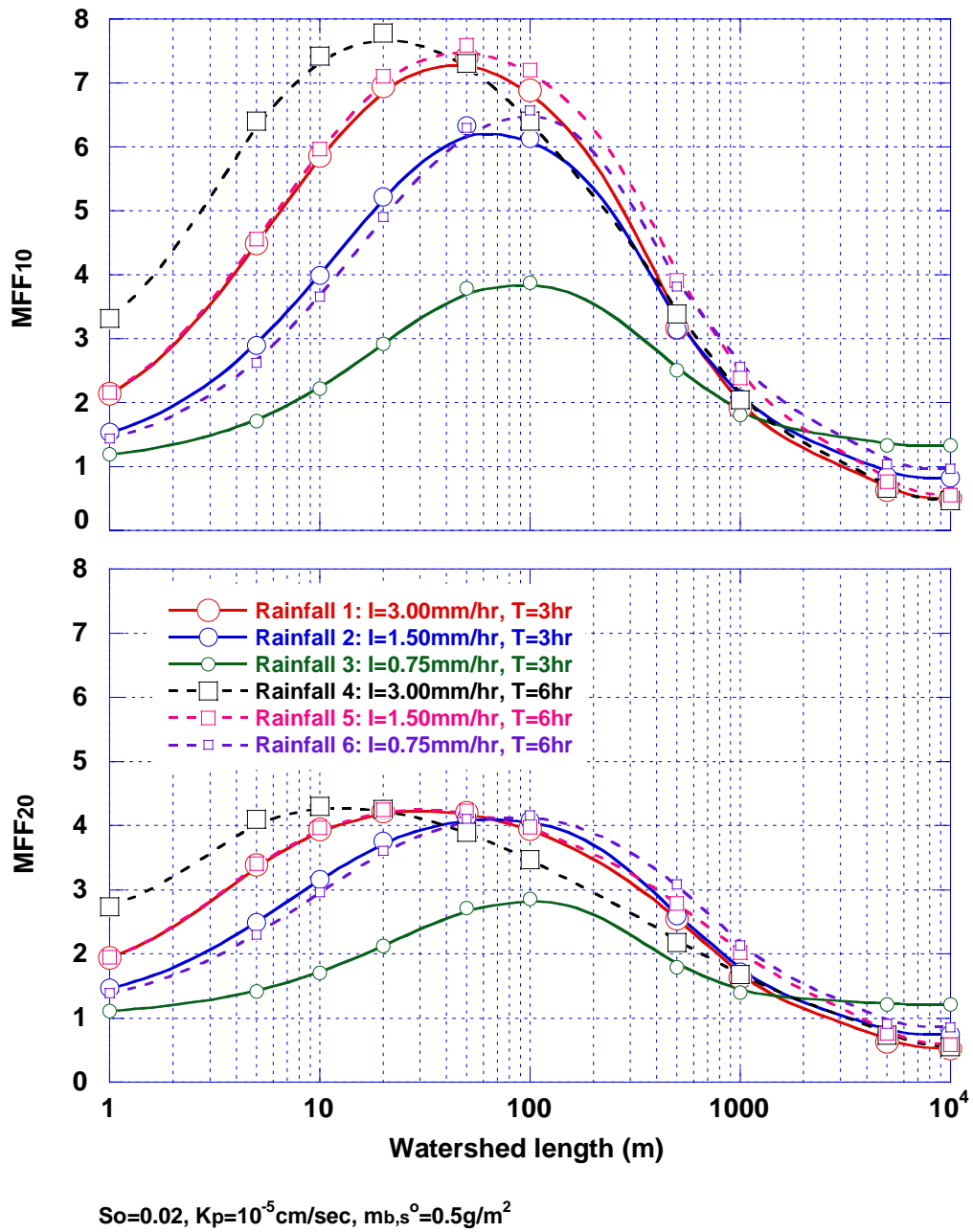


FIGURE 5.8 MFF₁₀ and MFF₂₀ with respect to the watershed length for different rainfall intensities and durations

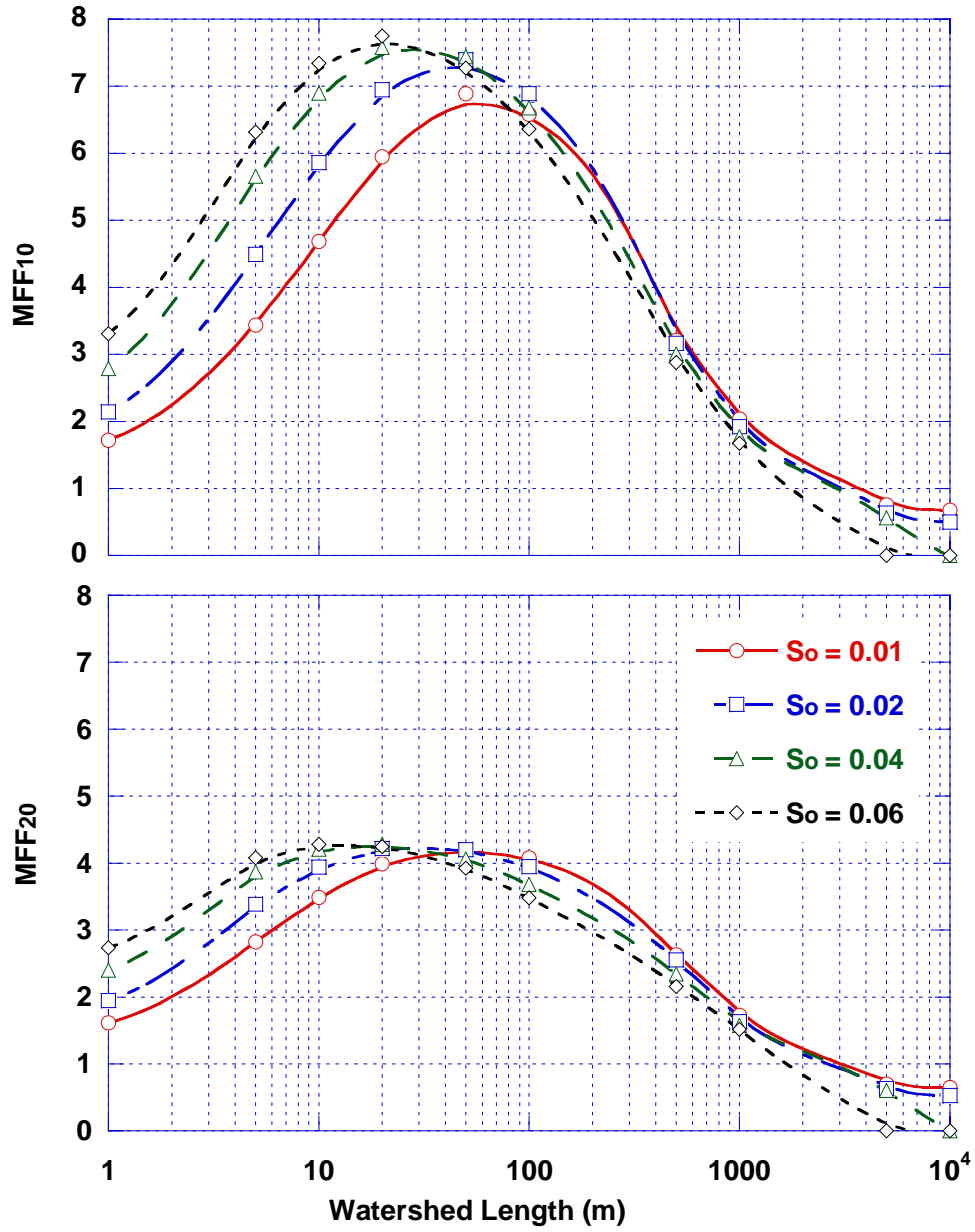


FIGURE 5.9 MFF_{10} and MFF_{20} with respect to the watershed length for different slopes ($I = 3$ mm/hr and $T = 3$ hr)

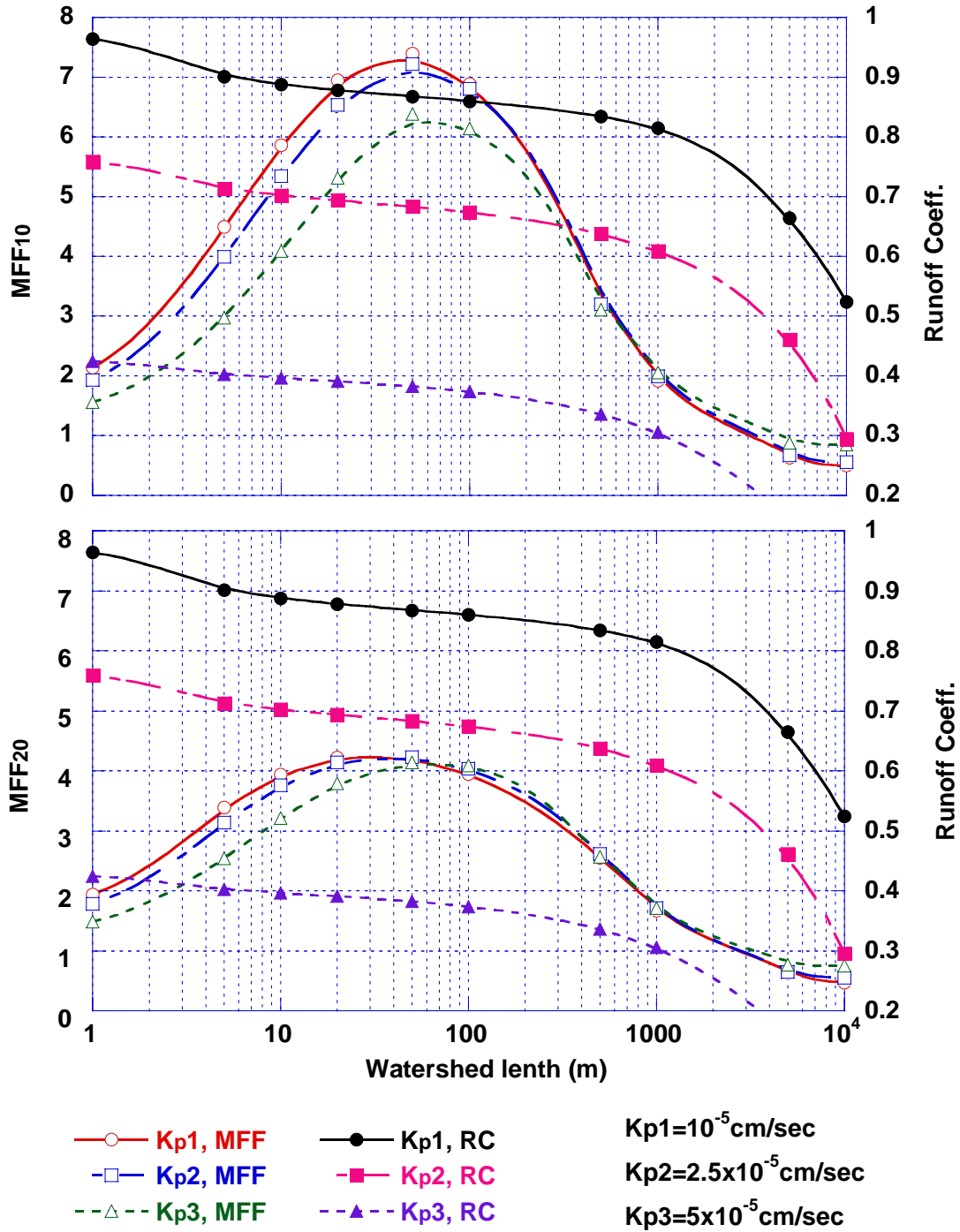


FIGURE 5.10 MFF₁₀ and MFF₂₀ with respect to the watershed length for different values of pavement hydraulic conductivity ($I = 3$ mm/hr and $T = 3$ hr)

Initial Mass ($m_{b,s}^0$) and Erosion Coefficients (ϵ_s, ϵ_l). Different values of $m_{b,s}^0$ were simulated as a function of WLs in Figure 5.11. As can be seen, larger $m_{b,s}^0$ yield greater MFF ratios and larger WL_{opt} for $MFF_{10, max}$ or $MFF_{20, max}$. Accumulated mass per unit distance strongly affects the MFF ratios in large watersheds. In contrast, the differences among the values of MFF_{10} or MFF_{20} for different values of $m_{b,s}^0$ were small in a very small watershed ($WL < 10$ m). With $m_{b,s}^0$ larger than 1 g/m^2 , there was little change in the curves of MFF ratio. In this case, short-term source becomes the dominant pollutant source, so that the total mass emission rate is primarily controlled by ϵ_s , not the absolute amount of total pollutant mass. As the ADD increases, the short-term pollutant accumulation approaches to maximum capacity. Therefore, the relationship between MFF and ADD becomes weaker as the ADD becomes longer because of limited mass accumulation as well as domination of the short-term source in the total pollutant mass. Figure 5.11 also implies MFF_{10} is more sensitive to the initial mass than MFF_{20} .

The pollutant erosion coefficients were also evaluated. Figure 5.12 shows the simulation results of MFF_{10} and MFF_{20} using two different values of erosion coefficient of the short-term source (ϵ_s). As shown in the figure, higher ϵ_s produces greater MFF ratios whereas the $MFF_{10, max}$ and $MFF_{20, max}$ are obtained at shorter WLs. MFF_n might be hardly influenced by changing ϵ_s in a relatively long watershed because the values of MFF_{10} or MFF_{20} for $\epsilon_s = 1$ and $\epsilon_s = 0.5$ are similar in watersheds longer than around 1,000 m.

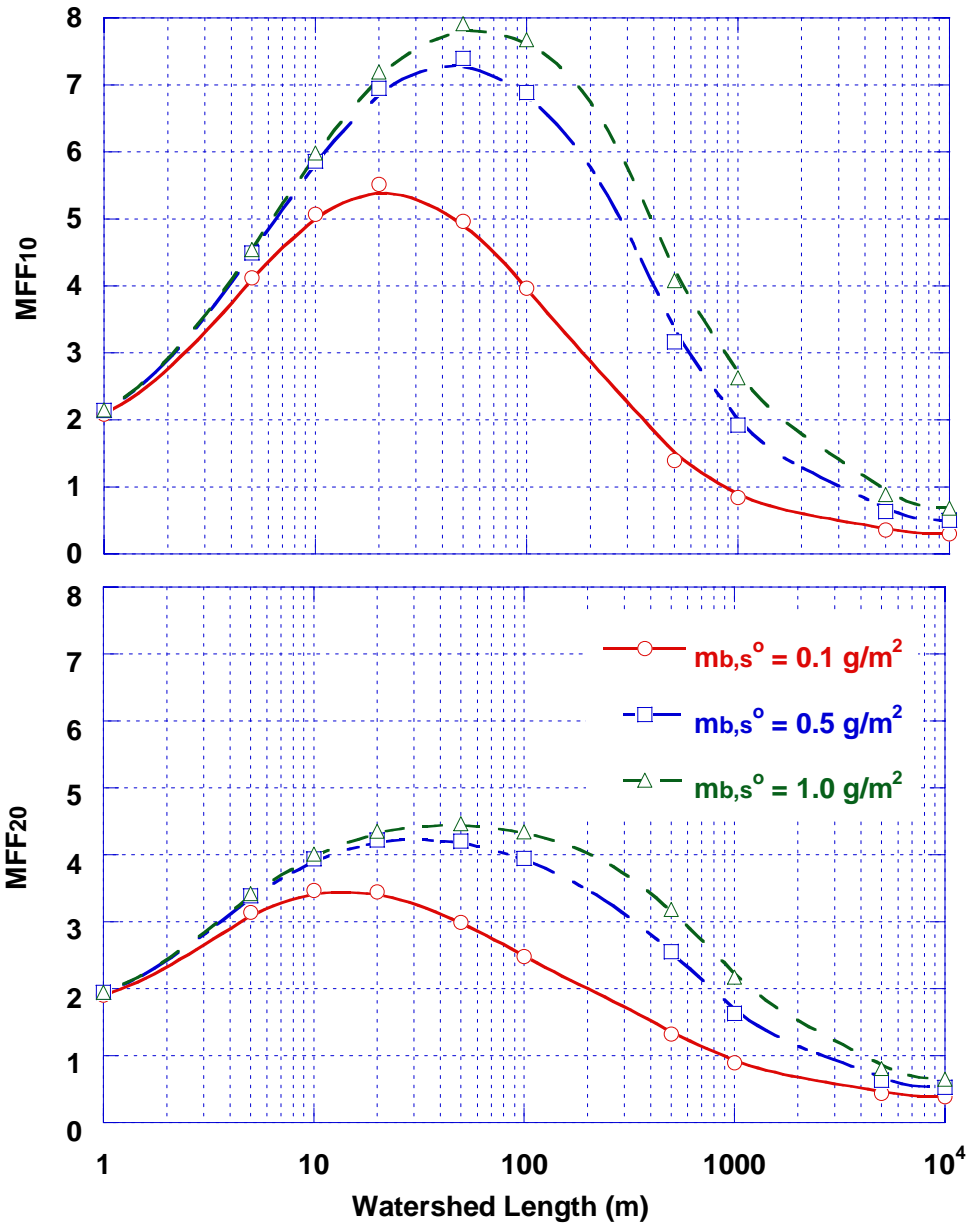


FIGURE 5.11 MFF₁₀ and MFF₂₀ with respect to the watershed length for different values of $m_{b,s}^{\circ}$ ($I = 3$ mm/hr and $T = 3$ hr)

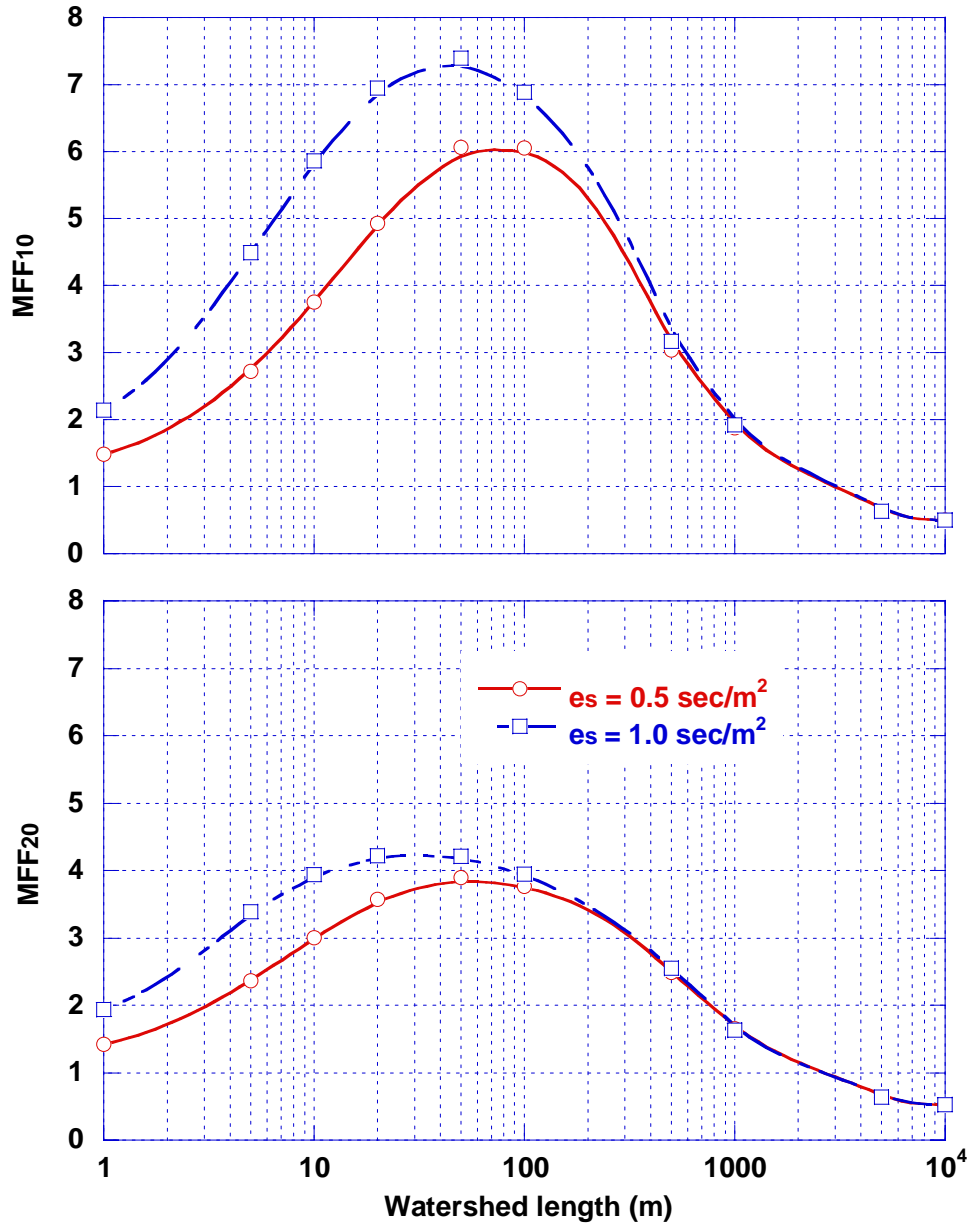


FIGURE 5.12 MFF₁₀ and MFF₂₀ with respect to the watershed for different erosion coefficients of short-term pollutant source ($I = 3 \text{ mm/hr}$ and $T = 3 \text{ hr}$)

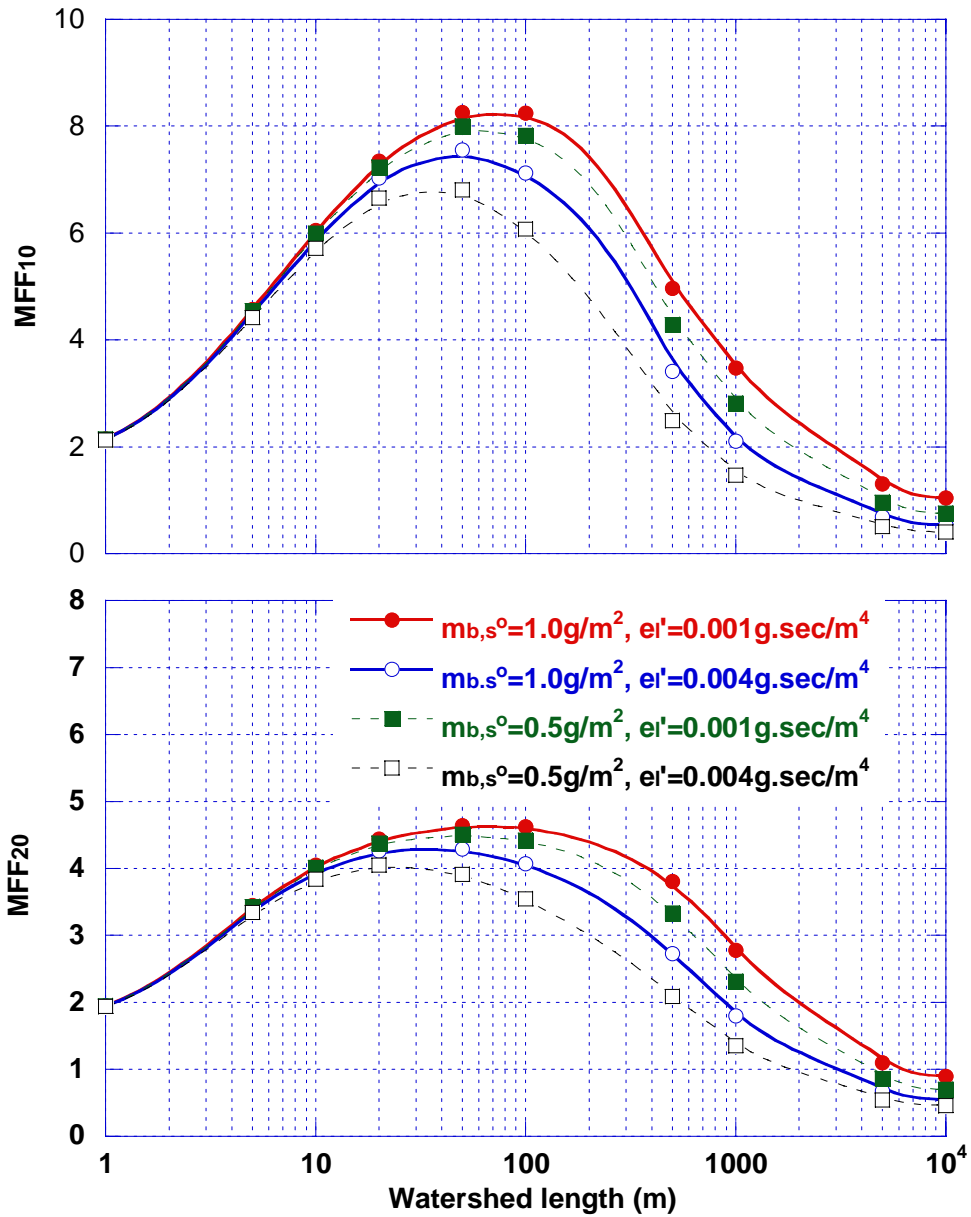


FIGURE 5.13 MFF₁₀ and MFF₂₀ with respect to the watershed for different erosion rates of long-term pollutant source ($I = 3 \text{ mm/hr}$ and $T = 3 \text{ hr}$)

Figure 5.13 shows the effect of the erosion coefficient of the short-term source (ϵ_l'). The MFF ratios are very sensitive to the change of ϵ_l' in the long watershed range, and

relatively insensitive to ε_s . For shorter watersheds, the opposite sensitivities are observed. As ε_l' increased from 0.001 to 0.004 g·sec/m⁴ (this is estimated range for ε_l' in the parameter estimation study previously performed in section 5.1.2), WL_{opt} , and WL at $MFF_{20} = 2.5$ decreased by $\Delta \ln(WL) \approx 0.7$ for both values of $m_{b,s}^0$. However, decreases in $MFF_{20, max}$, were relatively small. The sensitivity value of WL for ε_l' change ($\Delta \ln(WL)/\Delta \varepsilon_l' \approx 233$) may be considered in determining a design watershed length (WL_{des}) although more sensitivity studies will be required to establish the relationship among parameters.

As discussed above, the relative importance between pollutants from short-term and long-term sources strongly depends on $m_{b,s}^0$, ε_s and ε_l' , which determines the characteristics of MFF.

5.3 RADIAL FLOW SIMULATION

Irregular geometry can change MFF characteristics by converging or diverging water flow. To investigate the effect of geometry in 2-D watersheds, 2-D flow simulation is required, which is more complicated in numerical formulation and solution. However, the radial flow model, as a simple case of the 2-D flow model, can be used to obtain basic characteristics of the flow in a converging type watershed (converging flow). Converging flows are commonly observed in 2-D watersheds such as a parking lot as well as a large watershed that has a small number of inlets. A radial flow simulation will provide

fundamental information on MFF behavior in 2-D watersheds. The diffusion wave equation was used for the flow simulation because a strong effect of hydraulic diffusivity is predicted near the downstream where great volume of water accumulates.

Simulated I and T were 3 mm/hr and 3 hr respectively. Values of 0.02 and 0.5 were used for S_0 and $m_{b,s}^0$, respectively, for all radial flow simulations. Because the degree of flow converging depends on the ratio of the watershed length (WL = watershed radius – inlet radius) to the inlet radius (r_0), the effect of flow converging was investigated using different values for WL and r_0 . Simulated WL ranged from 1 to 200 m with different of r_0 s (i.e. 1, 5, 10 and 100 m). Watersheds longer than 200 m were not simulated because too much computing time was required.

Figure 5.14 shows the curves for MFF_{10} and MFF_{20} with respect to WL for different r_0 s. There were no significant differences in the WL_{opt} , $MFF_{10, max}$ and $MFF_{20, max}$ between each simulation. Figure 5.15 more clearly shows the maximum MFF ratios and corresponding values of WL_{opt} shown in Figure 5.14. As r_0 increases, MFF_{10} or MFF_{20} also increases although the rate of increase is small and WL_{opt} is little changed. Lower MFF in the converging flow is due to the tapering distribution of pollutant mass in the flow direction (Figure 5.16).

Figure 5.16 illustrates the mass distribution in a converging watershed. Assuming the mass accumulation per unit area is constant, the total mass in a discrete zone becomes larger as the distance of that discrete zone to the downstream boundary becomes longer. That is, less pollutant mass is available for the erosion although flow velocity is much higher near the downstream than the upstream. As a result, the accumulated pollutant

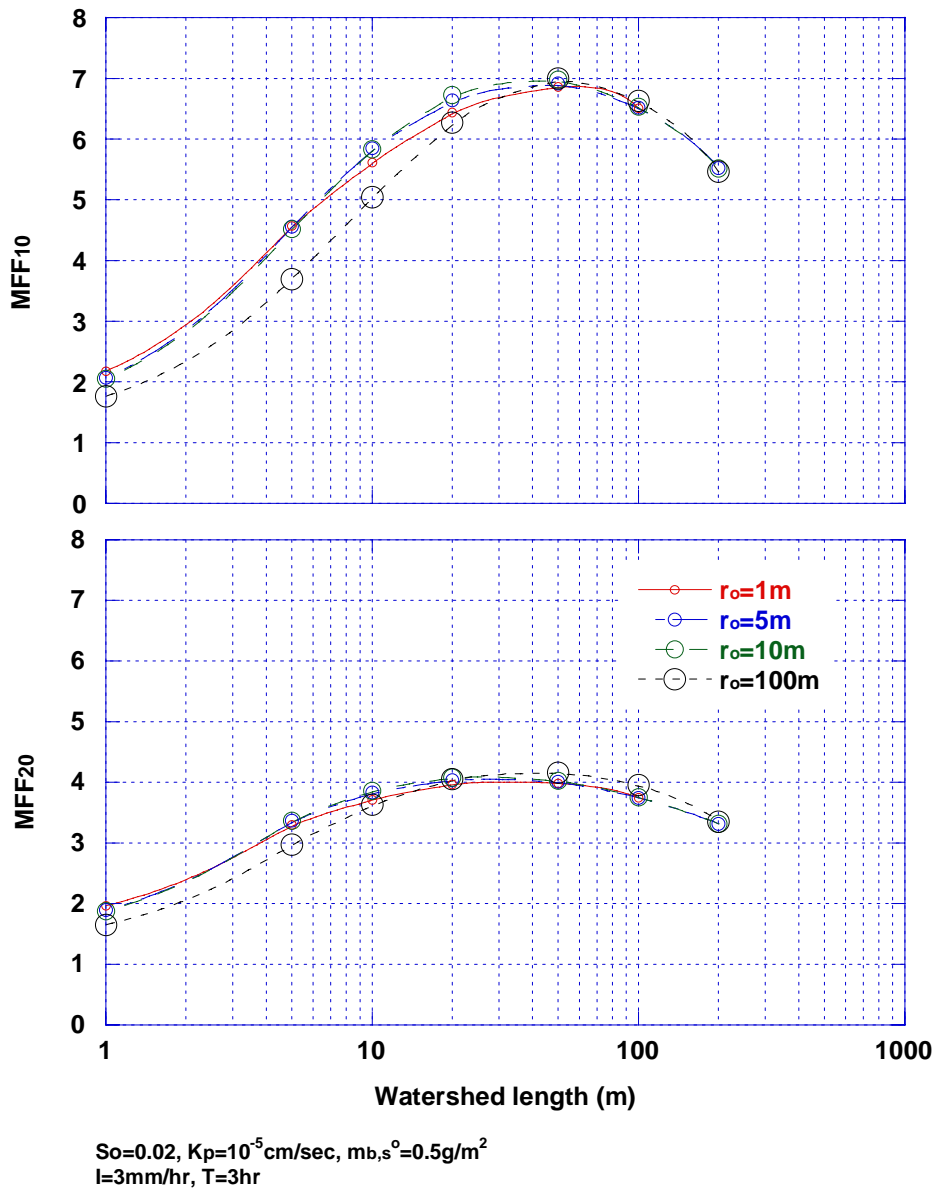


FIGURE 5.14 MFF₁₀ and MFF₂₀ with respect to the watershed length for different inlet radius in the radial flow

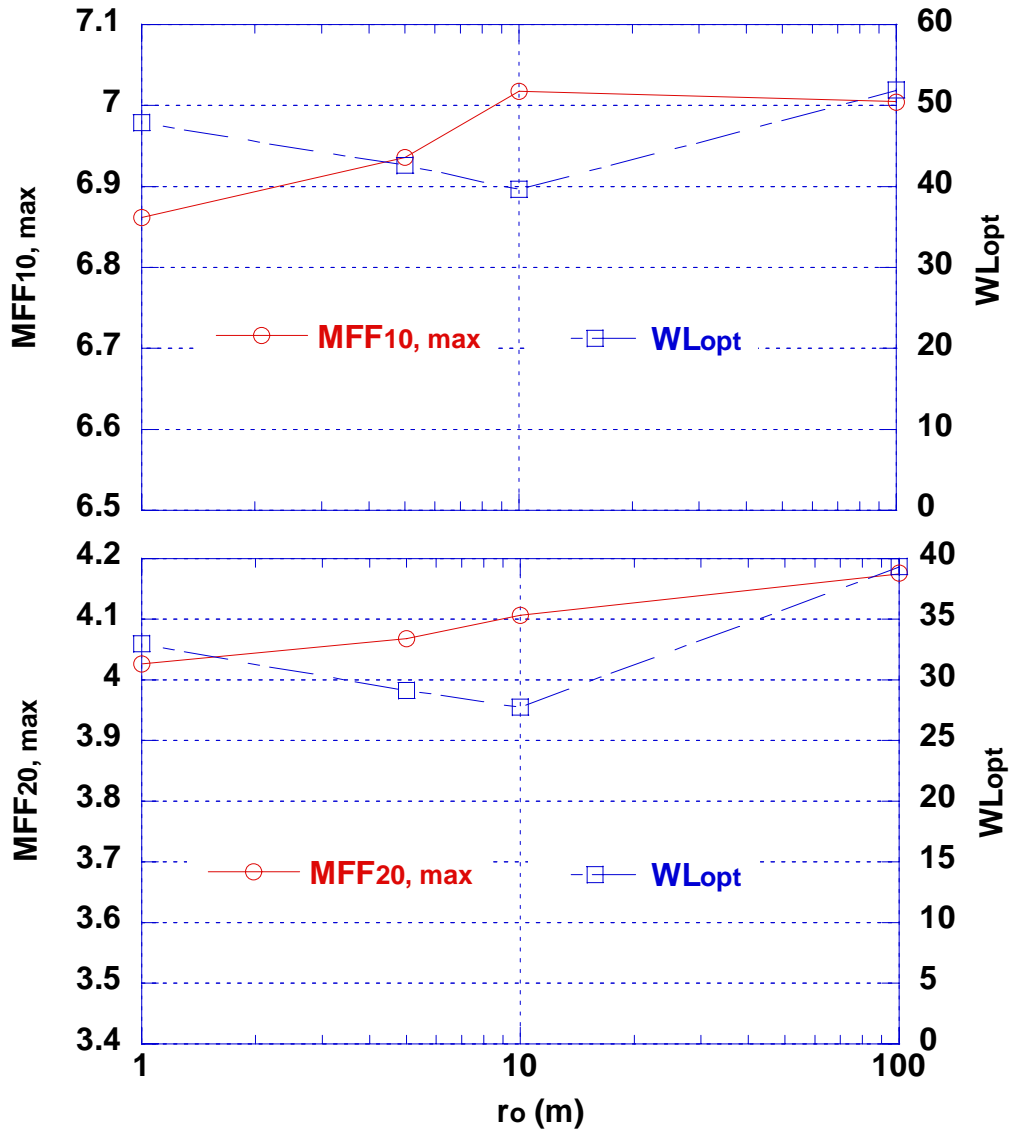


FIGURE 5.15 Maximum MFF ratio and optimum watershed length in the radial flow simulation in Figure 5.14

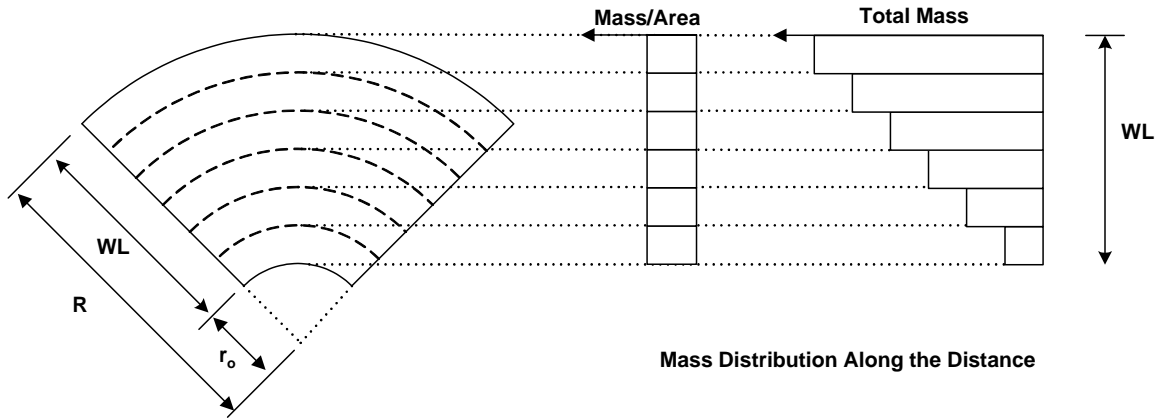


FIGURE 5.16 Mass distribution on the converging watershed

mass near the downstream is exhausted rapidly whereas the erosion of pollutant mass is comparatively less in the upstream area, where more pollutant mass is accumulated compared to the downstream. This uneven mass distribution affects on the MFF ratios but the difference was minimal when viewed as a whole.

5.4 DESIGN IMPLICATIONS

The 1-D highway runoff model developed in this study can be utilized for the BMP design in two ways. First, treatment capacity and operating conditions of a BMP can be determined using the runoff quantity and quality predicted by the model. Second, through simulation using various conditions, the best condition to obtain a desired MFF can be found and applied for designing storm-drain inlets and collection pipes. This study's focus is mainly on the collection system design described as the second purpose above.

5.4.1 MFF Ratio as a Design Parameter

Although many alternative choices for MFF ratio exist for a design parameter, MFF_{20} was considered an appropriate design parameter because the MFF simulation results (Figure 5.8 ~ Figure 5.13) shows that MFF_{20} is comparatively less sensitive to the varying conditions and thereby allows more robust design than designs using MFF_{10} .

A proper criterion should be established to use MFF_{20} as a design parameter because the design watershed length (WL_{des}) is determined by the design MFF_{20} ($MFF_{20, des}$). If a designer needs to maximize the pollutant mass to be treated in a BMP, $MFF_{20, max}$ can be used as a design criterion (i.e. $MFF_{20, des} = MFF_{20, max}$). $MFF_{20, des}$ can be also purposely adjusted to a lower level for more cost-effective design (e.g. $MFF_{20, des} = 2.5 < MFF_{20, max}$).

The MFF simulations from Figure 5.8 to Figure 5.13 provide a qualitative relationship between the MFF ratio and affecting factors as summarized in Table 5.5.

TABLE 5.5 Qualitative Relationship between MFF_{20} and Design factors

Design Factors to be Increased	$MFF_{20, max}$	WL_{opt}
Rainfall Intensity	Increase	Shorten
Rainfall Duration	Increase	Shorten
Slope	Increase	Shorten
Infiltration Rate	Decrease	Lengthen
ADD	Increase	Lengthen
Erosion coefficient for short-term source	Increase	Shorten
Erosion coefficient for long-term source	Decrease	Shorten

This qualitative result might be useful for screening before undertaking the full BMP design procedure. A universal design procedure will not be possible because of site specific conditions, due to the diversity in slope, rainfall and available mass of pollutant.

Comprehensive MFF simulations under various conditions of slope, rainfall and initial mass of the pollutant were conducted to generate a design tool for determining the watershed length. Table 5.6 shows the ranges of design factors that were used in the MFF simulations.

Figure 5.17 shows contours of WL_{opt} as a function of rainfall intensity and duration for different $m_{b,s}^0$ values at $S_0 = 0.02$. Similarly, contours of $MFF_{20, max}$ corresponding to the WL_{opt} were also constructed as shown in Figure 5.18. These two figures contain contours for four different values of $m_{b,s}^0$ (i.e. 0.1, 0.5, 1.0 and 1.5 g/m^2). Simulated rainfall intensity and duration were in the ranges of 1.2 ~ 12.0 mm/hr and 1 ~ 12 hr,

TABLE 5.6 Design Factors Applied in the MFF Simulations

Design Factors	Simulated Values
I (mm/hr)	1.2 ~ 12.0
T (hr)	1 ~ 12
S_0 (-)	0.01 ~ 0.06
$m_{b,s}^0$ (g/m^2)	0.1 ~ 1.5
K_p (cm/sec)	10^{-5}
ε_s (sec/m^2)	1.09
ε_l' ($g \cdot sec/m^4$)	0.0024

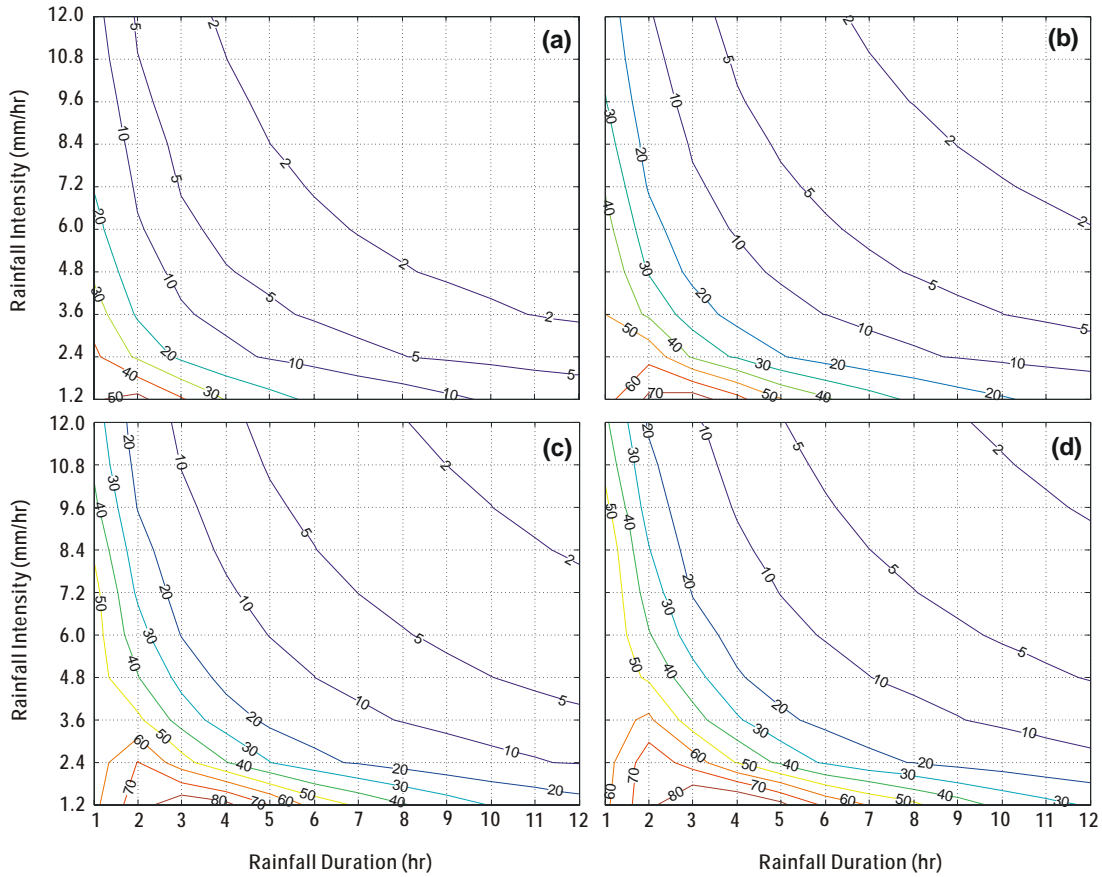


FIGURE 5.17 Contours of the optimal watershed length for maximum MFF_{20} as a function of rainfall intensity and duration for different values of $m_{b,s}^0$ at $S_o = 0.02$ and $K_p = 10^{-5}$ cm/sec: (a) $m_{b,s}^0 = 0.1$ g/m²; (b) $m_{b,s}^0 = 0.5$ g/m²; (c) $m_{b,s}^0 = 1.0$ g/m²; (d) $m_{b,s}^0 = 1.5$ g/m²

respectively, based on the rainfall data in site 3 (7-203). These contours can be used to decide the inlet location in highways or parking lots for a given characteristics of weather and watershed.

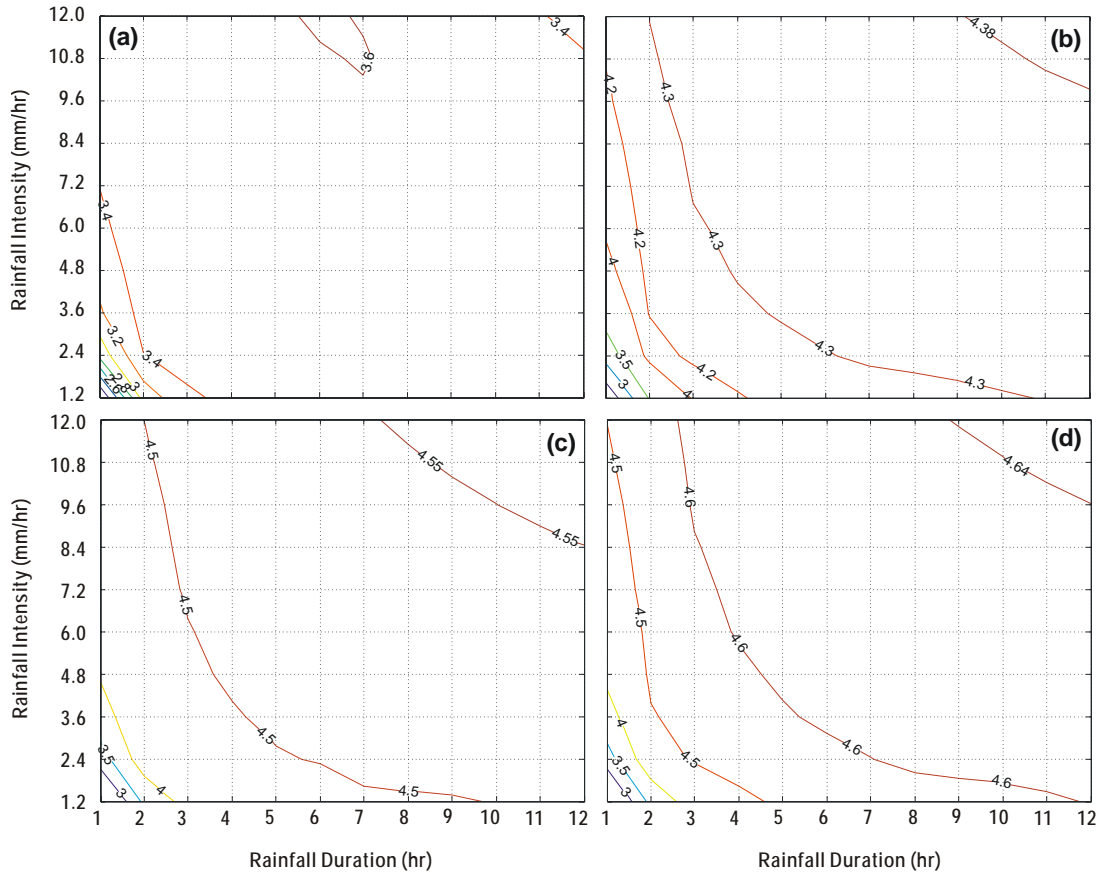


FIGURE 5.18 Contours of the maximum MFF_{20} as a function of rainfall intensity and duration for different values of $m_{b,s}^0$ at $S_o = 0.02$ and $K_p = 10^{-5}$ cm/sec: (a) $m_{b,s}^0 = 0.1$ g/m²; (b) $m_{b,s}^0 = 0.5$ g/m²; (c) $m_{b,s}^0 = 1.0$ g/m²; (d) $m_{b,s}^0 = 1.5$ g/m²

According to the contours in Figure 5.17, the values of WL_{opt} are less than 100 m for the entire range of the rainfall considered. If $MFF_{20, max}$ is a design criterion, the inlets should be installed at intervals of less than 100 m along the highway, which might result in undesirably high construction costs. For economic purpose, the design criteria for MFF_{20} ($MFF_{20, des}$) might be lowered to allow a longer WL_{des} . All aspects including costs and water quality should be therefore considered to determine $MFF_{20, des}$.

The broad peak of simulated MFF ratios implies a wide range of lengths to obtain high or favorable MFF₂₀ ratios. For example, the MFF₂₀ curve for *rainfall 1* in the Figure 5.8 shows that 2.5 or larger MFF₂₀ can be obtained at any WL between 2 and 400 m. This wide range of allowable WL provides a designer the alternative choices for WL_{des}. A strategy in determining WL_{des} can be selecting a value between WL_{opt} and the WL at a required MFF₂₀, which is the upper limit of allowable WL (i.e. the maximum WL among WLs yielding MFF₂₀s larger than a required value).

Figure 5.19 illustrates contours of the maximum WL at MFF₂₀ = 2.5 (if MFF_{20, max} < 2.5, MFF_{20, max} was used in the contours), which means 50% of the total mass washoff is in the first 20% of the runoff volume. A designer can select a value as a WL_{des} between the WL_{opt} from Figure 5.17 and the maximum WL from Figure 5.19.

Figure 5.20 contains contours for four different slopes at $m_{b,s}^0 = 1.0 \text{ g/m}^2$. This figure can be used for the watershed with slope ranged from 0.01 to 0.06. 1.0 g/m^2 of $m_{b,s}^0$ corresponds to 17 days of ADD based on the COD buildup estimated earlier.

In this manner, the design contour sets for possible conditions of slope and initial mass might be prepared and utilized as a design tool for installing storm-drain inlets.

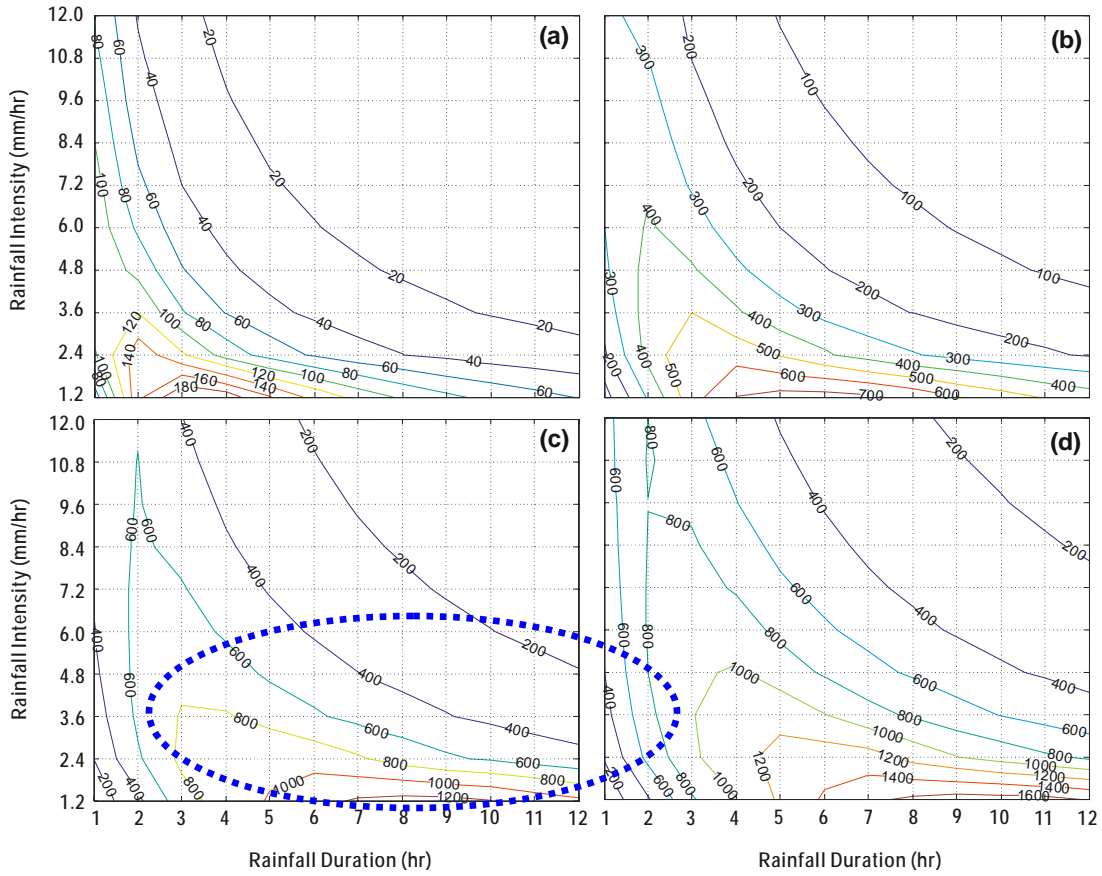


FIGURE 5.19 Contours of the maximum watershed length at $\text{MFF}_{20} = 2.5$ as a function of rainfall intensity and duration for different values of $m_{b,s}^0$ at $S_o = 0.02$ and $K_p = 10^{-5}$ cm/sec: (a) $m_{b,s}^0 = 0.1$ g/m²; (b) $m_{b,s}^0 = 0.5$ g/m²; (c) $m_{b,s}^0 = 1.0$ g/m²; (d) $m_{b,s}^0 = 1.5$ g/m²

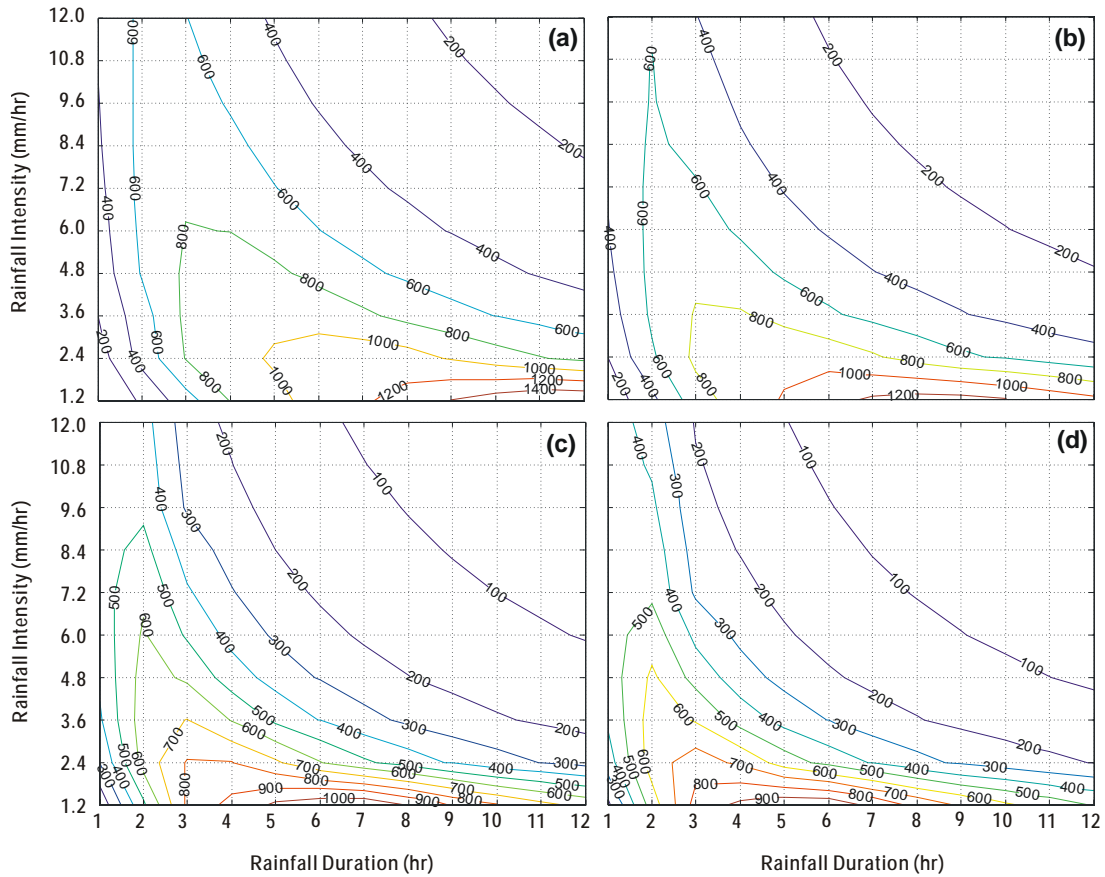


FIGURE 5.20 Contours of the maximum watershed length at $MFF_{20} = 2.5$ as a function of rainfall intensity and duration for different slopes at $m_{b,s} = 1.0 \text{ g/m}^2$ and $K_p = 10^{-5} \text{ cm/sec}$: (a) $S_o = 0.01$; (b) $S_o = 0.02$; (c) $S_o = 0.04$; (d) $S_o = 0.06$

5.4.2 BMP design for Highway Runoff

For treating MFF of highway runoff, the location and number of storm-drain inlets can be adjusted based on the WL_{des} for a given rainfall and slope condition of the catchment.

Figure 5.21 illustrates conceptual design of collection system in the highway runoff

BMPs. Inlet 1 and inlet 2 can be located based on the L_1 and L_2 , which are determined

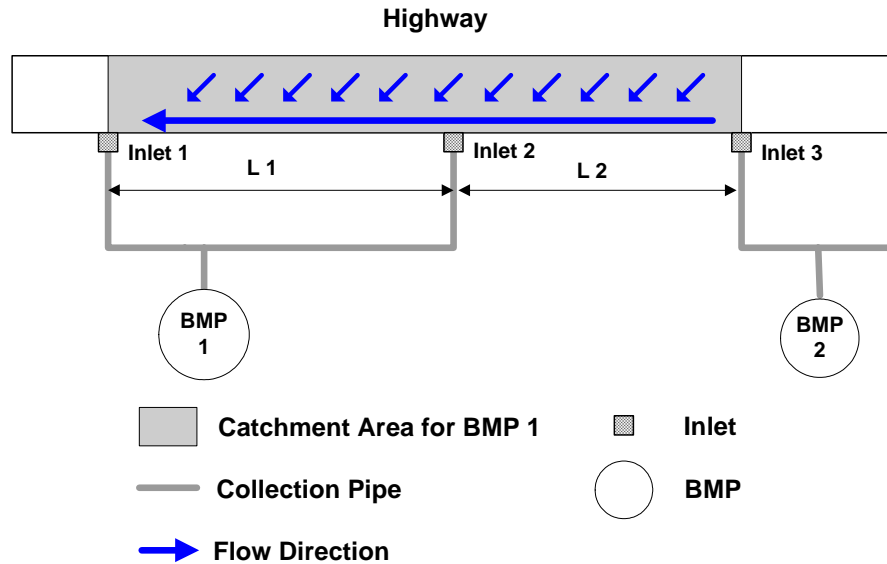


FIGURE 5.21 Collection system design in the highway runoff BMPs

as WLs to generate a required MFF ratio (e.g. $MFF_{20, \max}$). To determine a WL, the contours previously described can be used. The collection pipes can be designed to ensure rapid delivery of the runoff, minimizing attenuation of combined MFF ratio.

For example, when a designer needs to determine WL (i.e. L_1 or L_2 in Figure 5.21) for site 3, the contours in Figure 5.17 and Figure 5.19 can be used because the bed slope is 0.02. The ellipse in the Figure 5.19(c) shows the region corresponding to the mean values of observed rainfall intensity and duration ($I = 3.8$ mm/hr, $T = 8.2$ hr) surrounded by 1 standard deviation that were observed using three years' monitoring data at site 3. Although an alternative design rainfall can be chosen inside the ellipse area, the mean values are selected in this design example. The design value of $m_{b,s}^0$ is set to 1.0 g/m² assuming 17 days of ADD, which is three years' average during wet season in this site. Therefore, Figure 5.17(c) and Figure 5.19(c) can be used for these design conditions.

That is, a designer can select a value for WL_{des} between 8 m and 400 m, which can be read in Figure 5.17(c) and Figure 5.19(c) as the lower and upper boundaries of the WL, respectively.

5.4.3 BMP Design for Parking Lots

The concepts of design MFF ratio and watershed length can be also applied for the design of simple-geometric 2-D watersheds such as parking lots, which is known as a non-point pollutant source in urban landuses (Sonstrom et al, 2002). Although the dimension of the parking lots is generally determined by the site conditions, a typical geometry is a simple rectangle. Therefore, rectangular-type watersheds will be discussed in this study. For accurate MFF simulation for complex 2-D geometry, 2-D flow model might be necessary.

2-D flow can be characterized by the flow path and degree of flow convergence. From the case study of radial flow performed in the section 5.3, a dominant impacting factor on the MFF ratio is the watershed length (flow distance) rather than flow converging because little change in the curves of MFF ratio was observed in the radial flow compared to the 1-D flow. Therefore, MFF simulation of 1-D flow can be also applicable in BMPs for parking lots. In a rectangular watershed, flow path is determined by slope and inlet location. Therefore, the design concerning is how to locate inlets and slope in order to make the runoff flow a required distance for design MFF ratio (i.e. WL_{des}).

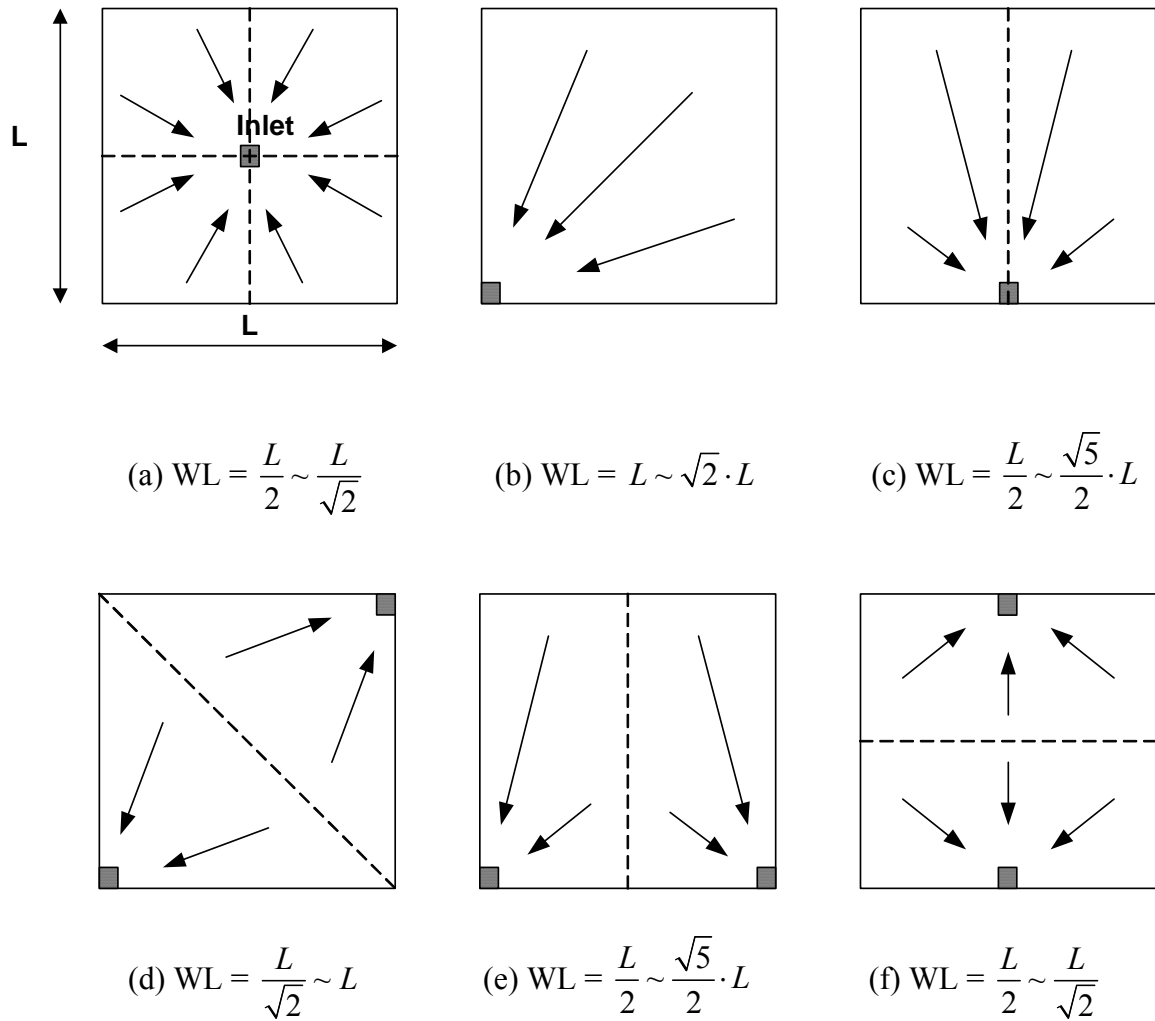


FIGURE 5.22 Different inlet location and watershed length in a square type watershed

Degree of slope is one of the important factors that determine WL_{des} . If the catchment dimension is too small, relatively steeper slope can be used for smaller WL_{des} in order to meet the criteria for MFF ratio. On the contrary, if the catchment dimension is large, lower slope can be used. Number and location of the inlets can be also adjusted under a fixed degree of slope to satisfy WL_{des} . Figure 5.22 shows how the flow direction and flow distance can be changed with different inlet locations in a given square type catchment

area. Slope directions were assumed to be always toward the location of inlets. The arrows represent the flow direction and WLs (flow distances) were calculated for six different cases from case (a) to (f). Case (a) and (f) are equivalent in terms of WL but have different numbers and locations of inlets. Case (a) is a better design than case (f) for the economic point of view because case (a) has fewer inlets. Similarly, case (c) and (e) are also equivalent watersheds for the same reason. Case (a), (b) and (c) containing only one inlet, have different WLs depending on the inlet location. According to the required MFF ratio, different strategies can be adapted in selecting the number and location of the inlets in a catchment area.

5.4.4 Potential Improvement of BMP Performance by Optimal Design

This section discusses the potential improvement of pollutant removal efficiency that can be obtained from different inlet designs for site 3. The design follows the procedure already described in the section 5.4.2. The evaluated pollutant for this discussion is Cu instead of COD because Cu is one of the most frequently observed and has relatively large emission rate among heavy metals in the highway runoff.

The $m_{b,s}^0$ for Cu at ADD = 17 days was calculated as 0.23 g/m^2 using the buildup formula provided in Table 5.3. Referring Table 5.2, ε_s and ε_l' for Cu were 0.88 sec/m^2 and $0.0016 \text{ g}\cdot\text{sec/m}^4$, respectively. Using those design parameters and design rainfall intensity and duration ($I = 3.8 \text{ mm/hr}$, $T = 8.2 \text{ hr}$), the MFF₂₀ curve for Cu can be obtained by the model simulation as shown in Figure 5.23 (Of course, contours of WL can be used instead if they are available). As shown in the figure, four different values of

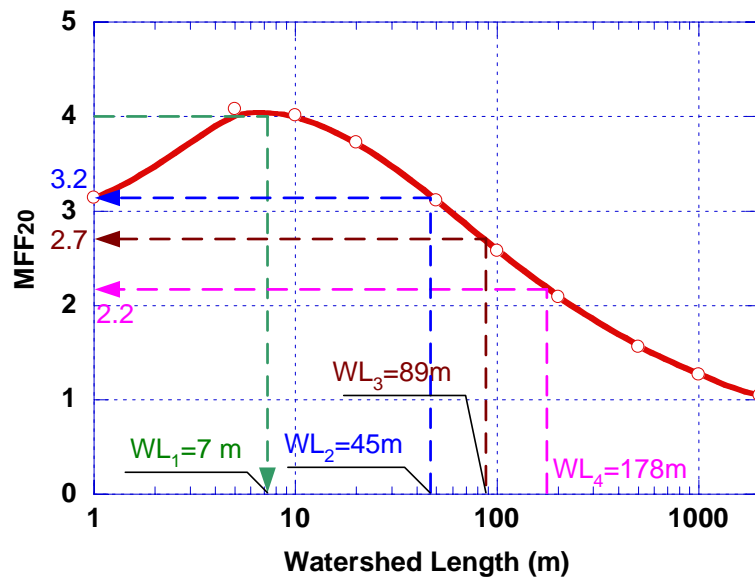


FIGURE 5.23 Determination of design watershed length based on a MFF₂₀ curve for Cu

WL were evaluated for WL_{des} (WL₁ = 7 m, WL₂ = 45 m, WL₃ = 89 m and WL₄ = 178 m). WL₁ was selected as WL_{opt} and the other WLs were selected based on different numbers of storm-drain inlets to be installed. The removal efficiency of Cu is evaluated for those different design conditions of storm-drain inlets with and without polymer addition. The removal efficiency with polymer addition was estimated based on the results of particle destabilization study described in Chapter 6 and Appendix F. Table 5.7 summarizes the final evaluation results assuming only 20% of total runoff was treated and removal efficiency of dissolved Cu is zero. There was little improvement in Cu removal using only gravity settling by maximizing MFF ratio because the settling efficiency is very low. As the removal efficiency increases, there is greater value in capturing the first flush. For

example, the removal efficiency increases from 16.4% to 30.2% by maximizing the first flush using only 24-hour settling. If polymer flocculation used, the absolute particle removal efficiency increases to 37.2%, and maximizing the first flush increases the overall efficiency to 67.6%. The optimum inlet design provides greater benefit with more efficient particle removal processes.

TABLE 5.7 Performances of BMPs with Different Designs

Parameter Evaluated		WL _{des}			
		WL ₁ (7 m)	WL ₂ (45 m)	WL ₃ (89 m)	WL ₄ (178 m)
Number of Inlets		26	4	2	1
Design MFF ₂₀		4.0	3.2	2.7	2.2
Removal Efficiencies of Particulate Cu ^a	24h Gravity Settling	30.2%	23.8%	20.1%	16.4%
	72h Gravity Settling	30.6%	24.4%	20.6%	16.8%
	Flocculation with Polymer (12h Settling)	67.6%	54.1%	45.7%	37.2%

^a It is assumed that only 20% of total runoff is treated

Particle Destabilization in Highway Runoff

6.1 PARTICLE AGGREGATION OVER TIME

Throughout the course of the experimental program, small changes in runoff samples were noted as storage time increased. By measuring the PSD, [Li et al \(2005a\)](#) was able to quantify the differences and develop a sampling protocol that avoided PSD change during storage. The natural aggregation of particles during sample storage is a problem for quantifying stormwater quality, but can be an advantage for BMP development. Increases in particle size generally improve settling and filtration performance.

To understand the magnitude of the changes in TDS and TSS, a series of experiments were performed to monitor changes over time. Figure 6.1 shows the result of one experiment and displays the concentration changes for TSS and TDS in the runoff water with respect to the time. The sample was collected on 2/6/05 and shows results with and

without slow mixing. Slow mixing was provided by a magnetic stirring bar operating at 100 rpm and providing a G factor of 9.3/s.

TSS concentration increased by about 30% and TDS concentrations decreased by about 10% of initial values during the first 100 hr for both mixed and unmixed samples. No significant changes in the concentration of TSS and TDS were observed after 240 hrs. In the mixed sample, TSS increased rapidly within 50 hrs and plateaued at about 300 mg/L after 100 hrs. The unmixed sample showed similar trends but required longer time to reach steady state. Steady state concentration of TSS in the unmixed sample was a little bit higher than that of mixed sample, although there are too few data points to evaluate significance. This might be because unmixed sample is free from fluid shear or agitation that would cause particle breakup. The decrease of TDS in the mixed and unmixed samples might imply that a portion of dissolved solid transforms to the suspended solid through aggregation. The increase in TSS does not balance the decrease in TDS, and this might be due to the definition of dissolved solids, which are defined as less than 0.45 μm , as opposed to being truly dissolved.

Figure 6.2 compares the PSD changes over time in the mixed and unmixed samples. The number of smaller particles decreased dramatically over time and larger particles increased in number. The particle change was more rapid in the mixed sample than unmixed sample. In the unmixed sample, there was an increase in particles smaller than 1 μm up to 48 hours and then a decrease with most particles disappearing after 264 h. Particles larger than 10 μm generally increased. For the mixed sample, changes in PSD occurred much more rapidly. The number of smaller particles at 24 and 48 hours was

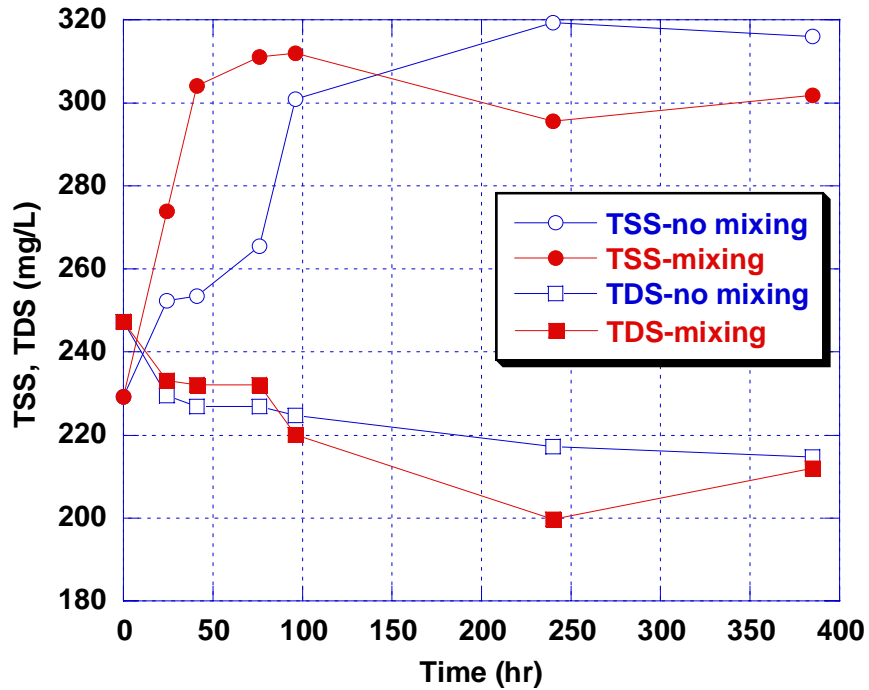


FIGURE 6.1 TSS and TDS changes over time from the observation of natural aggregation on 2/6/05

nearly the same as the original number and then decreased until 264 hours. The increase in small particles that occurred in the sample without mixing either did not occur with the mixed sample or occurred so rapidly that it was not observed (no observations were made between 0 and 24 hours).

This experiment demonstrates that the particles in highway runoff naturally aggregate over time and mixing can increase aggregation rate. However, the time required for the particle aggregation might not be sufficiently short for the practical application. As a result, additional efforts for destabilizing particles are needed.

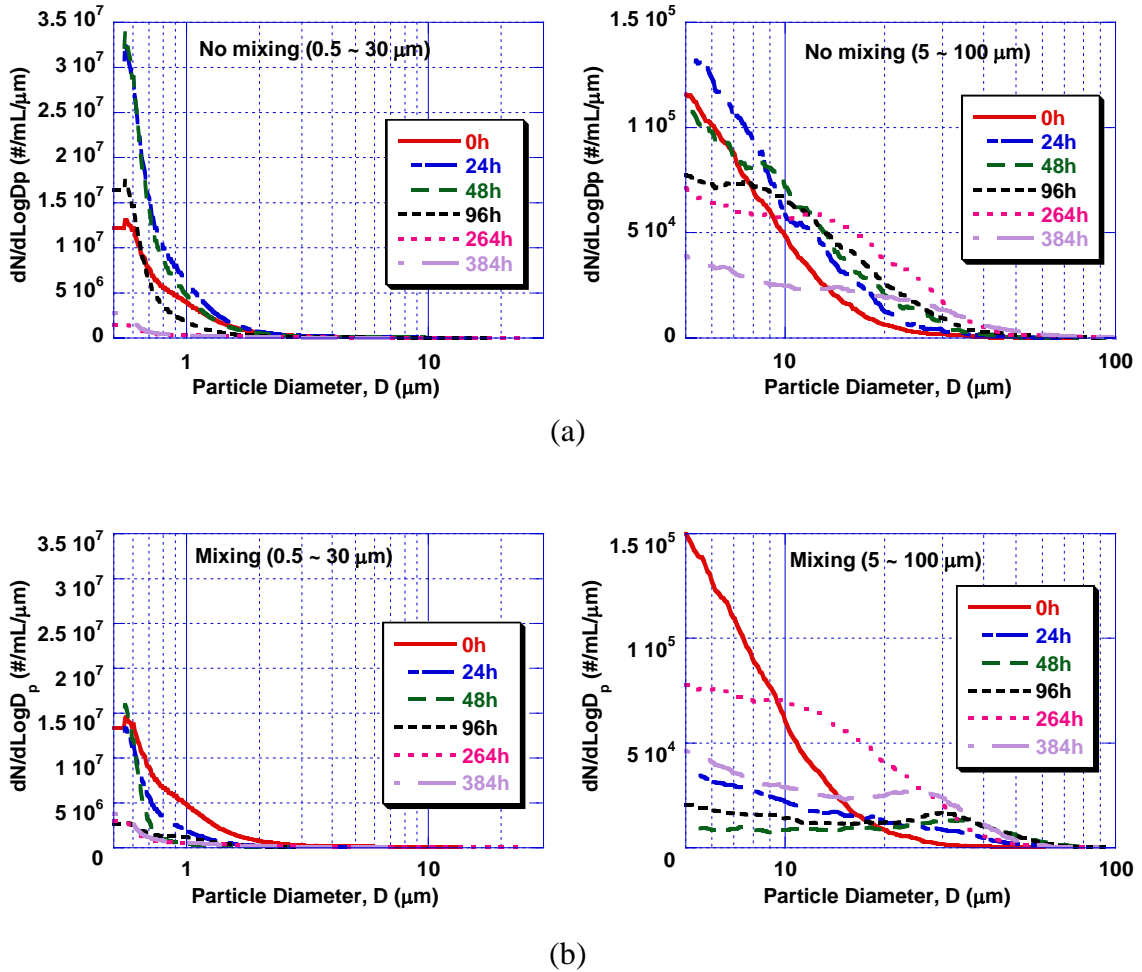


FIGURE 6.2 PSD changes over time on 2/6/05: (a) Without mixing; (b) With mixing

6.2 LOW DOSE FLOCCULATION

The first series of experiments used low dosages of coagulants to avoid pH changes that might occur with the low alkalinity runoff and to avoid the expense of high coagulant dose and resulting sludge production. Figure 6.3 shows the turbidity removals in the low

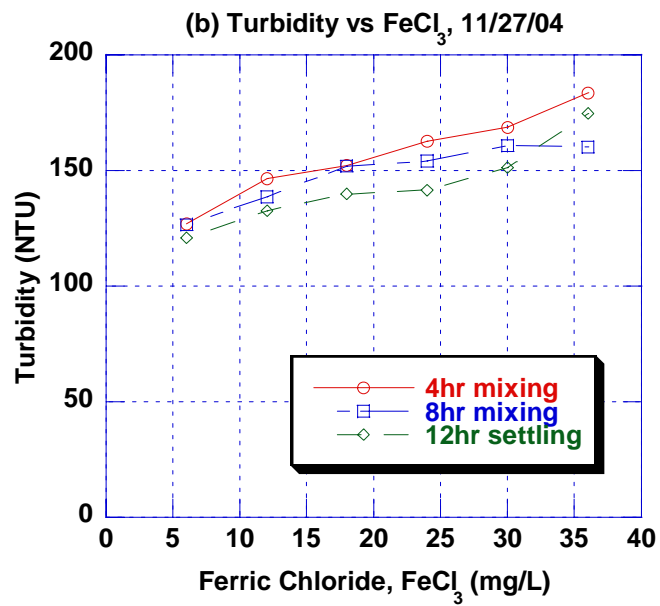
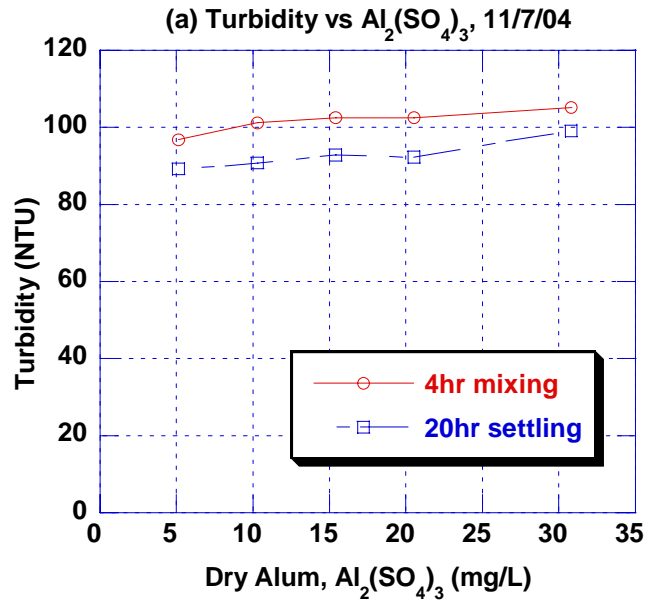


FIGURE 6.3 Turbidity changes in the samples in low dose coagulation: (a) Alum; (b) Ferric chloride

dose coagulation tests for two different storm events using alum and ferric chloride. In these tests, alum or ferric chloride was added in varying amounts up to 40 mg/L, which were did not produce sweep floc. Figure 4.25 shows that in low dosages, neither coagulant is able to produce settable particles but instead forms pin flocs, increasing turbidity. Settable particles were never produced even though extended periods of slow mixing were investigated. This conditioning might have been useful for granular media filtration, but was not investigated.

6.3 SWEEP FLOC COAGULATION

Figure 6.4 shows the results of turbidity removal using sweep floc coagulation with alum and ferric chloride respectively. Each storm event had a different optimum dose and the range was from approximately 40 to 500 mg/l. Optimum dose was defined as the minimum coagulant concentration required to produce less than 5 NTU.

The optimum does was plotted as a function of specific conductivity in Figure 6.5, showing that the optimum does is proportional to the initial conductivity. This relationship is not due to changing electro chemical properties with conductivity, but from the higher concentrations of dissolved and colloidal material, which consume more coagulants for destabilization. [Han, et al., \(2004\)](#) found that initial turbidity is related to dilution of the stormwater, with more heavily contaminated stormwater having higher initial conductivity. Other parameters such as TSS might be better indicators of coagulant

does, but conductivity can be easily measured in real-time, allowing it to be used for control. This result suggests that an automatic controller could use sample conductivity to adjust coagulant dose.

Figure 6.6 shows the turbidity and ZP changes as a function of alum and ferric chloride doses. For both alum and ferric chloride, the isoelectrical point of ZP could not be obtained, and sweep floc was routinely observed at -20 to -10 mV ZP. Alum was slightly more effective than ferric chloride in terms of turbidity removal and ZP reduction (all experiments performed at pH 7). The higher efficiency of alum over ferric chloride may result from its wider optimum pH range.

One test was performed to evaluate the impact of ionic strength on coagulation efficiency. Sodium chloride (NaCl) was added over the range of 10,000 to 50,000 mg/L in a series of jar tests. No significant drop in turbidity was observed in this range of salt concentration. However, at 30,000 mg/l NaCl the required alum or ferric chloride concentration was reduced to approximately 25% of the dose required without salt.

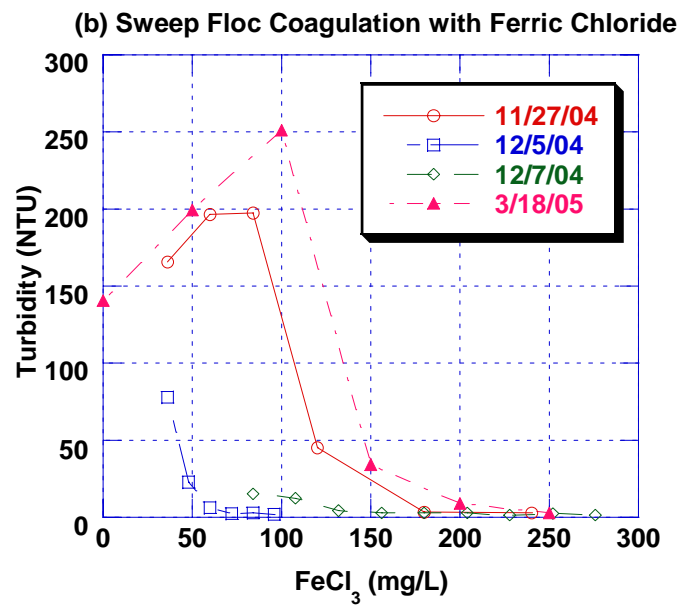
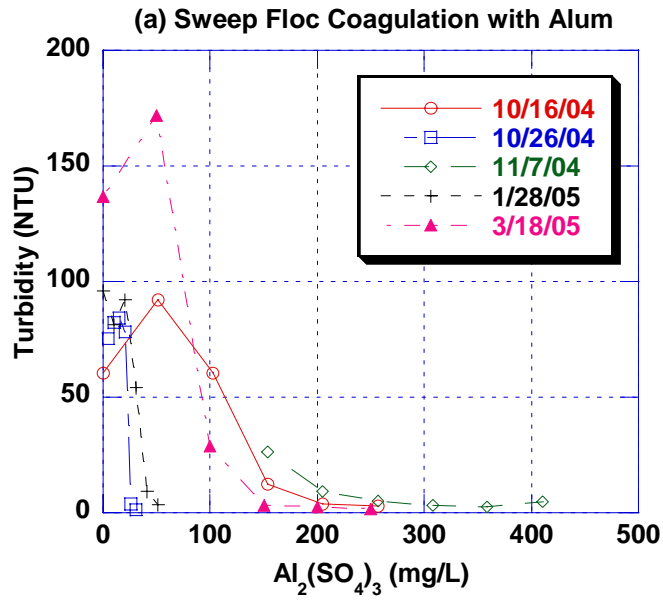


FIGURE 6.4 Turbidity removal from sweep floc coagulation: (a) Alum; (b) Ferric chloride

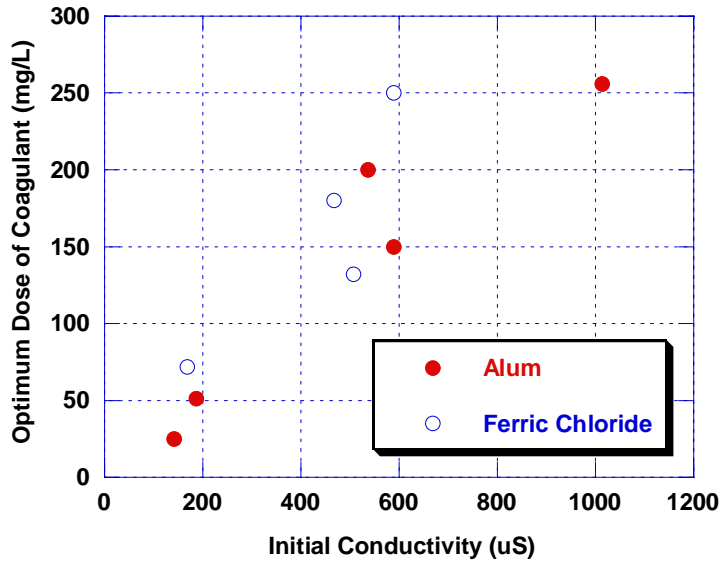


FIGURE 6.5 Optimum coagulant dose and initial conductivity

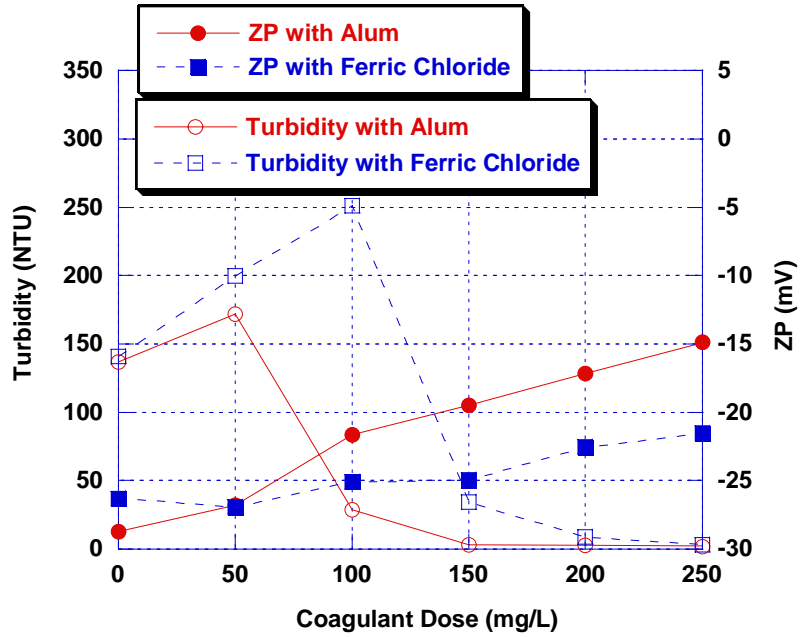


FIGURE 6.6 Turbidity and ZP changes after adding same serious of amounts for alum and ferric chloride on 3/18/05

6.4 FLOCCULATION WITH CATIONIC POLYMER

Figure 6.7 shows the ZP changes as a function of polymer dose for two different molecular weight polyDADMACs. Both polymers were equally effective in reducing the ZP. Figure 6.8 shows the isoelectric point as a function of initial conductivity, which is similar to the previous results showing optimum alum or ferric chloride dose related to initial conductivity.

Figure 6.9 shows the effect of mixing time on the turbidity removal with and without polymer. As can be seen, at least six hours were needed to reduce turbidity to less than 5 NTU after particles were destabilized. An extended mixing period might be required for particle aggregation and sedimentation even though the isoelectric point is reached by adding polymers.

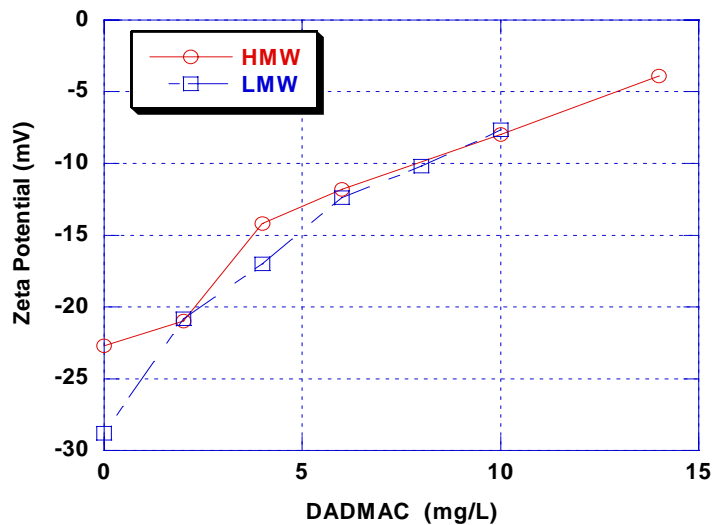


FIGURE 6.7 ZP changes in the sample after adding two different molecular weight polyDADMACs on 2/6/05

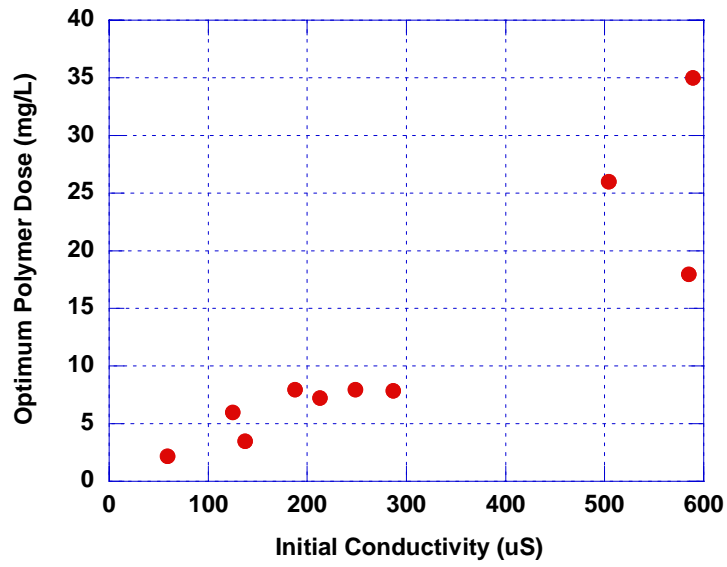


FIGURE 6.8 Optimum polymer dose and initial sample conductivity

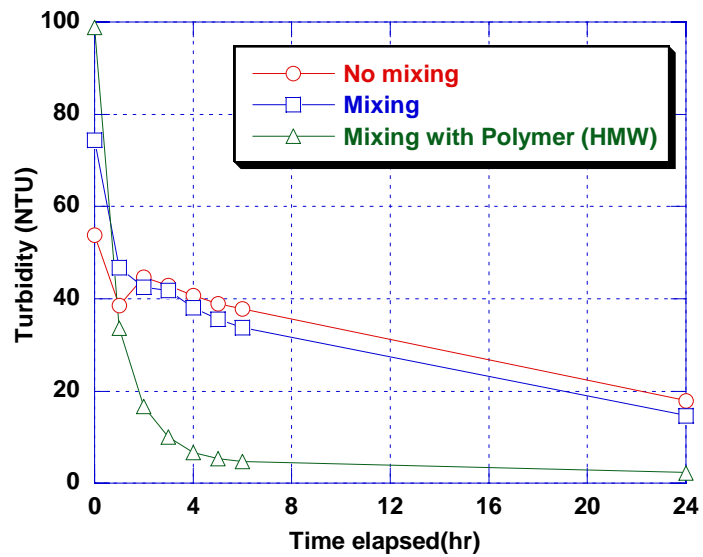


FIGURE 6.9 Effect of mixing time on the turbidity removal with and without polymer on 1/28/05

Figure 6.10 shows the effect of alum addition on the mixing time in the flocculation using the polymer on 1/28/05. Turbidity removals are displayed with slow mixing and after settling for different alum doses from 2.6 to 15.4 mg/L with 8 mg/L polymer dose, which was the optimum dose for this storm event. As more alum was added, shorter mixing time was required to reduce the turbidity in the supernatant. As a result, mixing time required for the flocculation by combining polymer and other coagulants such as alum or ferric chloride can be reduced.

Figure 6.11 shows that particle sizes were dramatically increased after coagulation. The vertical axis shows the relative decrease in the number of particles in a given size range, which is shown on the horizontal axis. Relative decrease is calculated relative to the initial particle concentrations. The various lines show a time series from just after rapid mixing to 8 hours and the final line shows the particle concentration after sedimentation. The graph shows that the relative number of smaller particles in the 2-3 μm to 20-30 μm ranges increases rapidly after dosage and initial mixing. This is direct evidence for particle aggregation. After settling the numbers of particles is much lower in all size ranges. The 12 hr settling line can also be thought of as removal efficiency. The low, medium (not shown) and high molecular weight polymers produced similar results.

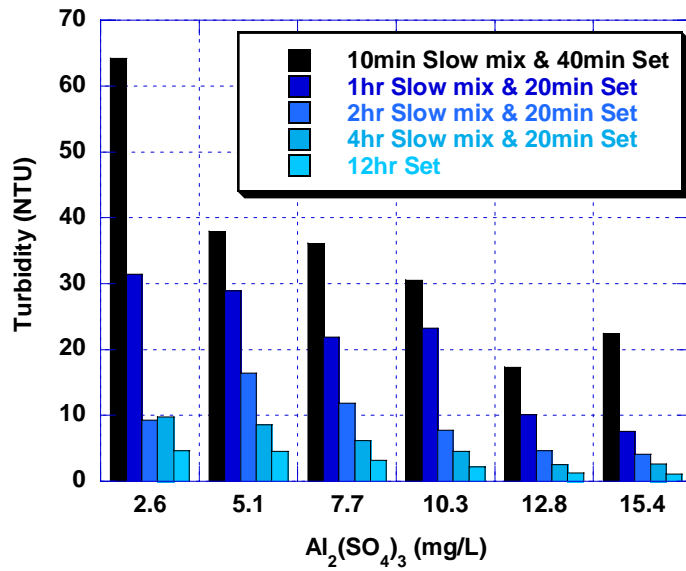


FIGURE 6.10 Effect of alum addition on the mixing time using polymer coagulation on 1/28/05 (polymer concentration was fixed at 8 mg/L)

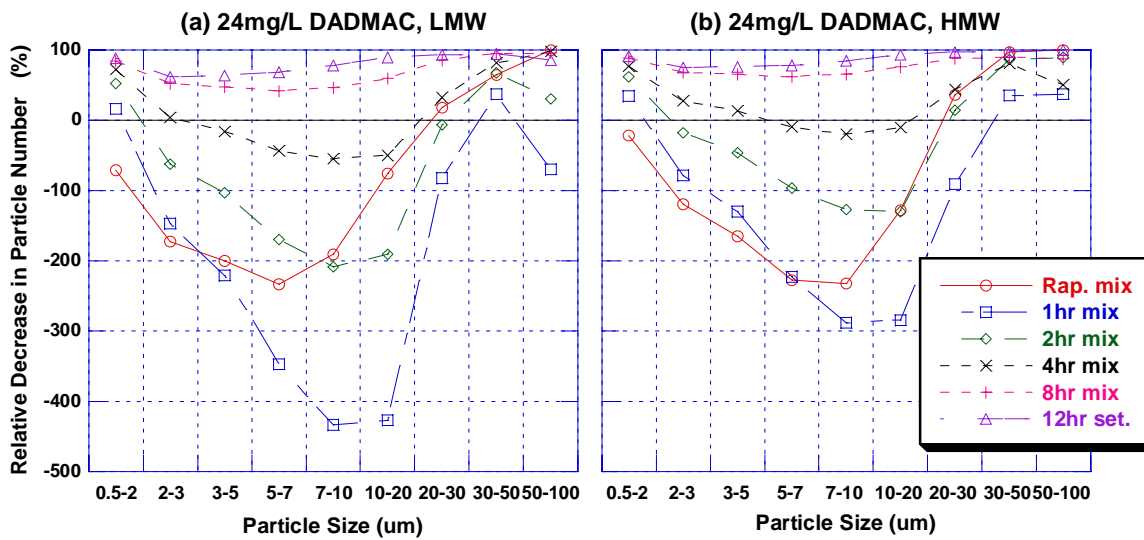


FIGURE 6.11 PSD changes with different molecular weight polymers on 2/11/05: (a) LMW; (b) HMW

6.5 REMOVAL OF DISSOLVED HEAVY METALS

Figure 6.12 displays the dissolved phase concentrations of seven species of heavy metals in the treated water from sweep floc coagulation with alum, ferric chloride and flocculation with polymer on 3/18/05. Figure 6.12(a) and (b) show that dissolved heavy metals except Ni can be reduced in proportion to the amount of alum or ferric chloride added. The removal efficiencies of dissolved Cr, As, Cd, As, Cu were over 50% at the sweep floc regimes of alum and ferric chloride. Dissolved Zn dramatically declined with the addition of alum or ferric chloride, and the maximum removal efficiency was over 85%. The spike of dissolved Pb at 50 mg/L of ferric chloride (Figure 4.12(b)) was probably due to sample contamination. PolyDADMAC was not effective in removing dissolved heavy metals as revealed in Figure 4.12(c) although dissolved Cr and Pb were selectively removed to some extent. Dissolved Ni could not be removed in both sweep floc coagulation and flocculation with polymer.

Figure 6.13 and 6.14 show turbidity, zeta potential, concentration and removal efficiency of dissolved metals in the treated runoff with combined polymer and alum dose at 8 and 16 mg/L. As can be seen, combinations of polymer and alum effectively remove turbidity with short mixing time (~10 min). Dissolved Pb was removed up to 60% with comparatively large amount of polymer (polyDADMAC > 6 mg/L). Dissolved As was removed up to 40% at alum = 16 mg/L. This removal may have been due to precipitation or it could be a result of aggregation of particles less than 0.45 μm . Metals adsorbed to particles less than 0.45 mm will be classified as suspended by the analytical methods. In no cases did the combination of polymer and alum achieve remarkable removal high removal of dissolved heavy metals.

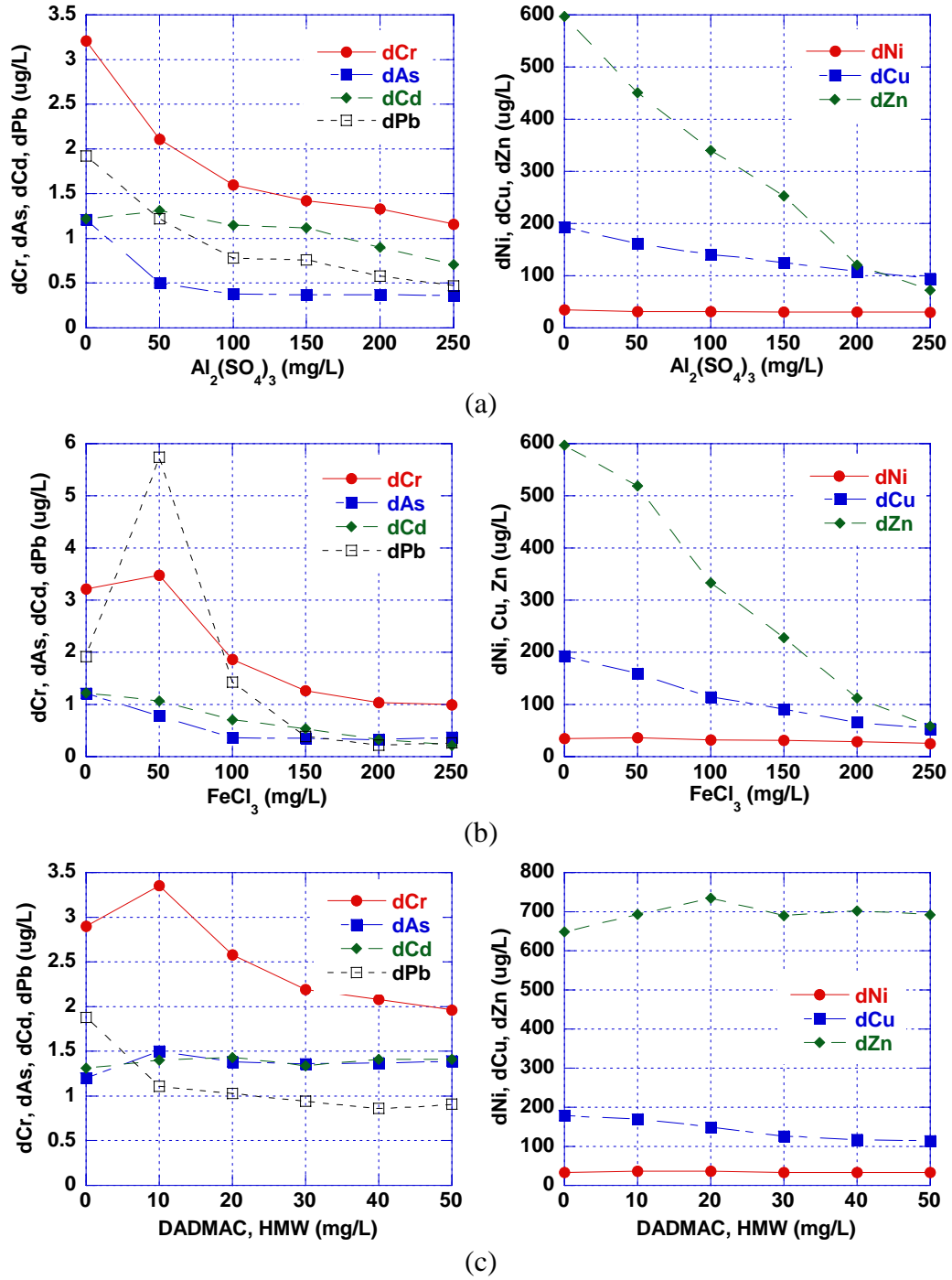


FIGURE 6.12 Dissolved metal concentrations in the treated runoff from different coagulation/flocculation tests on 3/18/05: (a) Sweep floc coagulation with alum; (b) Sweep floc coagulation with ferric chloride; (c) Flocculation with polymer

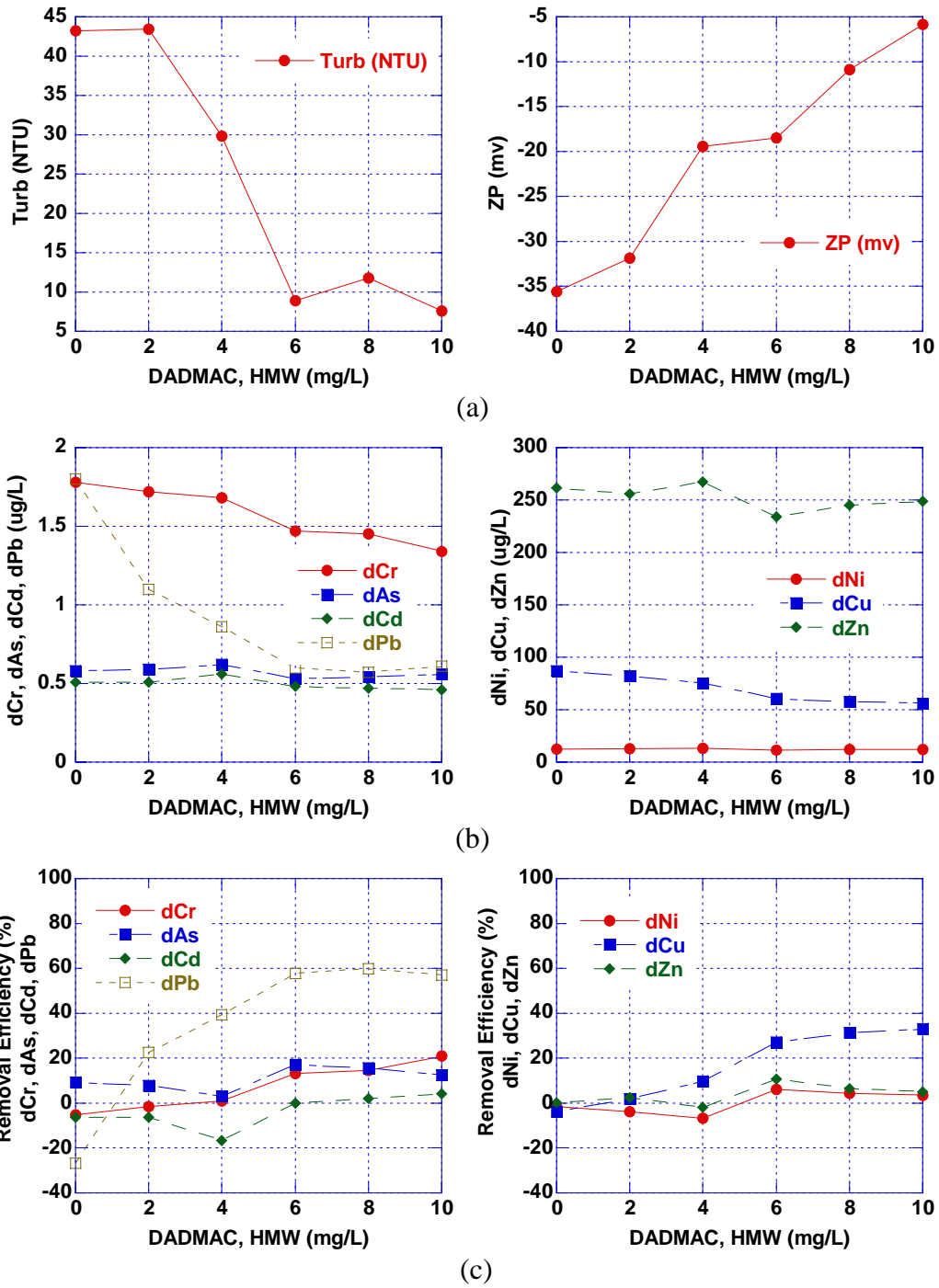


FIGURE 6.13 Coagulation results with different polymer doses at alum = 8 mg/L on 4/28/05: (a) Turbidity and zeta potential; (b) Concentrations of dissolved metals; (c) Removal efficiencies of dissolved metals

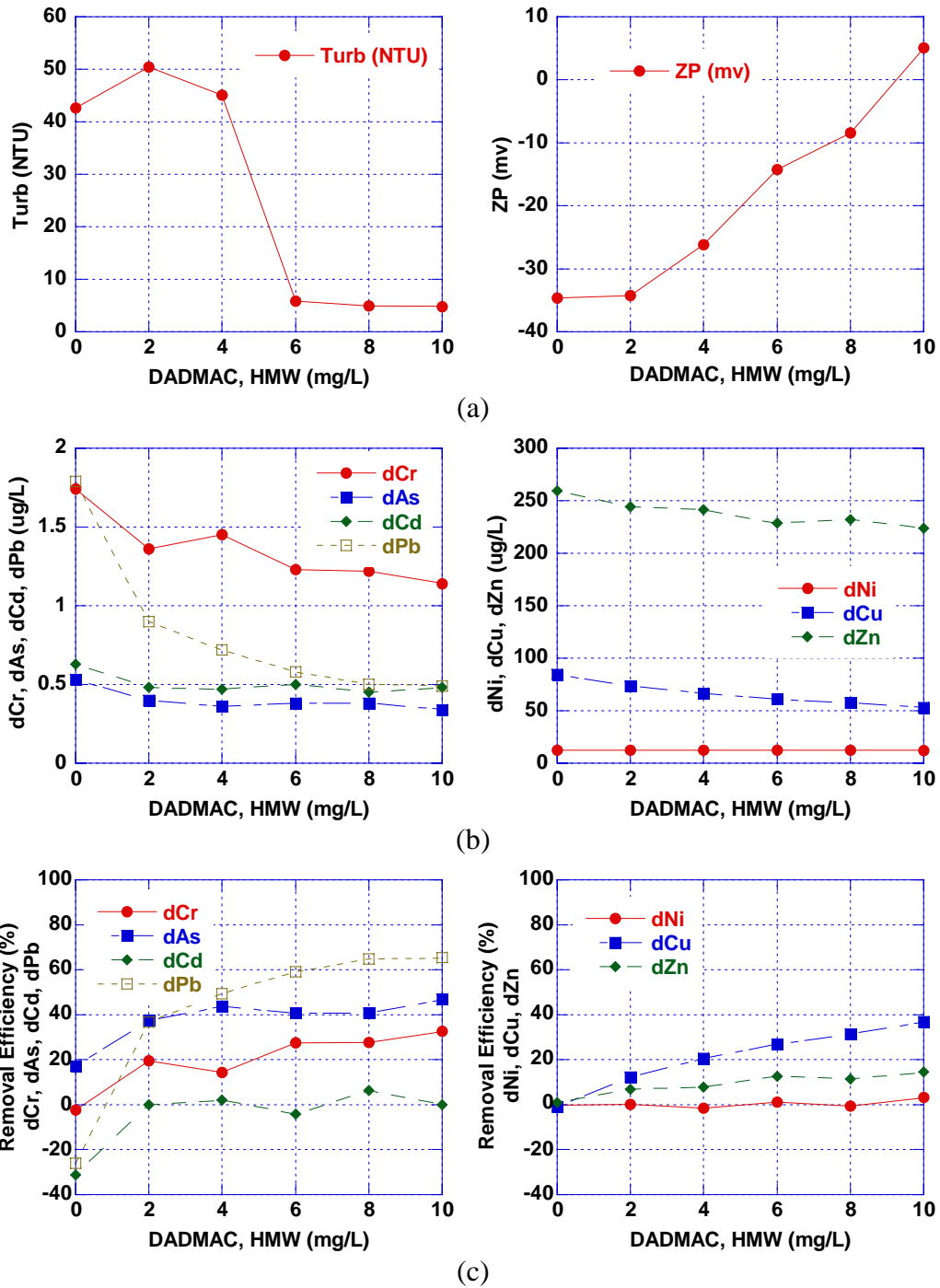


FIGURE 6.14 Coagulation results with different polymer doses at alum = 16 mg/L on 4/28/05: (a) Turbidity and zeta potential; (b) Concentrations of dissolved metals; (c) Removal efficiencies of dissolved metals

6.6 DISCUSSION

Coagulation can greatly increase particle sizes in stormwater runoff, which will make sedimentation BMPs much more efficient, especially for small particle removal. [Li, et al. \(2005b\)](#) proposed a two-compartment sedimentation tank with a first compartment to hold the initial runoff volume (first flush) for an extended period of time and a second compartment to treat the rest as a continuous flow clarifier. By holding the first flush and treating the remaining volume in a continuous flow clarifier, the two-compartment settling tank removed both small and large particles in stormwater runoff. This concept can be extended using coagulation and flocculation.

Based upon the results from particle settling experiments, only 27.1% and 27.5% particle mass reductions were possible for in settling basins with 24 and 72 hr retention times, respectively, using a storage tank designed to capture a 26 mm rainfall. In contrast, 90% of total particle mass was removed by providing 8 hr slow mixing and 4 hr settling with polymer addition.

Removal efficiencies of heavy metals were also evaluated utilizing the particle removal efficiency and metal-particle mass ratio reported by [Morquecho and Pitt \(2003\)](#) (refer to Table 2.1). The suspended solids reduction with polymer addition can reduce approximately 85% of particulate Cu and Zn, which correspond to the total removal efficiencies of 35% and 23% for Cu and Zn, respectively (see Appendix F).

Jar testing using metal salts was ineffective in removing particles at low concentrations and required high dosages well into the sweep floc regime for efficient

particle removal. The need for sweep floc increases costs due to coagulant cost and excess sludge production. In addition, the acidic nature of both metal salts will require neutralization, as well as further increase costs. A cationic polymer was effective in coagulating the stormwater runoff at low dosages and did not modify the pH. Additional mixing was necessary to effect efficient particle aggregation. The addition of small amounts of alum (2 to 15 mg/L) reduced the mixing time as well as dissolved heavy metals and suggests that a regime using polymer, followed by alum, is a good way to destabilize particles and enhance heavy metal removal in highway runoff.

BMPs in the field need unattended operation, as well as robustness because pollutant concentration in the highway runoff always changes as a function of rainfall characteristics, antecedent dry days, average daily traffic, and other factors. Therefore, runoff concentration is different for each storm event and BMPs must be able to cope with a range of influent concentrations and flow rates without special controls. A combination of cationic polymer with small amounts of alum and sufficient mixing time should enable effective colloid removal without close monitoring of dosages. Unattended polymer addition (automatic) to the first compartment can be also easily achieved by using the initial conductivity of the runoff and the fixed compartment volume. Unattended polymer addition to the continuous flow compartment needs further investigation due to the dynamic runoff retention time. Further studies on particle change with different mixing periods with polymer addition are on-going in our laboratory.

Conclusion

This dissertation developed a methodology for design and operation of best management practices (BMPs) for paved landuses such as highways and parking lots. To take the economic advantage of treating first flush, the MFF ratio can be maximized by means of adjusting the number and location of the storm-drain inlets, thereby changing the watershed length (i. e. catchment size). The developed 1-D model can be utilized to determine the watershed length to obtain the minimum required MFF ratio. In addition, the coagulation experiments revealed more efficient operating conditions for treating first flush in a settling basin, a common stormwater BMP.

Mass First Flush Modeling

Highway runoff was modeled as 1-D flow problem using the kinematic wave equation coupled with mass transport and erosion equation. The model parameters were calibrated using three years' monitoring data obtained from a highway site in west Los Angeles.

Calibrated parameters were initial mass and erosion equation coefficients developed by introducing two different pollutant source terms. Using the developed model, MFF simulations were performed. Through the first flush modeling study, the following conclusions are made:

1. The results from parameter estimation in 1-D model showed that there was no significant variations among the erosion coefficients for short-term sources for COD, conductivity, Zn and Cu. The initial mass and erosion rates of the long-term sources showed large differences among those constituents.
2. Different types of buildup formulas were fitted with calibrated initial mass and exponential and Michaelis-Menton type curves were useful to predict pollutant mass in a stormwater runoff.
3. The qualitative relationship between MFF and affecting factors such as rainfall intensity, duration, infiltration rate, slope, initial mass, erosion coefficients and watershed length were obtained using the developed 1-D model.
4. Mass first flush simulations showed that extremely short watershed lengths cannot develop sufficient flow energy for pollutant mobilization, and only low MFF can be observed. Extremely long watersheds also cannot achieve high MFF ratios due to long transport time. Therefore, it is necessary to optimize the size of catchment area so that the maximum MFF ratio can be captured by the BMPs.
5. Contours of watershed length constructed by MFF simulations using different conditions of weather and watershed geometry can be used in determining

location and number of storm-drain inlets for the BMPs for highway runoff.

Those contours are also applicable for the BMP design of simple 2-D structures with converging flow (radial flow) such as parking lots. Converging flow is common in 2-D watersheds and does not significantly change the mass first flush behavior that is observed in 1-D flow.

6. Although the MFF ratio may be maximized, improvement of pollutant removal cannot be guaranteed unless effective particle removal is obtained using additional particle destabilization process.

Coagulation/Flocculation

This research has shown that highway runoff can be effectively coagulated with a combination of metal salts (alum and ferric chloride) and organic cationic polymers. The following conclusions are made:

1. Alum or ferric chloride alone cannot effectively coagulate highway runoff at low concentrations (< 40 mg/L), suggesting that bridging and charge neutralization are not effective mechanisms for this application.
2. Alum and ferric chloride at high doses produced sweep floc that removed turbidity and suspended solids to low concentrations (< 5 NTU). Unfortunately the sludge production and the need for pH control limit this application. Alum appeared to be slightly more effective than ferric chloride. The dissolved

concentrations of As, Cu, Cr, Cd, Pb, and Zn were reduced by as much as 50% during these experiments. Dissolved Ni concentration was unchanged.

3. Small dosages (< 10 mg/L) of an organic polymer in three different molecular weights were useful in obtaining the isoelectric point. Gentle mixing ($G \sim 2.6/s$) over extended periods (~ 8 hrs) was effective in producing low effluent turbidity. Dissolved Pb concentration was reduced by 50% but other metal concentrations were unchanged.
4. The addition of alum (~8 mg/L) after optimal polymer dosing reduced mixing time by 50%.
5. Optimal dosage of metal salts and polymer was proportional to the initial conductivity of the runoff.
6. The removal of dissolved metals, with the possible exception of Pb, occurred only with high concentrations of metal salts. This suggests that removal occurred because of precipitation of truly dissolved metals, as opposed to removal of small particles (< 0.45 μm) that are classified as dissolved due to the working definition of soluble and particulate phases.

Further research is necessary to validate this work at larger scale and over a range of conditions to provide a robust and unattended operation.

Site Descriptions

Figure A.1 shows the map of three monitoring sites located in west Los Angeles, near UCLA campus. The catchments areas ranged from 3,900 to 16,900 m². Traffic loadings are over 269,000 vehicles per day in annual average daily traffic (AADT) and the average rainfall is approximately 330 mm. All sites were equipped with 950 Flow Meters (American Sigma, Loveland, Colorado), tipping bucket rain gauges and composite auto samplers. Site details are provided in Table A.1.

Model parameters were calculated using the rainfall and flow data from site 3 (7-203), which was chosen as an ideal model domain because the site is geometrically simple and meteorologically homogeneous. Site 3 is 21.6-m-wide and 178-m-long rectangular-shape catchment. The average slope is 0.02 with little local variation and there exists only one storm-drain inlet located on the freeway shoulder at the south-most end of the site.

The coagulation experiment was focused on site 2. Site 2 is the largest among the monitoring sites, producing enough runoff volume for the experiment in the first one hour of the storm.

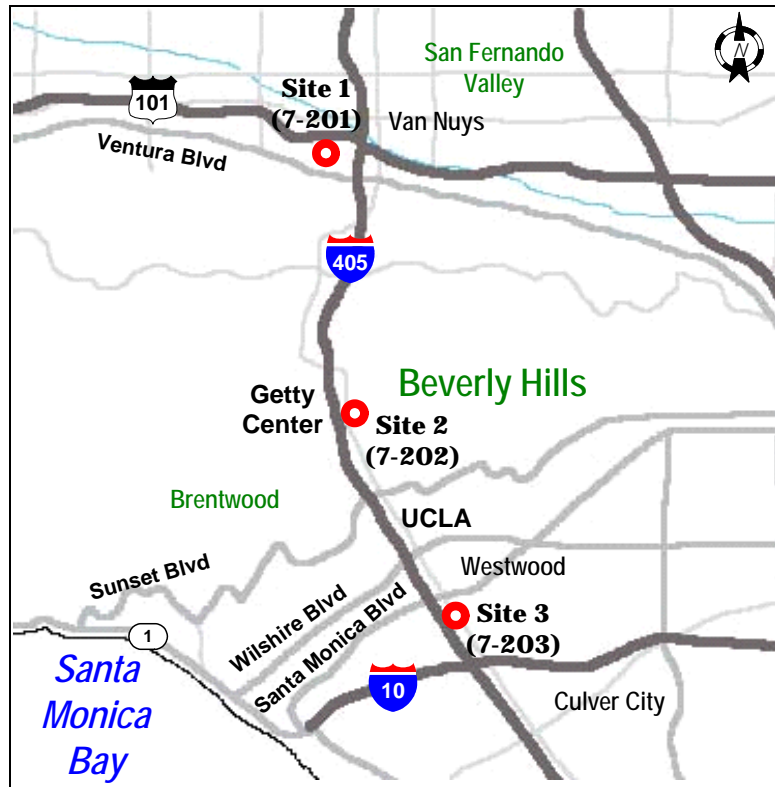


FIGURE A.1 Location of monitoring sites for highway runoff

TABLE A.1 Summary Description of Sampling Sites

Site No.	Location	Freeway / Post Miles	Area (h)	AADT (vehicle/day)	Imperviousness (%)
1 (7-201)	Eastbound US 101	HWY 101 PM 17	1.28	328,000	100
2 (7-202)	I-405 Freeway and Sepulveda Blvd	FW 405 PM 34	1.69	269,000	95
3 (7-203)	Santa Monica Blvd N. Bound Exit on I-405	FW 405 PM 30.8	0.39	322,000	100

Numerical Tests for Radial Flow Problem

A.1 CAM: $WL = 50$ m, $r_o = 1$ m

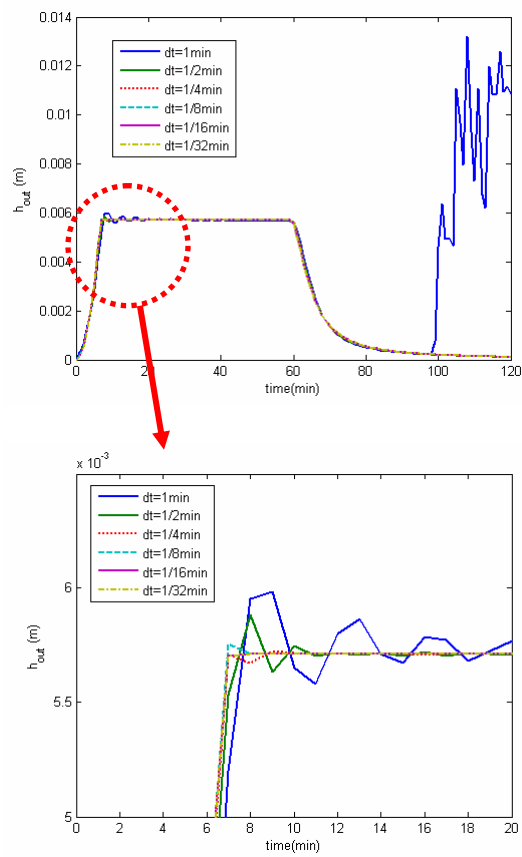
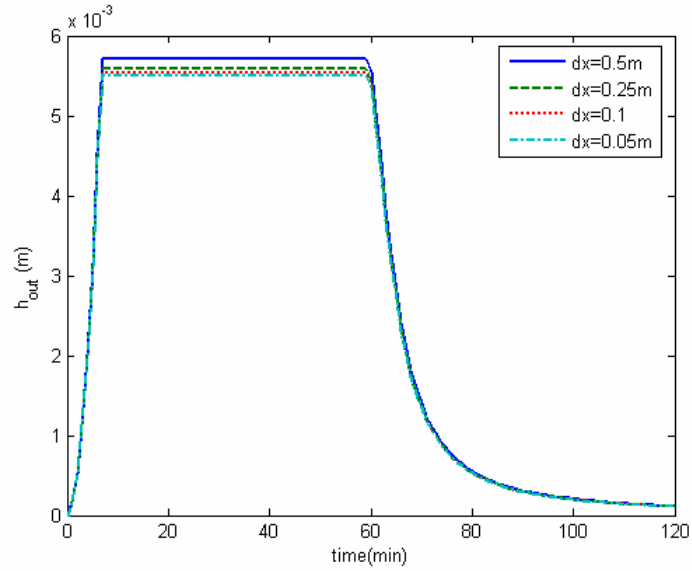
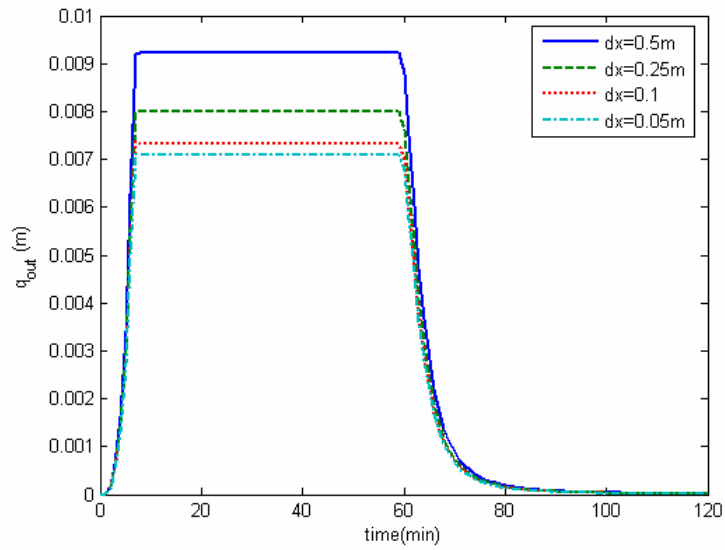


FIGURE A.1 Numerical solutions for the outflow depth using different values of Δt with $\Delta x = 0.5$ m



(a)



(b)

FIGURE A.2 Numerical solutions for the outflow using different values of Δx with $\Delta t = 1/16$ min: (a) depth; (b) flow rate

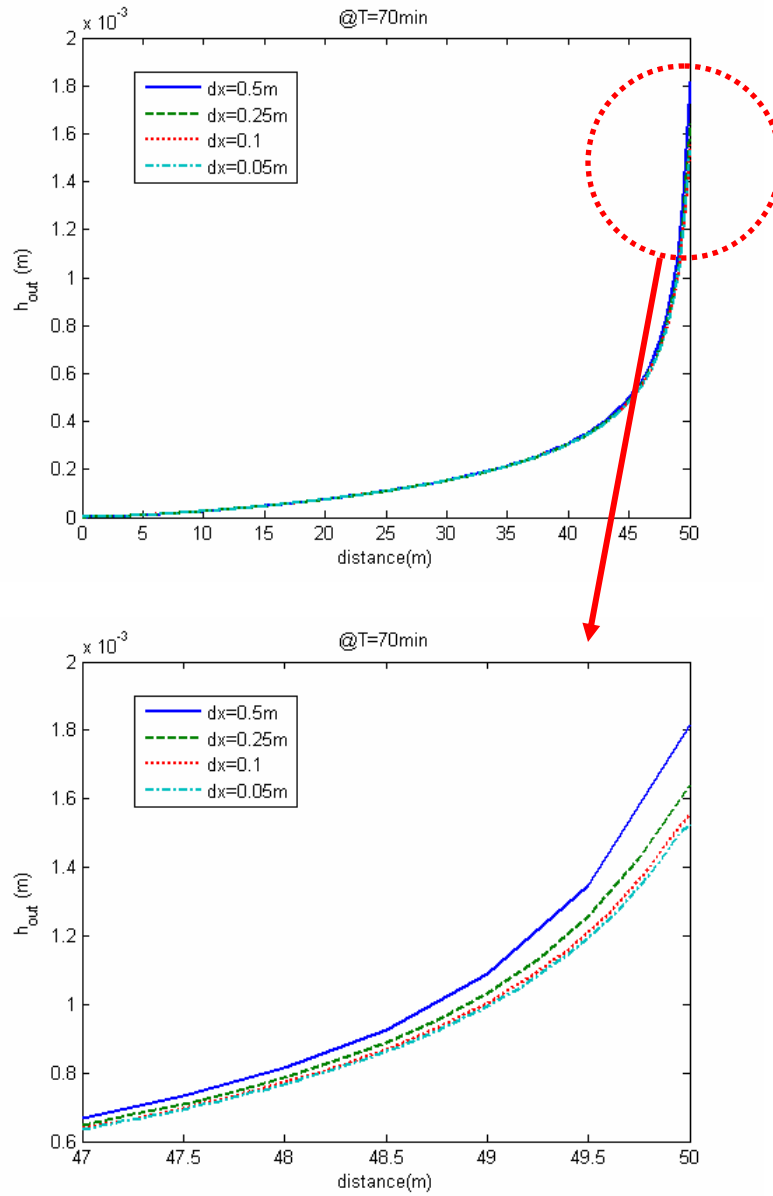


FIGURE A.3 Numerical solutions for the water depth profile along the distance using different values of Δx with $\Delta t = 1/16$ at $t = 70$ min

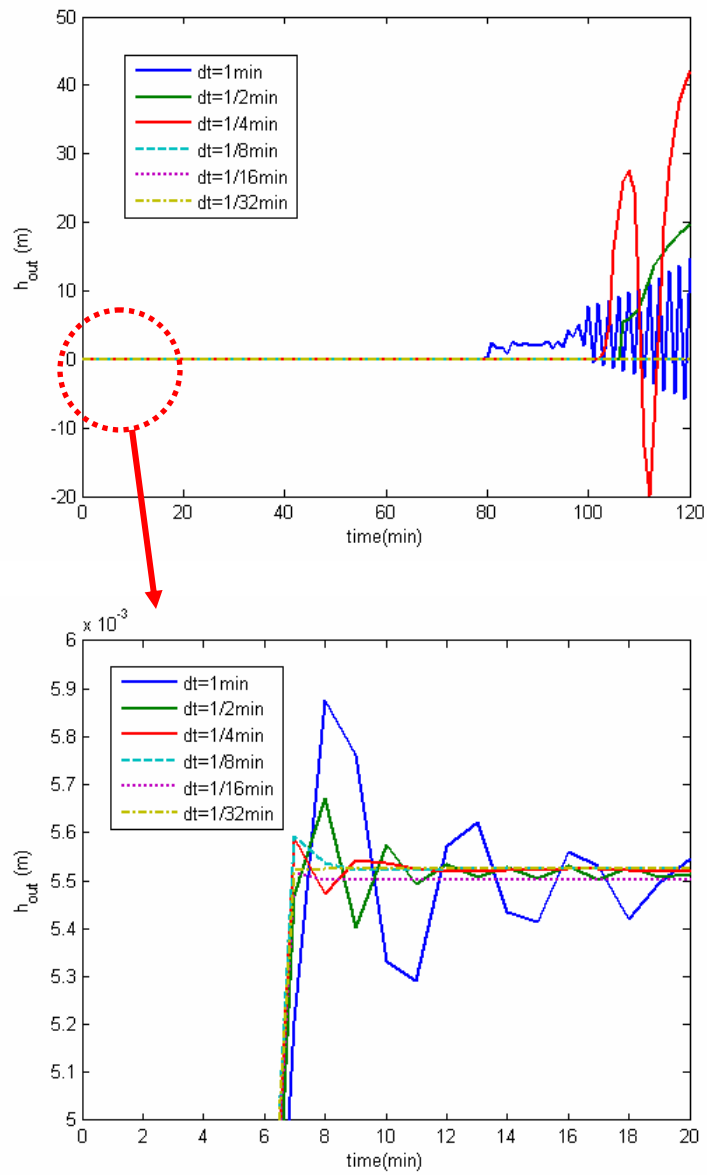


FIGURE A.4 Numerical solutions for the outflow depth using different values of Δt with $\Delta x = 0.05$ m

A.2 CAM: WL = 50 m, $r_o = 5$ m

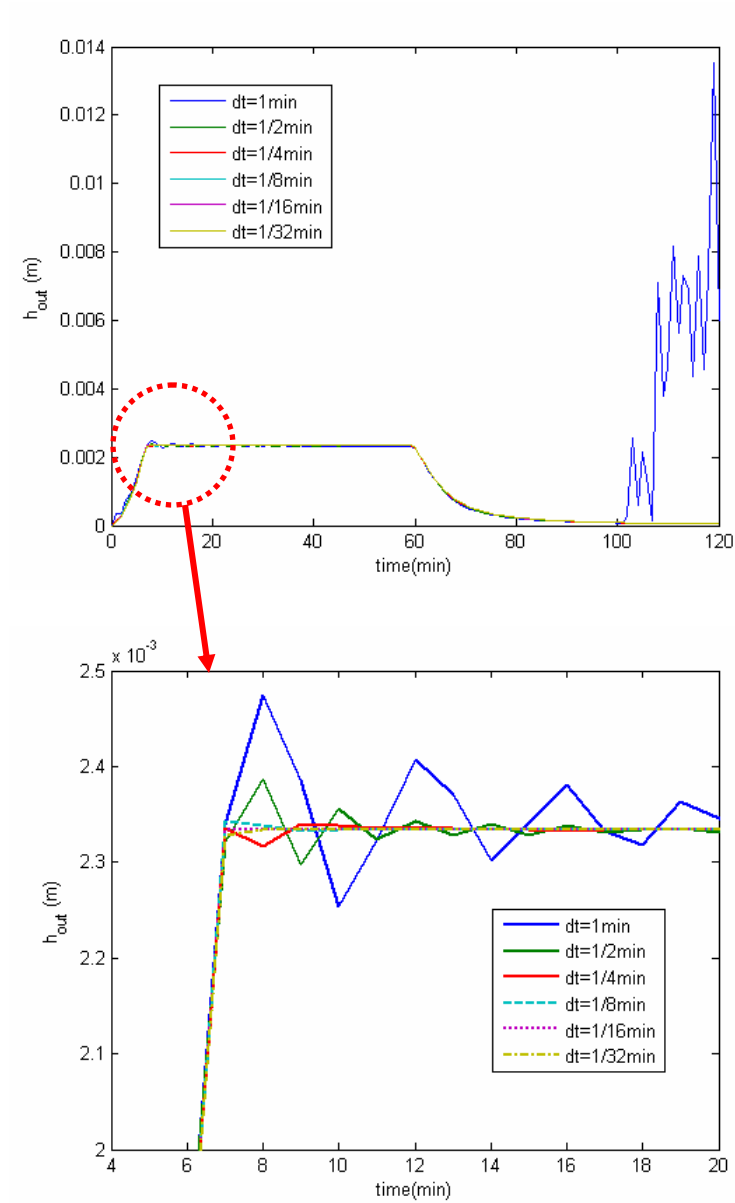
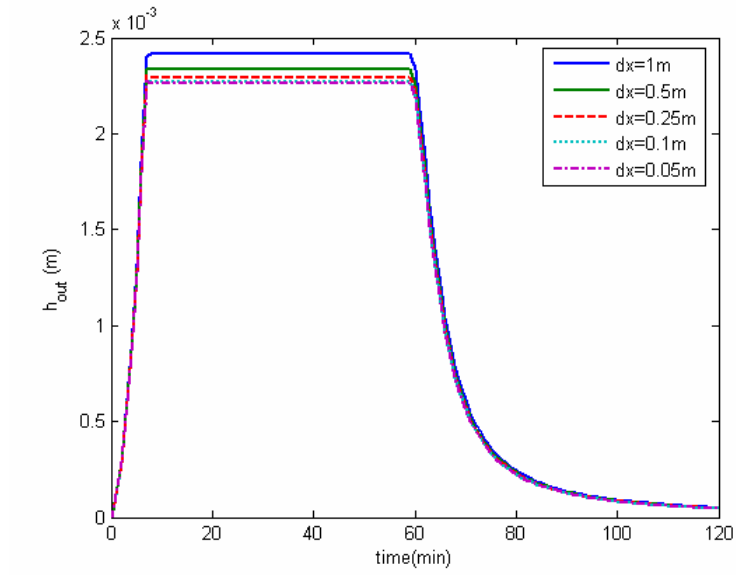
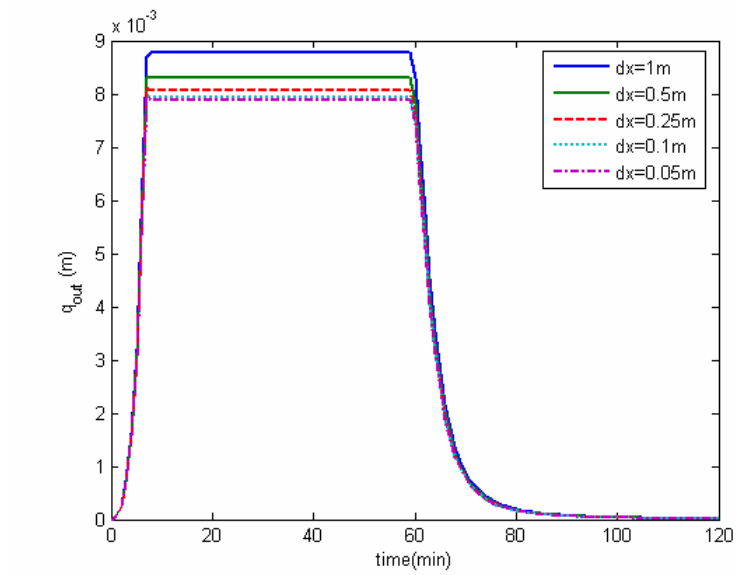


FIGURE A.5 Numerical solutions for the outflow depth using different values of Δt with $\Delta x = 0.5$ m



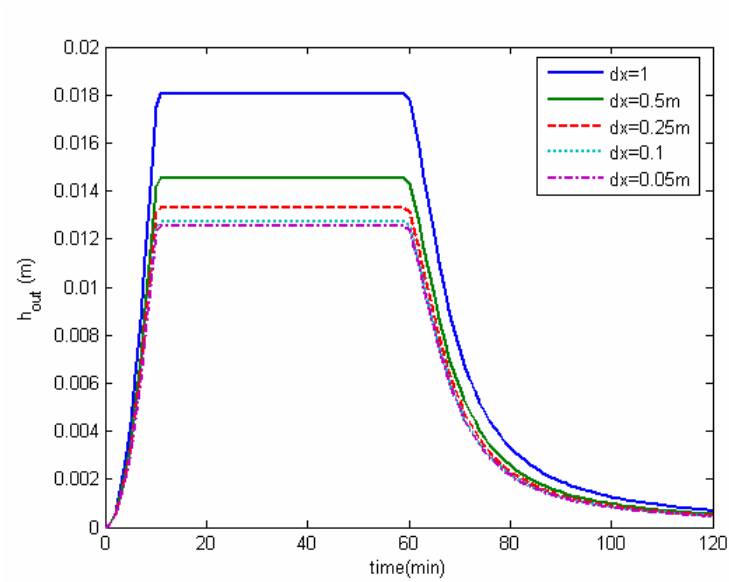
(a)



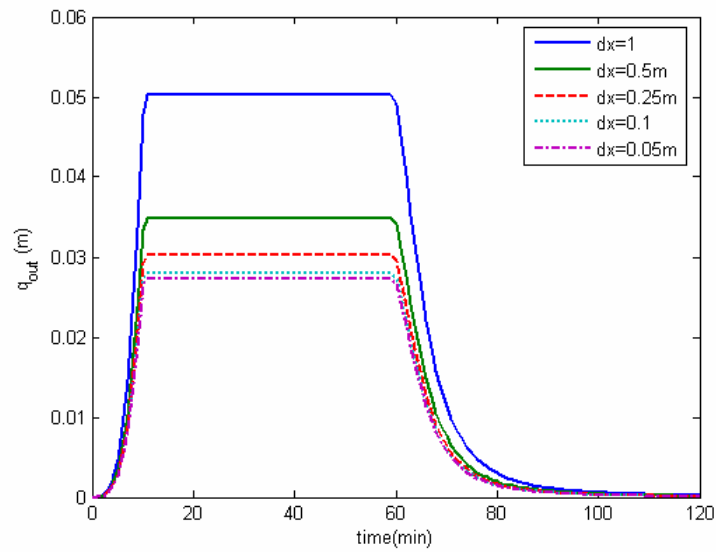
(b)

FIGURE A.6 Numerical solutions for the outflow using different values of Δx with $\Delta t = 1/16$ min: (a) depth; (b) flow rate

A.3 CAM: WL = 100 m, $r_o = 1$ m



(a)



(b)

FIGURE A.7 Numerical solutions for the outflow using different values of Δx with $\Delta t = 1/16$ min: (a) depth; (b) flow rate

A.4 CAM: WL = 100 m, $r_o = 5$ m

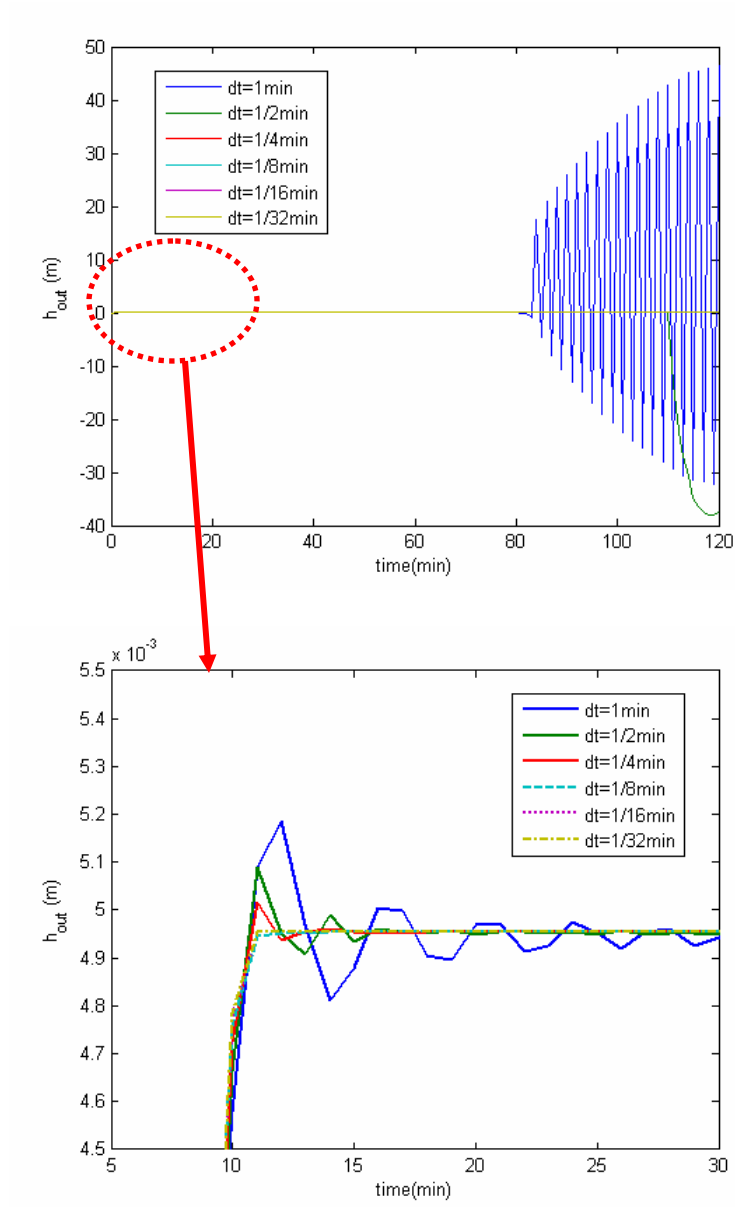
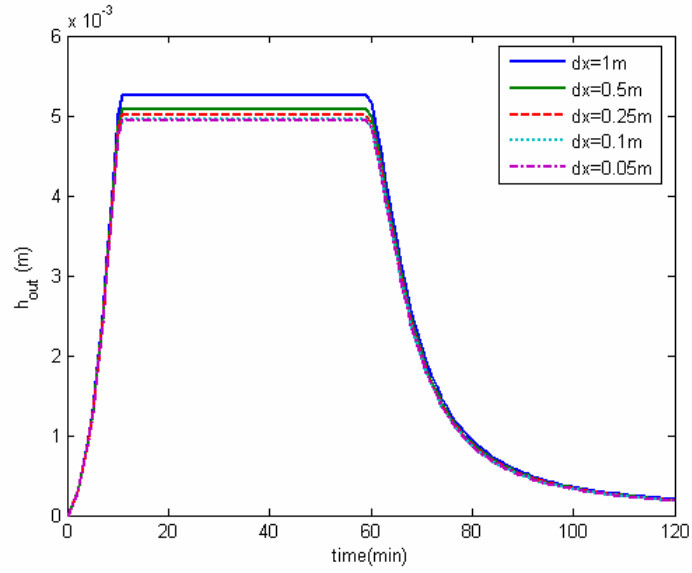
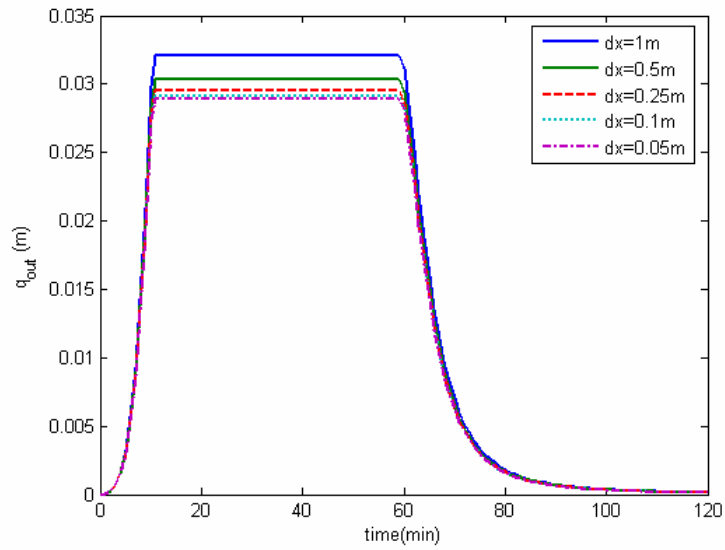


FIGURE A.8 Numerical solutions for the outflow depth using different values of Δt with $\Delta x = 0.1$ m



(a)



(b)

FIGURE A.9 Numerical solutions for the outflow using different values of Δx with $\Delta t = 1/16$ min: (a) depth; (b) flow rate

A.5 C-N: WL = 50 m, $r_o = 1$ m

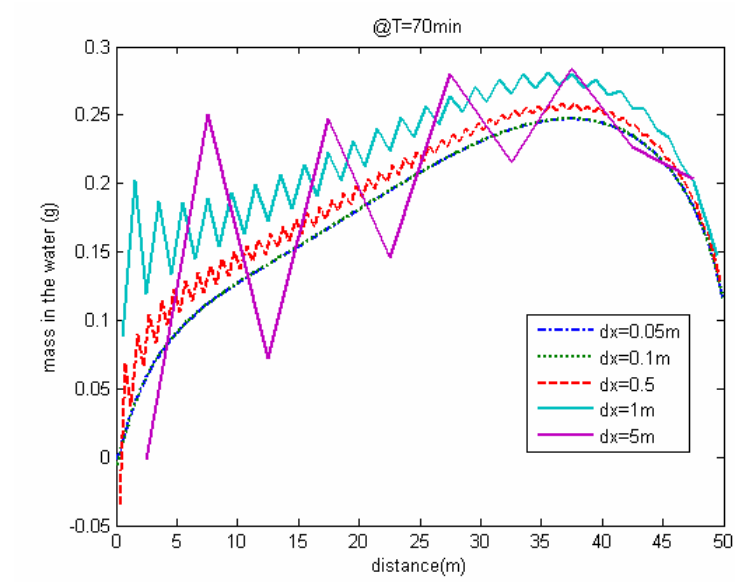


FIGURE A.10 Numerical solutions for the mass in the water along the distance using different values of Δx with $\Delta t = 1/16$ min at $t = 70$ min

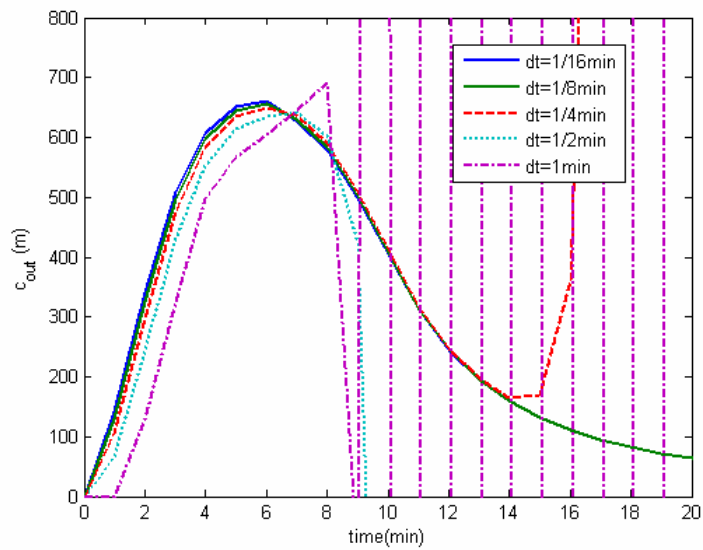


FIGURE A.11 Numerical solutions for the outflow concentration using different values of Δt with $\Delta x = 0.05$ m

Measured and Simulated Polluto-graphs

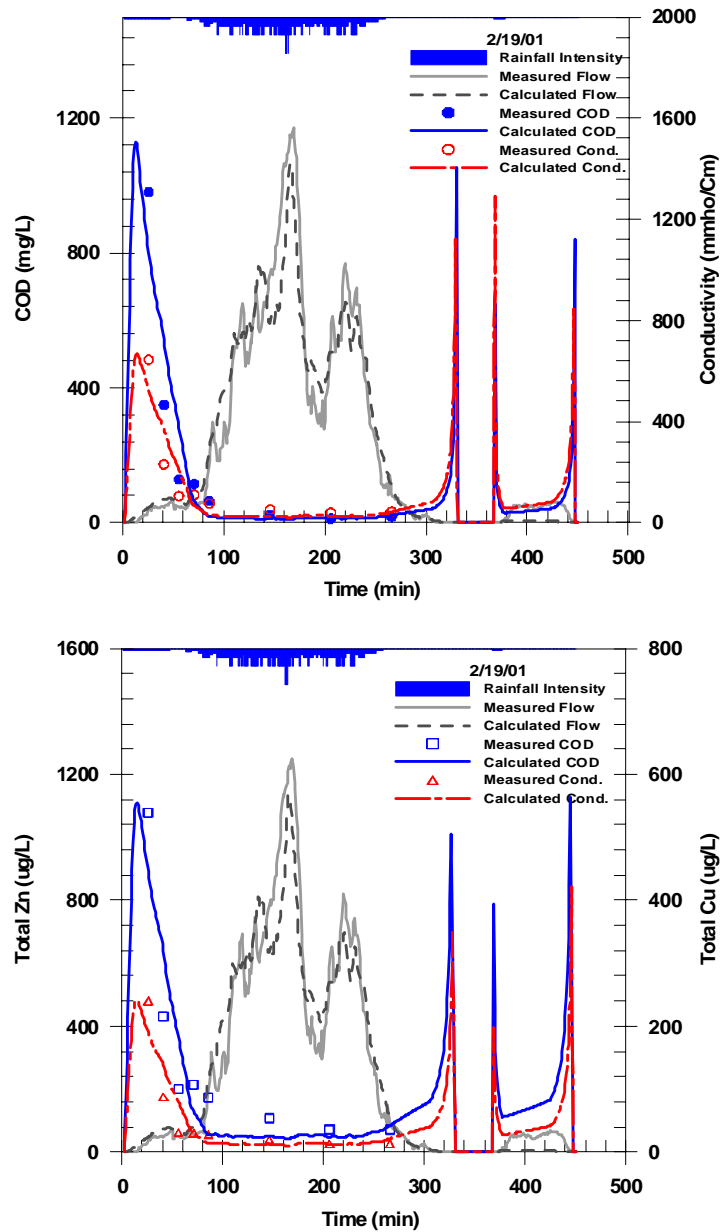


FIGURE C.1 Storm event on 2/19/01

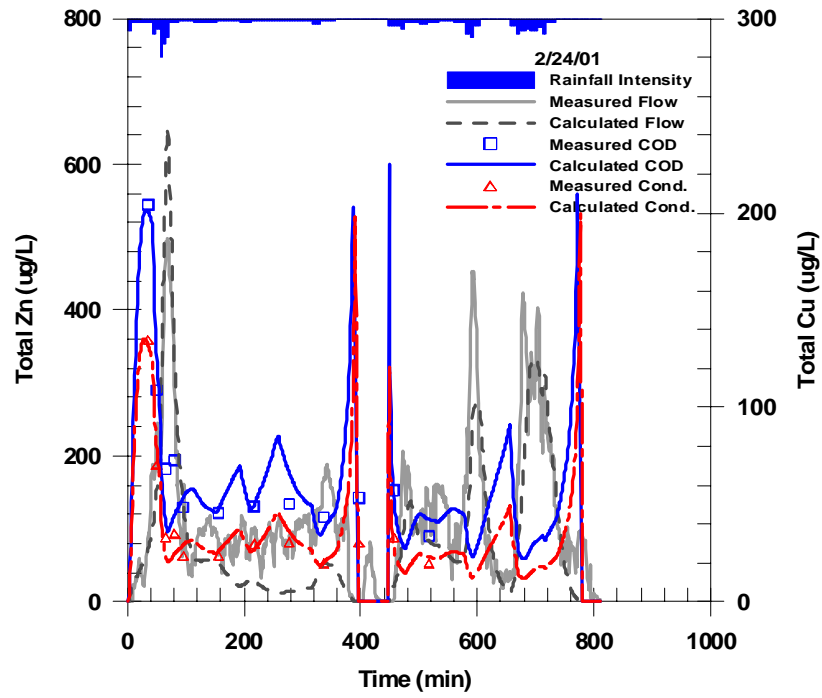
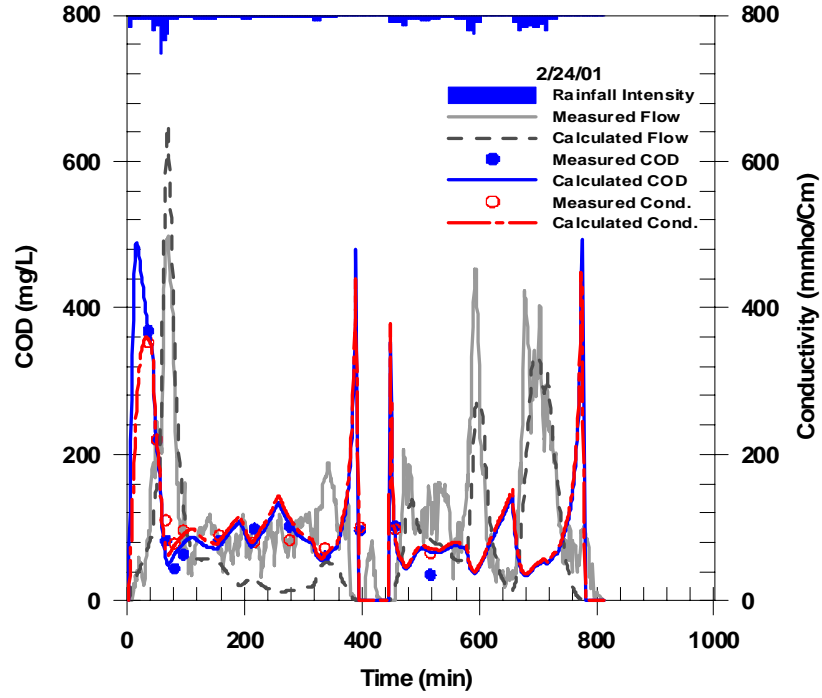


FIGURE C.2 Storm event on 2/24/01

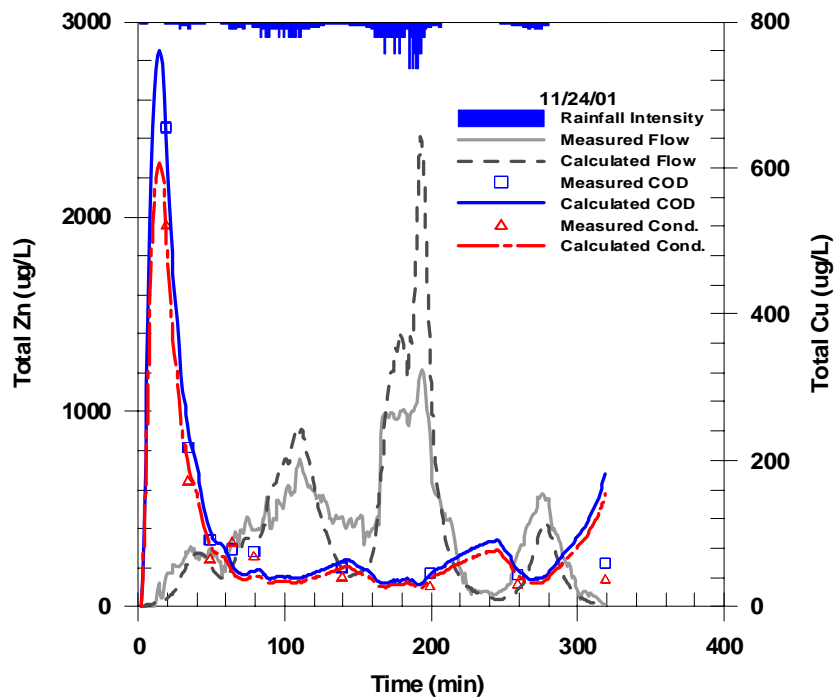
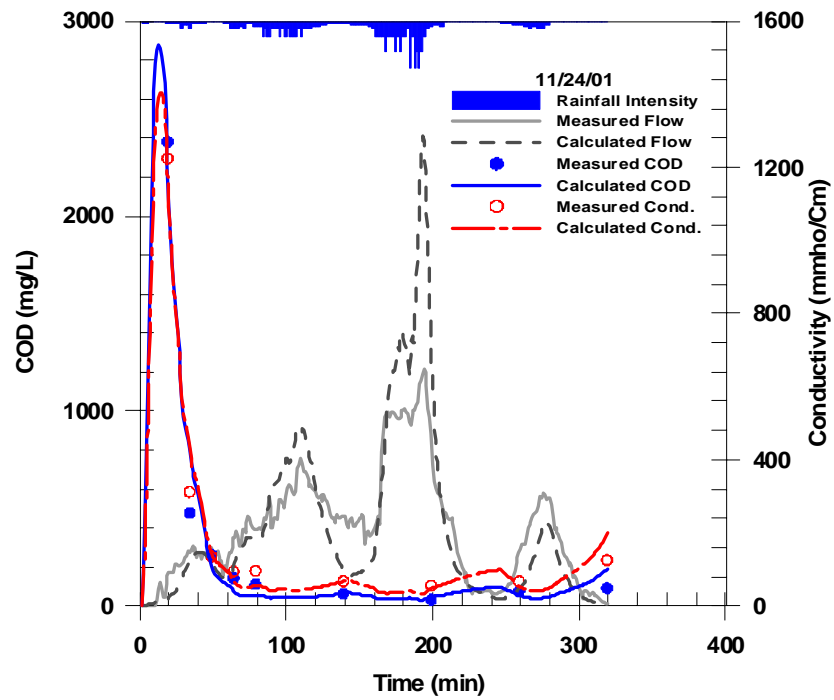


FIGURE C.3 Storm event on 11/24/01

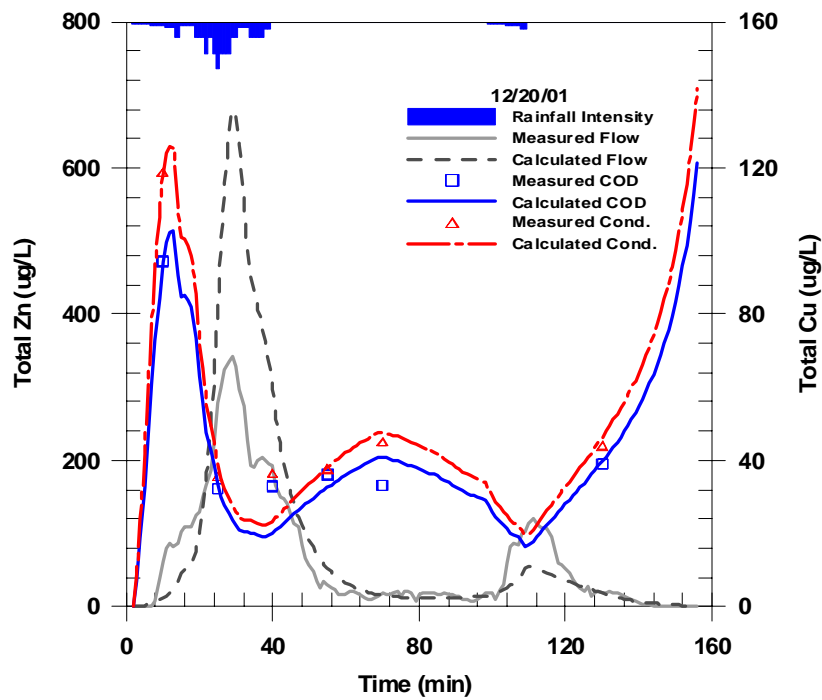
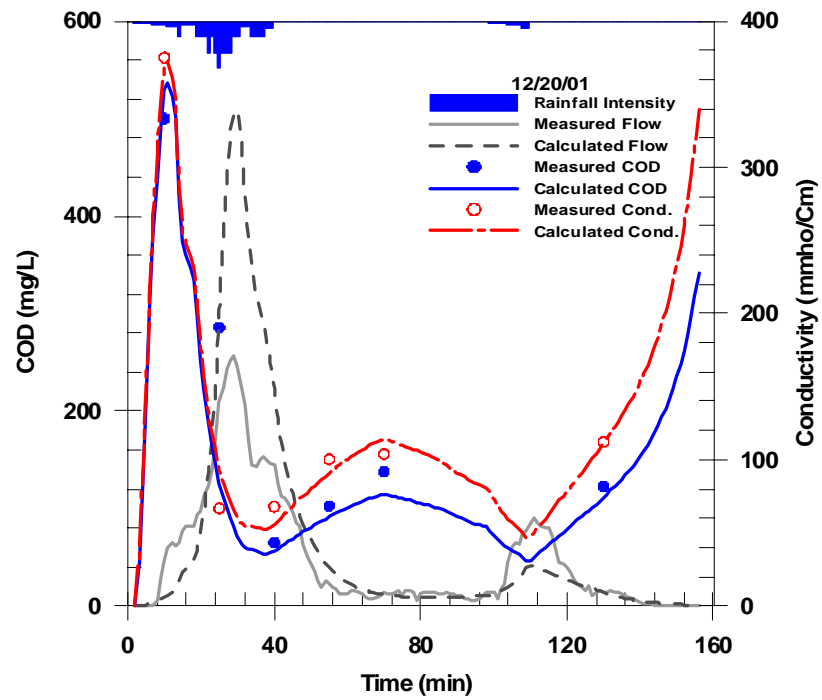


FIGURE C.4 Storm event on 12/20/01

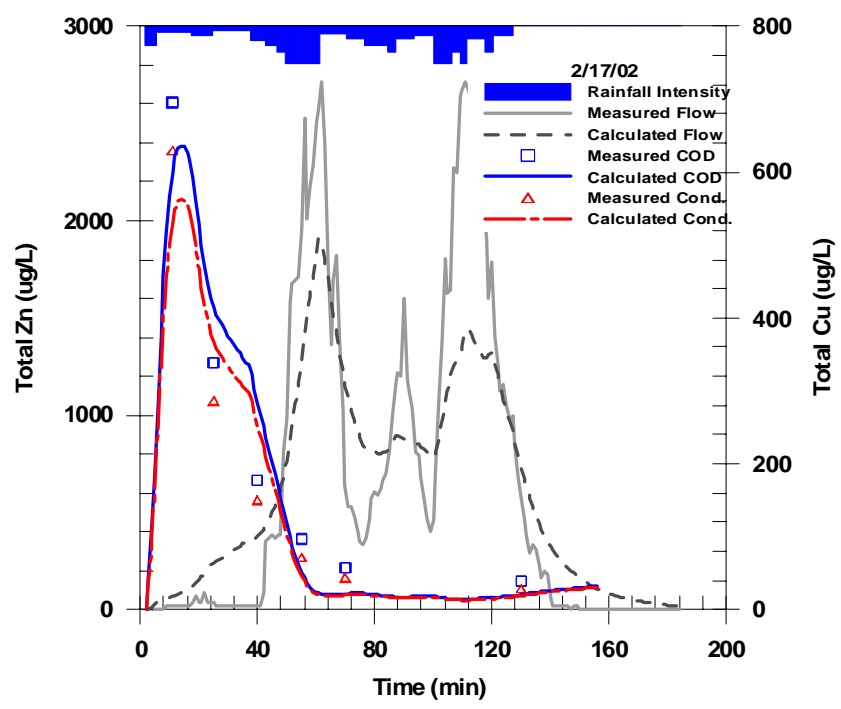
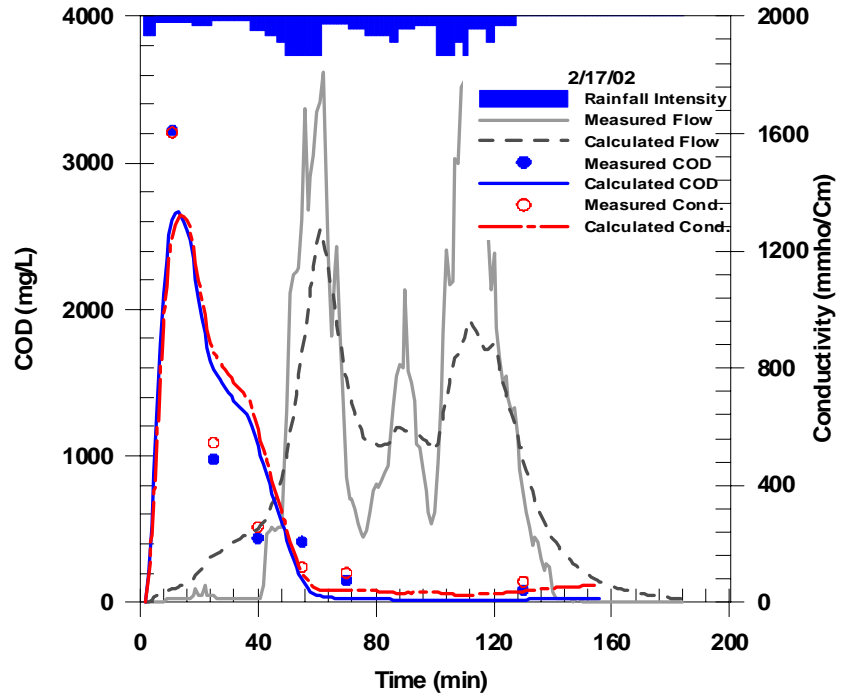


FIGURE C.5 Storm event on 2/17/02

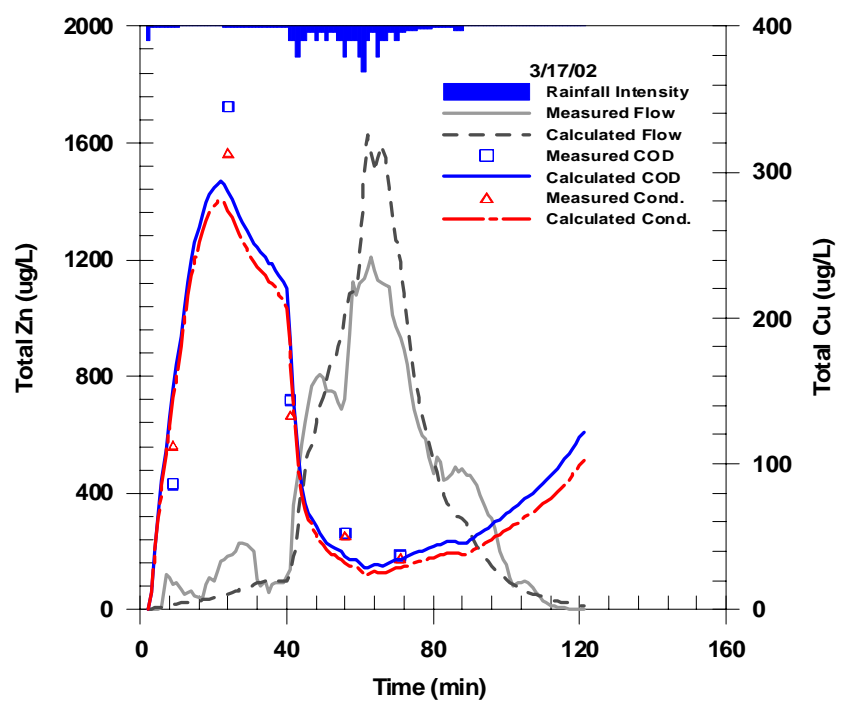
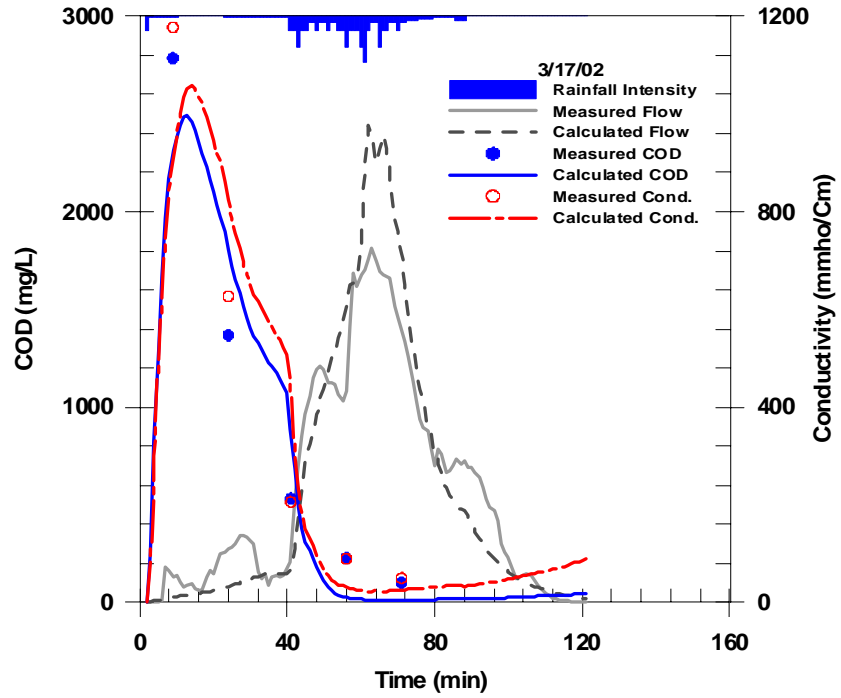


FIGURE C.6 Storm event on 3/17/02

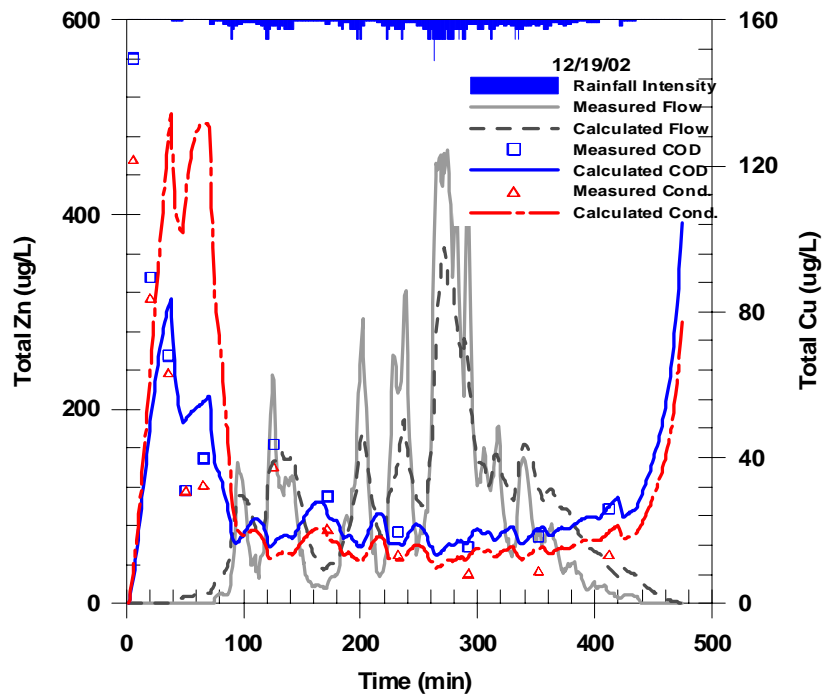
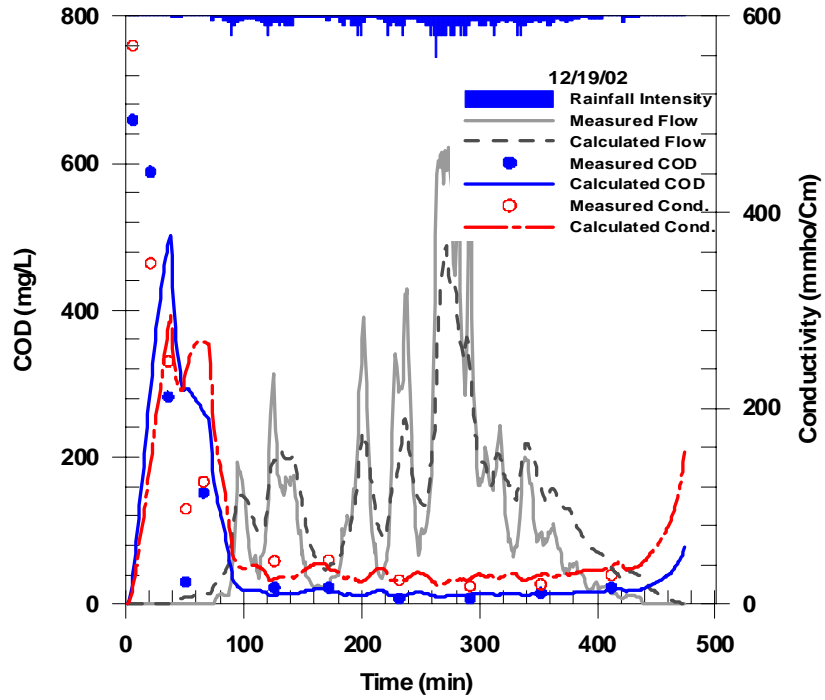


FIGURE C.7 Storm event on 12/19/02

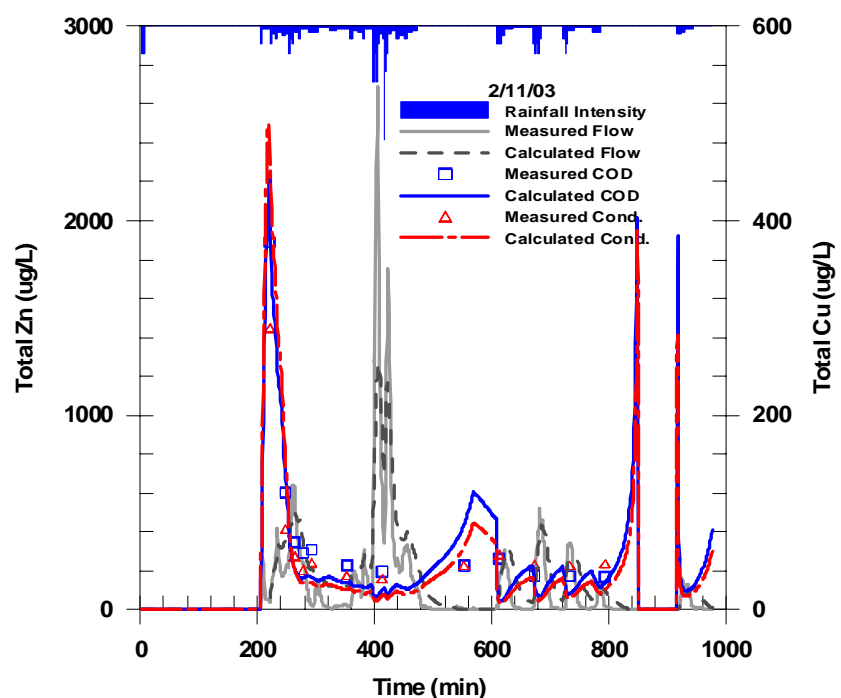
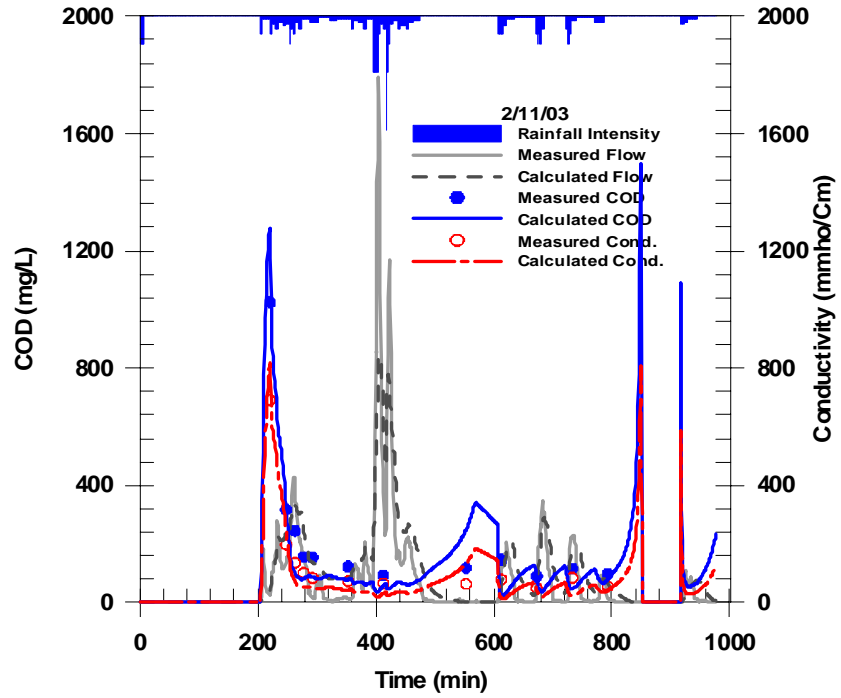


FIGURE C.8 Storm event on 2/11/03

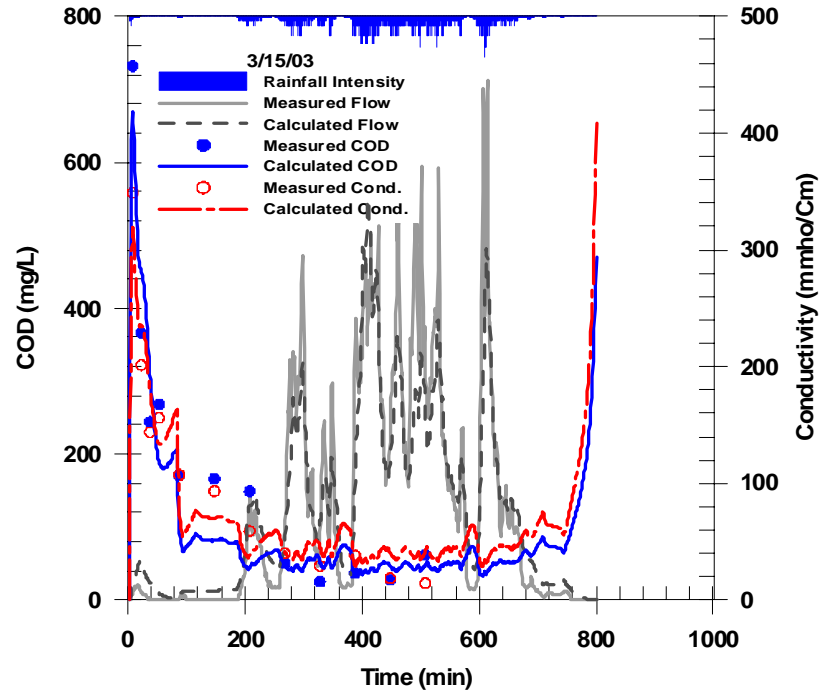


FIGURE C.9 Storm event on 3/15/03

Regressions for Buildup

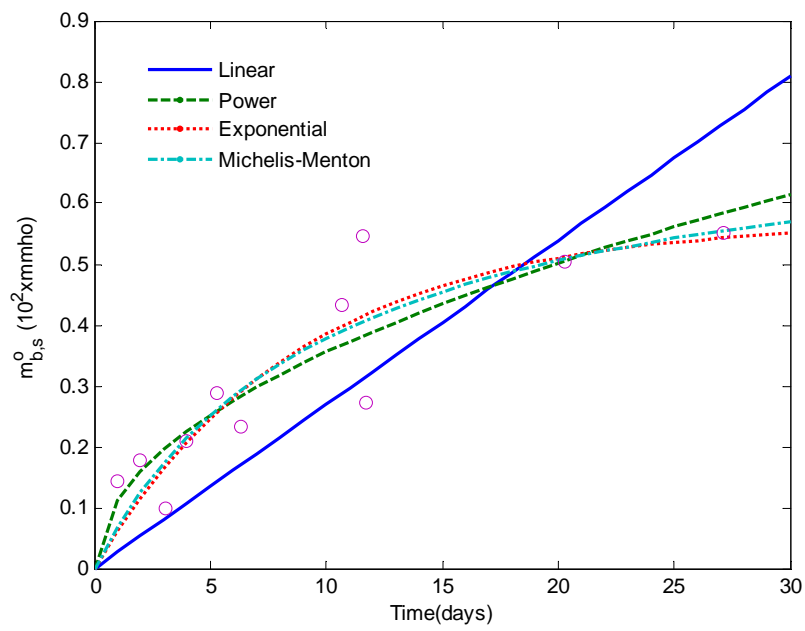


FIGURE D.1 Regression for conductivity buildup

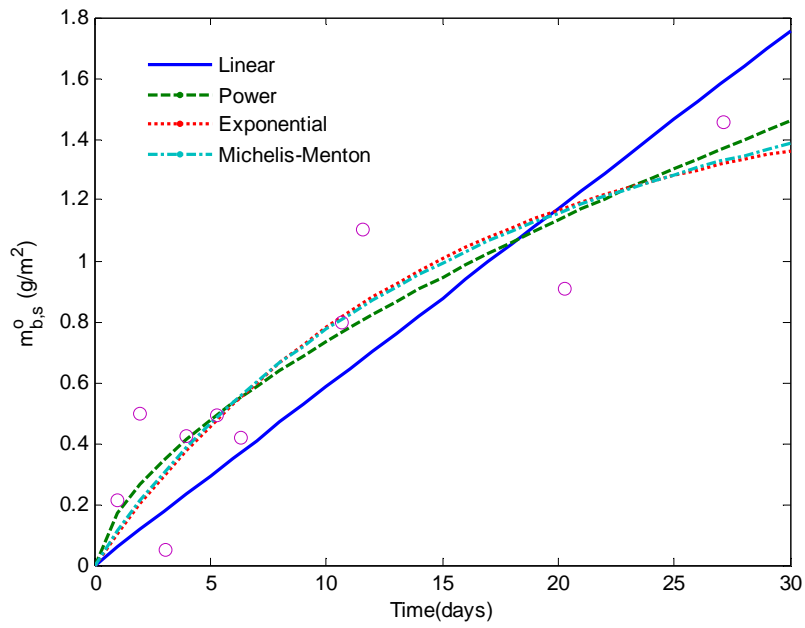


FIGURE D.2 Regression for Zn buildup

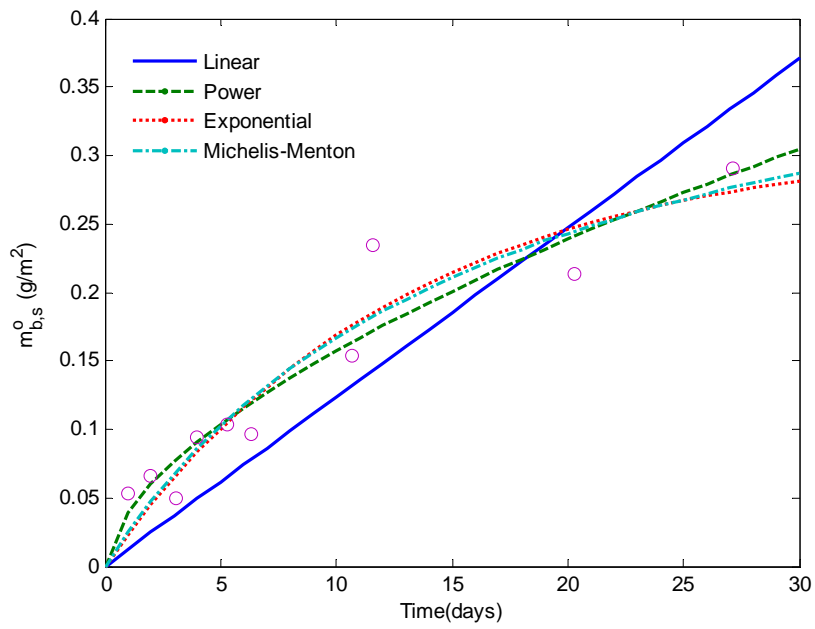


FIGURE D.3 Regression for Cu buildup

Program Codes (MATLAB)

Data matrices in the Input mat file

- **input**: flow, rainfall and corresponding time vectors
- **conc**: times and concentrations of constituents in the grab samples
- **metal**: concentrations of heavy metals in the grab samples

```
%=====
% PARAMETER OPTIMIZATION FOR 1-D FREEWAY RUNOFF MODEL %
%=====

close all; clear all; tic,

% Input Data (Rainfall, Pollutant Conc.)
load 021901s3.mat           % data for Feb.19,2001 in site3
rain=input(:,2);           % rainfall data [cm/min]
flow_m=1/60*input(:,3);    % measured flow [m3/min]->[m3/sec]

tc=conc(:,1);              % time for grab samle [min]
[tnn,ff]=size(tc); tc_m=tc(2:tnn-1);
c_m=conc(2:tnn-1,7);       % measured conc of a pollutant

% Watershed Dimension (Site3, L=244m, W=16m)
[nt,ff]=size(rain);
xmax=178; tmax=nt-1;
dx=2; dt=1/8;              % Grid Size, Time Step
mc=0.011 ;                 % manning's coeff
nx=int32(xmax/dx+1);       % Grid number
sx=0.02;                   % Slope in the flow direction

% Initializing matrices
h=zeros(nx,nt); h1=zeros(nx,2); di=zeros(nx,2);
hi=h; v1=h; hi_=h1;
hout=zeros(tmax,1);
v=h; q=h; vi=v;
```

```

vout=hout; gout=hout;

% Hydrologic Parameters
alpha=(sx^0.5)/mc; m=5/3;
imin=0.6e-5; % Minimum infiltration [m/min]
is=0.6e-6; % Infiltration rate with water depth [m]

% SUBPROGRAM 1 : Solution for Kinematic Wave Equation
% Method of Characteristics

tv=[0:tmax]; % Time vector
n=2; % index of time vector
t=0; % Real time in min
while n<nt

    t=t+dt; % real time
    xx=1; % index for x grid
    x_cum=0; % distance from x=0
    while x_cum < xmax
        xx=xx+1;
        p=interp1(tv,rain,t,'linear');
        if t==dt;
            h1(xx,2)=max(0,p*dt/100-(is*h1(xx-1,1)+imin)*dt);
            di(xx,2)=dx*(xx-1);
        else
            if xx==2;
                h1(xx,2)=max(0,p*dt/100-(is*h1(xx-1,1)+imin)*dt);
                di(xx,2)=dx;
            else
                c=alpha*m*h1(xx-1)^(m-1);
                if c==0;
                    h1(xx,2)=max(0,p*dt/100-(is*h1(xx-1,1)+imin)*dt);
                    di(xx,2)=di(xx,1);
                else
                    h1(xx,2)=max(0,h1(xx-1,1)+p*dt/100- ...
                        (is*h1(xx-1,1)+imin)*dt);
                    di(xx,2)=di(xx-1,1)+c*dt*60;
                end
            end
        end
        x_cum=di(xx,2);
    end

    % generation of velocity field based on the homogeneous node set
    dis=di(1:xx,2); hig=h1(1:xx,2); xxi=[0:dx:xmax];
    hi_=(interp1(dis,hig,xxi,'linear'))'; %rainfall vector
    v1=alpha*hi_.^(m-1);

    % saving solution at required time
    if fix(t)==t
        n=fix(t)+1; % vector index
        hi(:,n)=hi_;
        vi(:,n)=v1;
    end
end

```

```

    h1(:,1)=h1(:,2);
    di(:,1)=di(:,2);
end

for n=2:nt
    hout(n)=hi(nx,n);
    vout(n)=alpha*hout(n)^(m-1);
    qout(n)=vout(n)*hout(n);
end

% Generating velocity and water depth vectors for water quality calc.
nxx=nx-1; % number of cells
hi2=zeros(nxx,nt); vi2=zeros(nxx,nt);
for n=1:nt
    for i=1:nxx
        hi2(i,n)=(hi(i,n)+hi(i+1,n))/2;
        vi2(i,n)=alpha*hi2(i,n)^(m-1);
    end
end

% SUBPROGRAM 2 : Estimation of Parameters for Water Quality
% Transport Equation is calculated by C-N method
% Optimization tool box ("lsqcurvefit")
ko=[0.7 0.002 0.5]; % initial guess
lb=[0.6 0.001 0.3]; % lower boundary
ub=[1.2 0.005 1]; % upper boundary
options=optimset('MaxFunEvals',100);
[k,resnorm]=lsqcurvefit(@washoff4,ko,tc_m,c_m,lb,ub,options,...
    vi2,hi2,rain,nt,nxx,xmax,dt,dx,...
    tmax,tv,alpha,m,sx,qout)

% CALCULATION OF TRANSPORT WITH OPT. PARAMETERS
k1=k(1); kp=k(2); k2=2;
unit_mass0=k(3); %mass/length [g/m]
m2=zeros(nxx,nt); % remaining mass in watershed [g/m]
m1=m2; % mass in the solution [g/m]
m2(:,1)=unit_mass0*ones(nxx,1); % [g/m]
m2_2=unit_mass0*ones(nxx,2); m1_2=zeros(nxx,2);
tmass_re=zeros(nt,1); tmass_re(1,1)=unit_mass0*xmax;
m_emission=zeros(nt,1);
h2=zeros(nxx,1); v2=h2; % adjusted for cell base calculation

% Initialize tri-diagonal matrix
B=zeros(nxx,nxx); e=zeros(nxx,1);
Dt=dt*60; % [sec]
n=1; % time vector index (@t=0)
t=0; % real time
while t<=tmax-dt %for n=1:nt-1
    tt=fix(t);
    for i=1:nxx
        p=interp1(tv,rain,t,'linear'); % Precipitation [cm/min]
        if i==1

```

```

h2(i)=hi2(i,tt+1)-(t-tt)* ...
    (hi2(i,tt+1)-hi2(i,tt+2)); %interpolation
h2(i+1)=hi2(i+1,tt+1)-(t-tt)* ...
    (hi2(i+1,tt+1)-hi2(i+1,tt+2));
v2(i)=alpha*h2(i)^(m-1);
v2(i+1)=alpha*h2(i+1)^(m-1);
r=k1*v2(i)^k2; % [sec-1]
rc=kp*v2(i)^k2;
h_p=(h2(i+1)+h2(i))/2;
h_n=(h2(i)+0)/2;
us_p=sqrt(9.8*h_p*sx); % [m/sec]
us_n=sqrt(9.8*h_n*sx);
D_p=6.0*h_p*us_p; % [m2/sec]
D_n=6.0*h_n*us_n;
m2_2(i,2)=m2_2(i,1)-r*m2_2(i,1)*Dt;
B(i,i)=1+D_p*Dt/(2*dx^2)+D_n*Dt/(2*dx^2);
B(i,i+1)=-D_p*Dt/(2*dx^2)+v2(i+1)*Dt/(4*dx);
e(i,1)=(1-D_p*Dt/(2*dx^2)-D_n*Dt/(2*dx^2))*m1_2(i,1) ...
    +(D_p*Dt/(2*dx^2)-v2(i+1)*Dt/(4*dx))*m1_2(i+1,1) ...
    +r*m2_2(i,1)*Dt+rc*Dt;
elseif i==nxx
h2(i)=hi2(i,tt+1)-(t-tt)* ...
    (hi2(i,tt+1)-hi2(i,tt+2));
h2(i-1)=hi2(i-1,tt+1)-(t-tt)* ...
    (hi2(i-1,tt+1)-hi2(i-1,tt+2));
v2(i)=alpha*h2(i)^(m-1);
v2(i-1)=alpha*h2(i-1)^(m-1);
r=k1*v2(i)^k2; % [sec-1]
rc=kp*v2(i)^k2;
h_p=(h2(i)+h2(i))/2;
h_n=(h2(i)+h2(i-1))/2;
us_p=sqrt(9.8*h_p*sx);
us_n=sqrt(9.8*h_n*sx);
D_p=6.0*h_p*us_p; % [m2/sec]
D_n=6.0*h_n*us_n;
m2_2(i,2)=m2_2(i,1)-r*m2_2(i,1)*Dt;
B(i,i-1)=-D_n*Dt/(2*dx^2)-v2(i-1)*Dt/(4*dx);
B(i,i)=1+D_n*Dt/(2*dx^2)+v2(i)*Dt/(4*dx);
e(i,1)=(D_n*Dt/(2*dx^2)+v2(i-1)*Dt/(4*dx))*m1_2(i-1,1) ...
    +(1-D_n*Dt/(2*dx^2)-v2(i)*Dt/(4*dx))*m1_2(i,1) ...
    +r*m2_2(i,1)*Dt+rc*Dt;
else
h2(i)=hi2(i,tt+1)-(t-tt)* ...
    (hi2(i,tt+1)-hi2(i,tt+2));
h2(i-1)=hi2(i-1,tt+1)-(t-tt)* ...
    (hi2(i-1,tt+1)-hi2(i-1,tt+2));
h2(i+1)=hi2(i+1,tt+1)-(t-tt)* ...
    (hi2(i+1,tt+1)-hi2(i+1,tt+2));
v2(i)=alpha*h2(i)^(m-1);
v2(i-1)=alpha*h2(i-1)^(m-1);
v2(i+1)=alpha*h2(i+1)^(m-1);
r=k1*v2(i)^k2; % [sec-1]
rc=kp*v2(i)^k2;
h_p=(h2(i+1)+h2(i))/2;

```

```

        h_n=(h2(i)+h2(i-1))/2;
        us_p=sqrt(9.8*h_p*sx);
        us_n=sqrt(9.8*h_n*sx);
        D_p=6.0*h_p*us_p;           % [m2/sec]
        D_n=6.0*h_n*us_n;
        m2_2(i,2)=m2_2(i,1)-r*m2_2(i,1)*Dt;
        B(i,i-1)=-D_n*Dt/(2*dx^2)-v2(i-1)*Dt/(4*dx);
        B(i,i)=1+D_p*Dt/(2*dx^2)+D_n*Dt/(2*dx^2);
        B(i,i+1)=-D_p*Dt/(2*dx^2)+v2(i+1)*Dt/(4*dx);
        e(i,1)=(D_n*Dt/(2*dx^2)+v2(i-1)*Dt/(4*dx))*m1_2(i-1,1) ...
            +(1-D_p*Dt/(2*dx^2)-D_n*Dt/(2*dx^2))*m1_2(i,1) ...
            +(D_p*Dt/(2*dx^2)-v2(i+1)*Dt/(4*dx))*m1_2(i+1,1) ...
            +r*m2_2(i,1)*Dt+rc*Dt;
    end
end
m1_2(:,2)=inv(B)*e;
t=t+dt;
if fix(t)==t
    n=n+1; % vector index
    m1(:,n)=m1_2(:,2);
    m2(:,n)=m2_2(:,2);
    m_emission(n)=m1_2(nxx,2)*vi2(nxx,n);
end
m1_2(:,1)=m1_2(:,2);
m2_2(:,1)=m2_2(:,2);

end

% Concentration of constituent
for i=1:n
    if qout(i)<=1e-7 % minimum flow rate for constituent transport
        cout(i)=0;
    else
        cout(i)=m_emission(i)/qout(i);
    end
end

% RUNOFF COEFFICIENT
Total_rainfall=sum(rain)/100*xmax % [m2]
Total_runoff=sum(qout)*60
Runoff_coeff=Total_runoff/Total_rainfall

% MASS BALANCE (only holds for kp=0)
Inital_mass=tmass_re(1,1) % [g]
Mass_remaining=sum(m1(:,nt)+m2(:,nt))*dx
Mass_washoff=sum(m1(nxx,:).*vi2(nxx,:))*60
Calculated_mass=Mass_remaining+Mass_washoff

% PLOTS
% calc for measured data
time_c=conc(:,1); conc_m=conc(:,7);
time_f=input(:,1); flow_m=1/60*input(:,3);
c_m1=interp1(time_c,conc_m,time_f,'linear');
mass_m=c_m1.*flow_m;

```

```

tc=conc(:,1); [tnn,ff]=size(tc);

time=[0:tmax];
figure(1)
subplot(411),plot(time,rain),ylabel('p[cm/min]')
subplot(412),plot(time,flow_m,time,qout*21.9,'--'),ylabel('Q[m3/sec]')
subplot(413),...
    plot(tc(2:tnn-1),conc_m(2:tnn-1),'o',time,cout,'--') ...
    ,ylabel('Conc[ug/L]')
subplot(414),plot(time,mass_m,time,m_emission*16,'--') ...
    ,ylabel('Mass[mg/sec]')
xlabel('time[min]')
legend('measured','simulated')

% First Flush Plot
% calculated
tf=sum(qout); tf_m=sum(flow_m); tm=sum(m_emission);
% measured
cod_m=metal(:,3);
cod_m_i=interp1(time_c,cod_m,time_f,'linear');
cod_mass_m=cod_m_i.*flow_m;
tf_m=sum(flow_m); tm_cod_m=sum(cod_mass_m);
ncf=zeros(tmax+1,1); ncm=ncf; ncf_m=ncf; ncm_cod=ncf;
for i=2:tmax+1
    ncf(i)=ncf(i-1)+qout(i,1)/tf;
    ncf_m(i)=ncf_m(i-1)+flow_m(i,1)/tf_m;
    ncm(i)=ncm(i-1)+m_emission(i,1)/tm;
    ncm_cod(i)=ncm_cod(i-1)+cod_mass_m(i,1)/tm_cod_m;
end
t=linspace(0,1,m);
figure(2)
plot(ncf_m,ncm_cu,ncf,ncm,'--'),
grid,legend('Cu','Simulated')
axis([0 1 0 1]), axis('square')
figure(3)
plot(tc(2:tnn-1),conc_m(2:tnn-1),'o',time,cout,'--
'),ylabel('Conc(mg/L)')
toc

```

```

% SOLUTION FOR TRANSPORT EQUATION
% Crank-Nicolson Method

function F=washoff4(k, tcm, vi2, hi2, rain, nt, nxx, xmax, dt, dx, ...
    tmax, tv, alpha, m, sx, qout)

k1=k(1); kp=k(2); k2=2;
unit_mass0=k(3); %mass/length [g/m]
m2=zeros(nxx,nt); % remaining mass in watershed [g/m]
m1=m2; % mass in the water [g/m]
m2(:,1)=unit_mass0*ones(nxx,1); % [g/m]
m2_2=unit_mass0*ones(nxx,2); m1_2=zeros(nxx,2);

tmass_re=zeros(nt,1); tmass_re(1,1)=unit_mass0*xmax;
m_emission=zeros(nt,1);
h2=zeros(nxx,1); v2=h2; % adjusted for cell base
calculation

% Initialize tri-diagonal matrix
B=zeros(nxx,nxx); e=zeros(nxx,1);
Dt=dt*60; % [sec]
n=1; % time vector index (@t=0)
t=0; % real time
while t<=tmax-dt
    tt=fix(t);
    for i=1:nxx
        p=interp1(tv,rain,t,'linear'); % Precipitation [cm/min]
        if i==1
            h2(i)=hi2(i,tt+1)-(t-tt)*(hi2(i,tt+1)-hi2(i,tt+2));
            h2(i+1)=hi2(i+1,tt+1)-(t-tt)*(hi2(i+1,tt+1)-hi2(i+1,tt+2));
            v2(i)=alpha*h2(i)^(m-1);
            v2(i+1)=alpha*h2(i+1)^(m-1);
            r=k1*v2(i)^k2; % [sec-1]
            rc=kp*v2(i)^k2;
            h_p=(h2(i+1)+h2(i))/2;
            h_n=(h2(i)+0)/2;
            us_p=sqrt(9.8*h_p*sx); % [m/sec]
            us_n=sqrt(9.8*h_n*sx);
            D_p=6.0*h_p*us_p; % [m2/sec]
            D_n=6.0*h_n*us_n;
            m2_2(i,2)=m2_2(i,1)-r*m2_2(i,1)*Dt;
            B(i,i)=1+D_p*Dt/(2*dx^2)+D_n*Dt/(2*dx^2);
            B(i,i+1)=-D_p*Dt/(2*dx^2)+v2(i+1)*Dt/(4*dx);
            e(i,1)=(1-D_p*Dt/(2*dx^2)-D_n*Dt/(2*dx^2))*m1_2(i,1) ...
                +(D_p*Dt/(2*dx^2)-v2(i+1)*Dt/(4*dx))*m1_2(i+1,1) ...
                +r*m2_2(i,1)*Dt+rc*Dt;
        elseif i==nxx
            h2(i)=hi2(i,tt+1)-(t-tt)*(hi2(i,tt+1)-hi2(i,tt+2));
            h2(i-1)=hi2(i-1,tt+1)-(t-tt)*(hi2(i-1,tt+1)-hi2(i-1,tt+2));
            v2(i)=alpha*h2(i)^(m-1);
            v2(i-1)=alpha*h2(i-1)^(m-1);
            r=k1*v2(i)^k2; % [sec-1]
            rc=kp*v2(i)^k2;
            h_p=(h2(i)+h2(i))/2;

```

```

    h_n=(h2(i)+h2(i-1))/2;
    us_p=sqrt(9.8*h_p*sx);
    us_n=sqrt(9.8*h_n*sx);
    D_p=6.0*h_p*us_p;           % [m2/sec]
    D_n=6.0*h_n*us_n;
    m2_2(i,2)=m2_2(i,1)-r*m2_2(i,1)*Dt;
    B(i,i-1)=-D_n*Dt/(2*dx^2)-v2(i-1)*Dt/(4*dx);
    B(i,i)=1+D_n*Dt/(2*dx^2)+v2(i)*Dt/(4*dx);
    e(i,1)=(D_n*Dt/(2*dx^2)+v2(i-1)*Dt/(4*dx))*m1_2(i-1,1) ...
            +(1-D_n*Dt/(2*dx^2)-v2(i)*Dt/(4*dx))*m1_2(i,1) ...
            +r*m2_2(i,1)*Dt+rc*Dt;
else
    h2(i)=hi2(i,tt+1)-(t-tt)*(hi2(i,tt+1)-hi2(i,tt+2));
    h2(i-1)=hi2(i-1,tt+1)-(t-tt)*(hi2(i-1,tt+1)-hi2(i-1,tt+2));
    h2(i+1)=hi2(i+1,tt+1)-(t-tt)*(hi2(i+1,tt+1)-hi2(i+1,tt+2));
    v2(i)=alpha*h2(i)^(m-1);
    v2(i-1)=alpha*h2(i-1)^(m-1);
    v2(i+1)=alpha*h2(i+1)^(m-1);
    r=k1*v2(i)^k2;             % [sec-1]
    rc=kp*v2(i)^k2;
    h_p=(h2(i+1)+h2(i))/2;
    h_n=(h2(i)+h2(i-1))/2;
    us_p=sqrt(9.8*h_p*sx);
    us_n=sqrt(9.8*h_n*sx);
    D_p=6.0*h_p*us_p;           % [m2/sec]
    D_n=6.0*h_n*us_n;
    m2_2(i,2)=m2_2(i,1)-r*m2_2(i,1)*Dt;
    B(i,i-1)=-D_n*Dt/(2*dx^2)-v2(i-1)*Dt/(4*dx);
    B(i,i)=1+D_p*Dt/(2*dx^2)+D_n*Dt/(2*dx^2);
    B(i,i+1)=-D_p*Dt/(2*dx^2)+v2(i+1)*Dt/(4*dx);
    e(i,1)=(D_n*Dt/(2*dx^2)+v2(i-1)*Dt/(4*dx))*m1_2(i-1,1) ...
            +(1-D_p*Dt/(2*dx^2)-D_n*Dt/(2*dx^2))*m1_2(i,1) ...
            +(D_p*Dt/(2*dx^2)-v2(i+1)*Dt/(4*dx))*m1_2(i+1,1) ...
            +r*m2_2(i,1)*Dt+rc*Dt;
end
end
m1_2(:,2)=inv(B)*e;
t=t+dt;
if fix(t)==t
    n=n+1;                     % vector index
    m1(:,n)=m1_2(:,2);
    m2(:,n)=m2_2(:,2);
    m_emission(n)=m1_2(nxx,2)*vi2(nxx,n);
end
m1_2(:,1)=m1_2(:,2);
m2_2(:,1)=m2_2(:,2);
end

% Concentration of constituent
for i=1:n
    if qout(i)<=1e-7 % minimum flow rate for constituent transport
        cout(i)=0;
    else
        cout(i)=m_emission(i)/qout(i);
    end
end

```

```

    end
end

% Arbitrary function of pde solution
time=[0:tmax];
F = interp1(time,cout,tcn,'linear');

%=====
% Radial Flow Simulation      %
%=====
% Diffusive wave theory
% Characteristics averaging method

close all; clear all;
% Input Rainfall, [cm/min]
rain=[(0.005)*ones(180,1); zeros(41,1)];
% Model domain
[nt,ff]=size(rain);
xmax=10; tmax=nt-1;
dx=0.1; dt=1/16;
mc=0.014 ;           % manning's coeff
nx=int32(xmax/dx+1); % grid number
sx=0.02;
r0=1;               %[m] outlet radius
% Initializing vectors
h=zeros(nx,nt); h1=zeros(nx,2);
hi=h; hout=zeros(nt,1);
c=zeros(nx,1);
v=h; q=h;
vout=hout; qout=hout;
alpha=(sx^0.5)/mc; m=5/3;
% Infiltration parameters
imin=1e-5 % [cm/sec]
is=1e-6;  % [cm]
% Initialize tri-diagonal matrix
A=zeros(nx-1,nx-1); d=zeros(nx-1,1);
Dt=dt*60;
tv=[0:tmax];
n=1;t=0;
while t<=tmax
    p=interp1(tv,rain,t,'linear');
    for i=2:nx
        c(i)=alpha*m*h1(i)^(m-1);
        V=(c(i)+c(i-1))/2;
        h_=(h1(i-1,1)+h1(i,1))/2;
        D=(3/5)*V*h_/(2*sx);           % [m2/sec]
        if i==2
            A(i-1,i-1)=1/(2*Dt)+V/(2*dx)+D/(dx^2);
            A(i-1,i)=-D/(2*dx^2);
            d(i-1,1)=(1/(2*Dt)-V/(2*dx)+D/(2*dx^2))*h1(i,1)...
                +max(0,p/6000-(is*h1(i,1)+imin)/100) ...

```

```

        +alpha*h1(i,1)^m/(xmax+r0-(i-3/2)*dx);
elseif i==nx
    A(i-1,i-2)=-D/(dx^2)+1/(2*dt)-V/(2*dx);
    A(i-1,i-1)=1/(2*dt)+V/(2*dx)+D/(dx^2);
    d(i-1,1)=(1/(2*dt)-V/(2*dx)+D/(2*dx^2))*h1(i,1)...
        +(1/(2*dt)+V/(2*dx)-D/(dx^2))*h1(i-1,1)...
        +(D/(2*dx^2))*h1(i-2,1)...
        +max(0,p/6000-(is*h1(i,1)+imin)/100) ...
        +alpha*h1(i,1)^m/(xmax+r0-(i-3/2)*dx);
else
    A(i-1,i)=-D/(2*dx^2);
    A(i-1,i-1)=1/(2*dt)+V/(2*dx)+D/(dx^2);
    A(i-1,i-2)=1/(2*dt)-V/(2*dx)-D/(2*dx^2);
    d(i-1,1)=(1/(2*dt)-V/(2*dx)+D/(2*dx^2))*h1(i,1)...
        +(1/(2*dt)+V/(2*dx)-D/(dx^2))*h1(i-1,1)...
        +(D/(2*dx^2))*h1(i-2,1)...
        +max(0,p/6000-(is*h1(i,1)+imin)/100) ...
        +alpha*h1(i,1)^m/(xmax+r0-(i-3/2)*dx);
end
end
h1(2:nx,2)=inv(A)*d;
if fix(t)==t
    n=fix(t)+1;
    h(:,n)=h1(:,2);
    v(:,n)=alpha*h(:,n).^(m-1);
end
h1(:,1)=h1(:,2);
t=t+dt;
end
for n=2:nt
    hout(n)=h(nx,n); % [m]
    vout(n)=alpha*hout(n)^(m-1); % [m/sec]
    qout(n)=vout(n)*hout(n)*r0*pi; % [m3/sec]
end
% Runoff coeff.
Area=pi*((xmax+r0)^2-r0^2)/2;
Total_rainfall=sum(rain)/100*Area % [m3]
Total_runoff=sum(qout)*60
Runoff_coeff=Total_runoff/Total_rainfall

```

Calculation of Metal Removal Efficiency

**Particulate metal removal efficiency by 26mm design storm holding tank
(for Site 2, 1.69ha, tank volume 438m³ and surface area 146m²)**

Retention time	Particle mass removal	Particulate metal removal				Total metal removal			
		Pb	Zn	Cu	Fe	Pb	Zn	Cu	Fe
24h	27.12%	29.85%	28.96%	37.16%	26.27%	27.76%	8.11%	15.24%	25.48%
72h	27.46%	30.50%	30.00%	38.20%	26.57%	28.36%	8.40%	15.66%	25.78%
12h after polymer add	90.07%	85.29%	83.81%	84.54%	90.38%	79.32%	23.47%	34.66%	87.67%

Calculation of metal removal efficiency using polymer

Particles size range	Measured			Metal/Particl, ug/g (Morquecho)			
	ini_vol	vol after 12h	Rem. Eff.	Cu	Fe	Pb	Zn
0.45-2	2.31E+08	3.20E+07	86.19%	2894	29267	199	13540
2-10	4.45E+08	9.12E+07	79.51%	4668	18508	868	13641
10-45	6.21E+08	2.54E+07	95.91%	735	26221	229	1559
45-106	2.15E+08	1.55E+06	99.28%	1312	14615	226	2076
106-250	0.00E+00	0.00E+00	0.00%	2137	21730	375	3486
>250	0.00E+00	0.00E+00	0.00%	50	28604	117	266
total	1.51E+09	1.50E+08	90.07%				

Particles size range	Initial				12 set			
	Cu	Fe	Pb	Zn	Cu	Fe	Pb	Zn
0.45-2	6.7E+11	6.8E+12	4.6E+10	3E+12	9E+10	9E+11	6.4E+09	4E+11
2-10	2.08E+12	8.2E+12	3.9E+11	6E+12	4E+11	2E+12	7.9E+10	1E+12
10-45	4.56E+11	1.6E+13	1.4E+11	1E+12	2E+10	7E+11	5.8E+09	4E+10
45-106	2.82E+11	3.1E+12	4.9E+10	4E+11	2E+09	2E+10	3.5E+08	3E+09
106-250	0	0	0	0	0	0	0	0
>250	0	0	0	0	0	0	0	0
total	3.49E+12	3.4E+13	6.2E+11	1E+13	5E+11	3E+12	9.2E+10	2E+12

REFERENCES

- Abustan, I., and Ball, J.E. (1998). "Modelling the export of phosphorus from urban catchments." *Proc. HydraStorm'98*, Adelaide, Australia, 45-50.
- Aiguier, E., Ghassan C., Bertrand-Krajewske, J.-L., Gagné, B., and Hedges, P. (1998). "Analysis of the methods for determining the settling characteristics of sewage and stormwater solids." *Wat. Sci. Tech.*, 37(1), 53-60.
- Aiguier, E., Chebbo, G., Bertrand-Krajewske, J.-L., Hedges, P., and Tyack, N. (1996). "Methods for determining the settling velocity profiles of solid in storm sewage." *Wat. Sci. Tech.*, 33(9), 117-125.
- Aldheimer, G., and Bennerstedt, K. (2003). "Facilities for treatment of stormwater runoff from highways." *Wat. Sci. Tech.*, 48(9), 113-121.
- Allen, D.L. (2003). Analysis of field permeability and laboratory shear stresses for western Kentucky parkway milepost 18.240 to milepost 25.565 Caldwee-Hopkins Counties. Research Report, KTC-03-05/SPR245-02-1I, Kentucky Transportation Center, University of Kentucky, Lexington, Kentucky.
- Annadurai, G., Sung, S.S., and Lee, D.J. (2003) "Floc characteristics and removal of turbidity and humic acid from high-turbidity storm water" *J. Environ. Engrg.*, ASCE, 129, 571-575.
- Barbé, D.E., Cruise, J.F., and Mo, X. (1995) "Modeling the buildup and washoff of pollutants on urban watersheds." *Water Resources Bulletin*, AWRA, 32(3), 511-519.
- Borst, M., and Selvakumar, A. (2003). "Particle-associated microorganisms in stormwater runoff." *Wat. Res.*, 37, 215-223.
- Bowders, J.J., Blanco, A.M., and Parra, J.R. (2003). Characterization of permeability of pavement bases in Missouri Department of Transportation's System. Final Report, RDT 03-005, Research Investigation 01-006, Missouri Department of Transportation Research, Development and Technology, Jefferson City, Missouri.
- Charbeneau, R.J., and Barrett, M.E. (1998). "Evaluation of methods for estimating stormwater pollutant loads." *Wat. Env. Res.*, 70(7), 1295-1302.
- Characklis, W.G., and Wiesner, M.R. (1997). "Particle, metals, and water quality in runoff from large urban watershed." *J. Environ. Engrg.*, ASCE, 123(8), 753-759.

- Chien, N., and Wan, Z. (1999). *Mechanics of Sediment Transport*. ASCE Press, Reston, Virginia.
- Cristina C.M, Tramonte J., and Sansalone J. J. (2002). "A granulometry-based selection methodology for separation of traffic-generated particles in urban highway snowmelt runoff." *Water, Air, and Soil Pollution*, 136, 33-53.
- Cristina, C.M., and Sansalone, J.J. (2003a). "'First Flush", Power law and particle separation diagrams for urban storm-water suspended particulates." *J. Environ. Engrg.*, ASCE, 129(4), 298-307.
- Cristina, C.M., and Sansalone, J.J. (2003b). "Kinematic wave model of urban pavement rainfall-runoff subject to traffic loadings." *J. Environ. Engrg.*, ASCE, 129(7), 629-636.
- Deletic, A. (2001). "Modelling of water and sediment transport over grassed areas." *Journal of Hydrology*, 248, 168-182.
- Deletic, A.B., and Maksimovic, C.T. (1998). "Evaluation of water quality factors in storm runoff from paved areas." *J. Environ. Engrg.*, ASCE, 124(9), 869-879.
- Deng, Z.Q., Lima, J.L.M.P., and Singh, V.P. (2005). "Fractional kinetic model for first flush of stormwater pollutants." *J. Environ. Engrg.*, ASCE, 131(2), 232-241.
- Einstein, H.A. (1950). "The bed load function for sediment transportation in open channel flows." Tech. Bulletin, No.1026, United States Dept. of Agriculture.
- Elder, J.W. (1959). "The dispersion of marked fluid in a turbulent shear flow." *J. Fluid Mech.*, 5(4), 544-560.
- Fennema, R.J., and Chaudhry, M.H. (1986). "Explicit numerical schemes for unsteady free-surface flows with shocks." *Water Resour. Res.*, 22(13), 1923-1930.
- Fennema, R.J., and Chaudhry, M.H. (1990). "Explicit methods for 2-D transient free-surface flows." *J. Hydr. Engrg.*, ASCE, 116(8), 1013-1034.
- Fennema, R.J., Neidrauer, C.J., Johnson, R.A., MacVicor, T.K., and Perkins, W.A. (1994). "A computer model to simulated natural Everglades hydrology." *Everglades, The Ecosystem and its Restoration*, Eds. Davis, S.M and Ogden, J.C, St. Luice Press, FL, 249-289.
- Fiedeler, F.R., and Ramirez, J.A. (2000). "A numerical method for simulating shallow flow over an infiltrating surface." *Int. J. Numer. Meth. Fluids*, 32, 219-240.

- Furumai, H., Balmer, H., and Boller, M. (2002). "Dynamic behavior of suspended pollutants and particle size distribution in highway runoff." *Wat. Sci. Tech.*, 46(1), 413-418.
- Gabet, E.J., and Dunne, T. (2003). "Sediment detachment by rain power." *Water Resource Res.* 39(1), 1002.
- Geiger, W. (1987). "Flushing effects in combined sewer systems." *Proceedings of the 4th Int. Cont. on Urban Drainage*, 40-46, Lausanne, Switzerland.
- German J., and Svensson G. (2002). "Metal content and particle size distribution of street sediments and street sweeping waste." *Wat. Sci. Tech.*, 46(6-7), 191-198.
- Govindaraju, R.S., Jones, S.E., and Kavvas, M.L. (1988). "On the diffusion wave model for overland flow, 1. Solution for steep slopes." *Water Resour. Res.*, 24(5), 734-744.
- Graf, W.H. (1998). *Fluvial hydraulics*. John Wiley & Sons, Inc., New York, USA.
- Grottker, M. (1987). "Runoff quality from a street with medium traffic loading." *Sci. Total Environ.*, 59, 457.
- Guo, J.C.Y. (2004). "Hydrology-based approach to storm water detention basin design using new routing schemes." Technical Notes, *J. Hydrol. Engrg*, ASCE, 9(4), 333-336.
- Gupta, K., and Saul, A.J. (1996). "Specific relationship for the first flush load in combined sewer lows." *Wat. Res.*, 30(5), 1244-1252.
- Han, Y-H, Lau, S-L., Kayhanian, M., and Stenstrom, M.K. (2004). "Correlation analysis among highway stormwater runoff pollutants and characteristics." Paper 1E-III-4, *IWA Diffuse Pollution Conference*, Kyoto, Japan.
- Haque, M.A. (2002). "Study of surface runoff using physical models." *Environmental Geology*, 41, 797-805.
- Heinzmann, B. (1994). "Coagulation and flocculation of stormwater from a separate sewer system – A new possibility for enhanced treatment." *Wat. Sci. Tech.*, 29, 267-278.
- Henderson, F.M., and Wooding, R.A. (1964). "Overland flow and groundwater flow from a steady rainfall of finite duration." *J. Geophys. Res.*, 69(8), 1531-1540.

- Herrmann, R. (1981). "Transport of polycyclic aromatic hydrocarbons through a partly urbanized river basin." *Water, Air and Soil Pollution*, 16(4), 445-467.
- Herricks, E.E. (1995). Stormwater runoff and receiving systems. CRC Press, Inc., Boca Raton, Florida, USA.
- Hewitt, C.N., and Rashed, M.B. (1992). "Removal rates of selected pollutants in the runoff waters from a major rural highway." *Wat. Res.*, 26(3), 311-319.
- Hoffman, E.J., Latimer, J.S., Hunt, C.D., Mills, G.L., and Quinn, J.G. (1985). "Stormwater runoff from highways." *Water, Air and Soil Pollution*, 25(4), 349-364.
- Hunter, J.V., Balmat, J., Wilber, W., and Sabatino, T. (1981). "Hydro-carbons and heavy metals in urban runoff." *Urbanization, stormwater runoff and the aquatic envir.*, George Mason Univ., Fairfax, Va.
- Jaber, F.H., and Mohtar, R.H. (2002). "Dynamic time step for one-dimensional overland flow kinematic wave solution." *J. Hydro. Engrg.*, ASCE, 7(1), 3-11.
- Jacopin, C.J., Bertrand-Krajewski, J.L., and Desbordes, M. (1999). "Characterisation and settling of solids in an open, grassed, stormwater sewer network detention basin." *Wat. Sci. Tech.*, 39(2). 135-144.
- Jacopin, C.J., Desbordes, M., and Bourgoigne, P. (2001). "Optimisation of operational management practices for the detention basins." *Wat. Sci. Tech.*, 44(2-3), 277-285.
- James, W., and Shivalingaiah, B. (1985). "Storm water pollution modeling: buildup of dust and dirt on surfaces subject to runoff." *Can. J. Civ. Eng.*, 12, 906-914.
- Johnston, J., and Patel, D. (2004) "Small-scale pilot studies using coagulants for turbidity and phosphorus removal at Lake Tahoe." *3rd Annual North American Surface Water Quality Conference (StormCon)*.
- Kamalakkannan, R., Zettel, V. Goubatchev, A. Stead, K., and Ward, N.I. (2004). "Chemical (polycyclic aromatic hydrocarbon and heavy metal) levels in contaminated stormwater and sediments from a motorway dry detention pond drainage system." *J. Environ. Monit.*, 6, 175-181.
- Kang, J.-H., Li, Y., Lau, S., Kayhanian, M., and Stenstrom, M.K. (2005). "Application of particle size distribution in highway runoff: Optimization of settling tank design to remove particles." *Proceedings of The 4th South pacific conference on stormwater and aquatic resource protection*, Auchland, New Zealand.

- Kim, L.-H. (2002). "Monitoring and modeling of pollutant mass in urban runoff: Washoff, buildup and litter." *Ph.D. Dissertation*. University of California, Los Angeles.
- Kim, L.-H., Kayhanian, M., and Stenstrom, M.K. (2004). "Event mean concentrations of litter from highways during storms." *Sci. of the Total Envir.*, 330, 101-113.
- Kim, L.-H., Kayhanian, M., Lau, S.-L., and Stenstrom, M.K. (2005). "A new modeling approach for estimating first flush metal mass loading." *Wat. Sci. Tech.*, 51(3-4), 159-167.
- Kranck, K., and Milligan, T.G. (1991). Grain size in oceanography. In: Syvitski, J.P.M. (Ed.), principles, methods, and application of particle size analysis. Cambridge University Press, New York, 332-345.
- Krein, A., and Schorer, M. (2000). "Road runoff pollution by polycyclic aromatic hydrocarbons and its contribution to river sediments." *Wat. Res.*, 34(16), 4110-4115.
- Krishnappan, B.G., Marsalek, J., Watt, W.E., and Anderson, B.C. (1999). "Seasonal size distributions of suspended solids in a stormwater management pond." *Wat. Sci. Tech.*, 39(2), 127-134.
- Latimer, J.S., Hoffman, E.J., and Quinn, J.G. (1990). "Sources of petroleum hydrocarbons in urban runoff." *Wat. Air Soil Pollut.*, 52, 1-21.
- Lau S.-L., and Stenstrom M. K. (2005). "Metals and PAHs adsorbed to street particles." *Wat. Res.*, 39(17), 4083-4092.
- Lee, H., Lau, S.-L., Kayhanian, M., and Stenstrom, M.K. (2004). "Seasonal first flush phenomenon of urban stormwater discharges." *Wat. Res.*, 38, 4153-4163.
- Lee, J.H., Yu, K.W., Bang, K.W., and Choe, J.S. (2003). "Evaluation of the methods for first flush analysis in urban watersheds." *Wat. Sci. Tech.*, 48(10), 167-176.
- Legret, M., and Pagotto, C. (1999). "Evaluation of pollutant loadings in the runoff waters from a major rural highway." *Sci. of the Total Envir.*, 235, 143-150.
- Li, X.-Y., Zhang, J.-J, and Lee, J.H.W. (2004). "Modelling particle size distribution dynamics in marine waters." *Wat. Res.*, 38, 1305-1317.
- Li, Y., Lau, S.-L., Kayhanian, M., and Stenstrom, M. K. (2005a). "Particle size distribution in highway runoff." *J. of Envir. Engrg.*, ASCE, 131(9), 1267-1276.

- Li, Y., Lau, S.-L., Kayhanian, M., and Stenstrom, M. K. (2005b). "Dynamic characteristics of particles size distribution in highway runoff: implications for settling tank design." *J. of Envir. Engrg.*, ASCE, in press.
- Ma, M., Khan, S., Li, S., Kim, L.-H., Ha, S., Kayhanian, M., and Stenstrom, M.K. (2002). "First flush phenomena for highways: how it can be meaningfully defined." *Proceedings of 9th International Conference on Urban Drainage*, September, Portland, Oregon.
- Manning, M.J., Sullivan, R.H., and Kipp, T.M. (1977). Nationwide evaluation of combined sewer overflows and urban stormwater discharges-vol.III: characterization of discharges. EPA-600/2-77-064c (NTIS PB-2721207), USEPA.
- McAnally, W.H., and Mehta, A.J. (2000). "Aggregation rate of fine sediment." *J. Hydr. Engrg.*, ASCE, 126(12), 883-892
- Mehta, A.J. (1994). Hydraulic behavior of fine sediment - Coastal estuarial, and harbour engineer's reference book. Chapman & Hall, London, UK
- Milligan, T.G., and Loring, D.H. (1997). "The effect of flocculation on the size distributions of bottom sediment in coastal inlets: implications for contaminant transport." *Water, Air and Soil Pollution*, 99, 33-42.
- Moramarco, T., and Singh, V.P. (2002). "Accuracy of kinematic wave and diffusion wave for spatial-varying rainfall excess over a plane." *Hydrol. Process.*, 16, 3419-3435.
- Morquecho, R., and Pitt, R. (2003). "Stormwater heavy metal particulate associations." *Proceedings of WEFTEC*, Water Environment Federation, Los Angeles, California, October 11-15, 2003.
- Ngabe, B., Bidleman, T.F., and Scott, G.I. (2000). "Polycyclic aromatic hydrocarbons in storm runoff from urban and coastal South Carolina." *Sci. of the Total Envir.*, 255, 1-9.
- Oliver, B.G., Milne, J.B., and LaBarre, N. (1974). "Chloride and lead in urban snow." *Journal of the Water Pollution Control Federation*, 46(4), 766-771.
- Ongley, E.D., Bynoe, M.C., and Percival, J.B. (1981). "Physical and geochemical characteristics of suspended solids, Wilton Creek, Ontario." *Canadian Journal of Earth Sciences*, 18(8), 1365-1379.

- Perigault, J.G., Leckie, J.O., and Kitanidis, P.K. (2000). "Modeling particle transport and aggregation in a quiescent aqueous environment using the residence-time scheme." *Water Resources Research*, 36(8), 2249-2261.
- Persson, J., and Wittgren, H.B. (2003). "How hydrological and hydraulic conditions affect performance of ponds." *Ecological Engineering*, 21, 259-269.
- Pettersson, T.J.R. (1998). "Water quality improvement in a small stormwater detention pond." *Wat. Sci. Tech.*, 38(10), 115-122.
- Ponce, V.M., and Klabunde, A.C. (1999). "Parking lot storage modeling using diffusion waves." *J. Hydro. Engrg.*, ASCE, 4(4), 371-376.
- Roger, S., Montréjaud-Vignoles, M., Andral, M.C., Herremans, L., and Fortune, J.P. (1998). "Mineral, physical and chemical analysis of the solid matter carried by motorway runoff water." *Wat. Res.*, 32(4), 1119-1125.
- Rouse, H. (1938). *Fluid mechanics for hydraulic engineers*. Dover Publ., New York, USA.
- Saget, A., Chebbo, G., and Bertrand-Krajewski, J.L. (1996). "The first flush in sewer systems." *Wat. Sci. Tech.*, 33(9), 101-108.
- Sansalone, J.J., and Buchberger, S.G. (1997). "Characterization of solid and metal element distributions in urban highway stormwater." *Wat. Sci. Tech.*, 36(8-9), 155-160.
- Sansalone, J.J., Koran, J.M., Smithson, J.A., and Buchberger, S.G. (1998). "Physical characteristics of urban roadway solids transported during rain events." *J. Environ. Engrg.*, ASCE, 124(5), 427-440.
- Sansalone, J.J., and Cristina, C.M. (2004). "First flush concepts for suspended and dissolved solids in small impervious watersheds." *J. Environ. Engrg.*, ASCE, 130(11), 1301-1314.
- Sartor, J.D., and Boyd, G.B. (1972). *Water pollution, aspects of street surface contaminants*. EPA-R2-72-081, USEPA.
- Schillinger, J.E., and Gannon, J.J. (1985). "Bacterial adsorption and suspended particles in urban stormwater." *J. Wat. Pollut. Control.*, 57, 384-389.
- Schueler, T.R. (1987). *Controlling urban runoff: A practical manual for planning and designing urban BMPs*. Metropolitan Washington Council of Governments, Washington, D.C., USA.

- Shaheen, D.G. (1975). Contribution of urban roadway usage to water pollution. Environmental Protection Technology Series, EPA-600/2-75-004, USEPA. Cincinnati, OH.
- Shapiro, R. (1975). "Linear filtering." *Mathematics of Computation*, 29(132), 1094-1097.
- Singh, V.P. (1996). Kinematic wave modeling in water Resources: Surface Water Hydrology. Wiley, New York.
- Singh, V.P. (2002a) "Kinematic wave solutions for pollutant transport by runoff over an impervious plane, with instantaneous or finite-period mixing." *Hydrol. Process.*, 16, 1831-1863.
- Singh, V.P. (2002b) "Kinematic wave solutions for pollutant transport over an infiltrating plane with finite-period mixing and mixing zone." *Hydrol. Process.*, 16, 2441-2477.
- Sonstrom, R.S., Clausen, J.C., and Askew, D.R. (2002). "Treatment of parking lot stormwater using a stormtreat system." *Environ. Sci. Technol.*, 36, 4441-4446.
- Stenstrom, M.K., and Silverman, G.S., and Bursztynsky, T.A. (1984). "Oil and grease in urban stormwaters." *J. Environ. Engrg.*, ASCE, 110(1), 58-72.
- Stenstrom, M.K., and Strecker, E. (1993). Assessment of storm drain sources of contaminants to Santa Monica Bay, volume I, annual pollutant loadings to Santa Monica Bay from stormwater runoff. School of Engineering and Applied Science, UCLA.
- Stenstrom, M.K. (1996). Mathematical models for water quality. Lecture Notes, University of California, Los Angeles.
- Stenstrom, M.K., and Kayhanian, M, (2005). First flush phenomenon characterization. CTSW-RT-05-73-02.6, California Department of Transportation, Division of Environmental Analysis, Sacramento, CA., USA.
- Stuck, J.D., Izuno, F.T., Pickering, N., Cambell, K.L., and Bottcher, A.B. (2001). "Mathematical modeling of suspended solids and particulate phosphorus transport in farm conveyance systems of the Everglades agricultural area." *Transactions of the ASAE*, 44(5), 1117-1126.
- Stumm, W., and O'Melia, C.R. (1968) "Stoichiometry of coagulation." *J. AWWA*, May1968, 515-539.

- Taebi, A., and Droste, R.L. (2004). "First flush pollution load of urban stormwater runoff." *J. Environ. Eng. Sci.*, 3, 301-309.
- Takada, H., Harada, M., and Ogura, N. (1991). "Distribution and sources of polycyclic aromatic hydrocarbons (PAHs) in street dust from the Tokyo metropolitan area." *Sci. Total Env.*, 107, 45-69.
- Thomson, N.R., Mcbean, E.A., Snodgrass, W., and Monstrenko, I.B. (1997). "Highway stormwater runoff quality: development of surrogate parameter relationships." *Water, Air and Soil Pollution*, 94, 307-347.
- Tomanovic, A., and Maksimovic, C. (1996) "Improved modeling of suspended solids discharge from asphalt surface during storm event." *Wat. Sci. Tech.*, 33(4-5), 363-369.
- Trejo-Gaytan, J., Bachand, P., and Darby, J. (2005). "Treatment of urban runoff at Lake Tahoe: low intensity chemical dosing." *Wat. Env. Res.*, In press.
- U.S.EPA (1983). Results of nationwide urban runoff program, Vol.1-Final report. Water Planning Division, WH-554, Washington, DC, 20460.
- Vaze, J., and Chiew, F.H.S. (2002). "Experimental study of pollutant accumulation on an urban road surface." *Urban Wat.*, 4, 379-389.
- Von Rosenberg, D.U. (1969). Methods for the numerical solution of partial differential equations. Elsevier, New York.
- Vorreiter, L., and Hickey, C. (1994). "Incidence of the first flush phenomenon in catchments of the Sydney region." *National Conference Publication-Institute of Engineers*, Australia, 3, 359-364.
- Wasantha Lal, A.M. (1998). "Performance comparison of overland flow algorithms." *J. Hydr. Engrg.*, ASCE, 124(4), 342-349.
- Wood, W.L. (1993). Introduction to numerical methods for water resources. Oxford University Press, New York.
- Zhang, G.H., Liu, B.Y., Nearing, M.A., Huang, C.H., and Zhang, K.L. (2002). "Soil detachment by shallow flow." *Technical note*, ASAE. 45(2), 351-357.
- Zartman, R.E., Ramsey III, R.H., and Huang, A. (2001). "Variability of total and dissolved elements in stormwater runoff." *J. Soil & Wat. Conservation*, 56(3), 263.
- Zoppou, C. (2001). "Review of urban storm water models." *Environmental Modelling & Software*, 16, 195-231.